THE REGULATION OF TNF SIGNALING IN METABOLISM-RELATED DISEASES

Inaugural-Dissertation
zur Erlangung des

Doktorgrades
der Mathematisch-Naturwissenschaftlichen Fakultät

der **Universität zu Köln**

Önay Veli
Aus Nicosia, Cyprus
PhD Dissertation – 2024

Examination Committee

Reviewers/Examiners

Dr. Alessandro Annibaldi

Prof. Ana García Saéz

Prof. Andreas Morandi

Chair

Prof. Guenter Schwarz

Minutes taker

Jun. Prof. Nieves Peltzer

Day of examination: 04/12/2024

TABLE OF CONTENTS

INDEX OF FIGURES

INDEX OF TABLES

Abstract

Tumor necrosis factor (TNF) is a proinflammatory cytokine with a well-established role in diabetes pathogenesis. In addition to driving inflammation, TNF can induce cell death; yet the contribution of TNF-induced cell death to β-cell loss in diabetes remains unclear. Receptor-interacting protein kinase 1 (RIPK1) is a key regulator of TNF-induced cell death. The kinase function of RIPK1 is essential for TNF-induced necroptosis and under certain circumstances, apoptosis. In contrast, the scaffolding function of RIPK1 is essential to limit cell death. We studied the role of TNF-induced cell death in the pathogenesis of diabetes by dissecting the kinase versus scaffold function of RIPK1.

To study the role of this important checkpoint in TNF signaling in β-cells, we used two models that induce hyperglycemia by either β-cell toxicity or insulin resistance. These are the Multiple Low Dose Streptozotocin (MLDSTZ) and the high-fat diet models, respectively. Using *Ripk1*^{D138N} mice, which express a kinase-inactive version of RIPK1, we demonstrated that RIPK1 kinase activity does not drive the pathogenesis of type 1 diabetes (T1D), at least in the Multiple Low Dose Streptozotocin (MLDSTZ) model. We then generated *Ripk1*$^{\beta\text{-}KO}$ mice, which lack RIPK1 specifically in pancreatic β-cells. Notably, these mice are viable and have normal glycemic control over their lifespan. Moreover, *Ripk1*$^{\beta\text{-}KO}$ mice were not sensitized to MLDSTZ or high-fat diet (HFD). Hence, although RIPK1 is vital for the survival of many cell types, including keratinocytes and immune cells, its deletion in β-cells did not result in any spontaneous phenotype.

Islets isolated from *Ripk1*$^{\beta\text{-}KO}$ mice were resistant to TNF-induced cell death and were not sensitized to cytokine cocktail-induced cell death. While RIPK1 is crucial for the survival of many cell types, its deletion in β-cells did not sensitize them to cell death. Interestingly, we found that β-cells express high levels of cFLIP relative to Caspase-8, likely conferring resistance to TNF-induced apoptosis. Additionally, β-cells exhibited low RIPK3 expression, explaining their resistance to necroptosis. These findings suggest that β-cells fine-tune the expression of prosurvival and pro-death proteins to limit TNF-induced cell death, thereby preserving β-cell mass and maintaining normoglycemia.

In a second project, we investigated the role of LUBAC, another important checkpoint of TNF signaling in glycogen metabolism. LUBAC, an E3 ubiquitin ligase, acts downstream of various immune and cytokine receptors and is crucial for limiting TNF-induced cell death. In humans, LUBAC deficiency leads to autoinflammation and immunodeficiency. Unexpectedly, many patients also develop cardiomyopathy and myopathy due to toxic polyglucosan (a less-branched form of glycogen) accumulation in cardiac and skeletal muscles.

To explore LUBAC's role in glycogen metabolism, we generated *Hoip*$^{Muscle\text{-}KO}$ mice, lacking HOIP, the main catalytic component of LUBAC, in cardiac and skeletal muscle. These mice were viable and displayed no overt phenotypes. However, histological analysis revealed polyglucosan accumulation in the heart, reinforcing the hypothesis that LUBAC regulates glycogen metabolism through an unknown mechanism. Our preliminary results suggest that LUBAC may regulate autophagy, as ATG16L1, a key scaffold protein for LC3 lipidation, was significantly downregulated in *Hoip*$^{Muscle\text{-}KO}$ hearts. The precise mechanism by which LUBAC controls glycogen metabolism warrants further investigation.

In summary, my work revealed that β-cells regulate TNF-mediated cell death pathways in an alternative way, independent of classical checkpoints. While elevated cFLIP levels may play a key role in this resistance, other molecular mechanisms are likely involved and warrant further investigation. Additionally, LUBAC, a critical checkpoint in TNF signaling, appears to regulate glycogen metabolism, potentially by facilitating autophagy-mediated clearance of polyglucosan bodies.

Zusammenfassung

Tumornekrosefaktor (TNF) ist ein proinflammatorisches Zytokin mit einer gut etablierten Rolle in der Pathogenese von Diabetes. Neben der Förderung von Entzündungen kann TNF auch den Zelltod induzieren; dennoch bleibt der Beitrag des TNF-induzierten Zelltods zum Verlust von β-Zellen bei Diabetes unklar. Das Rezeptor-interagierende Proteinkinase 1 (RIPK1) ist ein Schlüsselregulator des TNF-induzierten Zelltods. Die Kinasefunktion von RIPK1 ist essenziell für die TNF-induzierte Nekroptose und unter bestimmten Umständen auch für die Apoptose. Im Gegensatz dazu ist die Gerüstfunktion von RIPK1 entscheidend, um den Zelltod zu begrenzen. Wir untersuchten die Rolle des TNF-induzierten Zelltods in der Pathogenese von Diabetes, indem wir die Kinase- und Gerüstfunktion von RIPK1 differenzierten.

Um die Rolle dieses wichtigen Kontrollpunkts in der TNF-Signalübertragung in β-Zellen zu untersuchen, verwendeten wir zwei Modelle, die durch β-Zelltoxizität oder Insulinresistenz Hyperglykämie induzieren. Diese sind das Multiple Low Dose Streptozotocin (MLDSTZ)-Modell und das Hochfettdiät-Modell. Mithilfe von *Ripk1*^{D138N}-Mäusen, die eine Kinase-inaktive Version von RIPK1 exprimieren, konnten wir zeigen, dass die Kinaseaktivität von RIPK1 die Pathogenese von Typ-1-Diabetes (T1D) im MLDSTZ-Modell zumindest nicht antreibt. Anschließend generierten wir *Ripk1*$^{\beta\text{-}KO}$-Mäuse, denen RIPK1 spezifisch in pankreatischen β-Zellen fehlt. Bemerkenswerterweise sind diese Mäuse lebensfähig und zeigen über ihre gesamte Lebensspanne eine normale glykämische Kontrolle. Zudem waren *Ripk1*$^{\beta\text{-}KO}$-Mäuse weder gegenüber MLDSTZ noch einer Hochfettdiät (HFD) sensibilisiert. Obwohl RIPK1 für das Überleben vieler Zelltypen, einschließlich Keratinozyten und Immunzellen, entscheidend ist, führte seine Deletion in β-Zellen zu keinem spontanen Phänotyp.

Von *Ripk1*$^{\beta\text{-}KO}$-Mäusen isolierte Inselzellen waren resistent gegenüber TNF-induziertem Zelltod und nicht sensibilisiert für den Zelltod, der durch einen Zytokin-Cocktail induziert wurde. Während RIPK1 für das Überleben vieler Zelltypen entscheidend ist, machte seine Deletion β-Zellen nicht einmal empfindlich gegenüber Zelltod. Interessanterweise stellten wir fest, dass β-Zellen hohe cFLIP-Spiegel im Vergleich zu Caspase-8 exprimieren, was ihnen wahrscheinlich eine Resistenz gegenüber TNF-induzierter Apoptose verleiht. Darüber hinaus zeigten β-Zellen eine geringe RIPK3-Expression, was ihre Resistenz gegenüber Nekroptose erklärt. Diese Erkenntnisse deuten darauf hin, dass β-Zellen die Expression von prosurvival und pro-death Proteinen fein abstimmen, um den TNF-induzierten Zelltod zu begrenzen, wodurch die β-Zellmasse erhalten bleibt und die Euglykämie aufrechterhalten wird.

In einem zweiten Projekt untersuchten wir die Rolle von LUBAC, einem weiteren wichtigen Kontrollpunkt in der TNF-Signalübertragung im Glykogenstoffwechsel. LUBAC, eine E3-Ubiquitin-Ligase, wirkt stromabwärts von verschiedenen Immun- und Zytokinrezeptoren und ist entscheidend, um den TNF-induzierten Zelltod zu begrenzen. Beim Menschen führt ein LUBAC-Mangel zu Autoinflammation und Immunschwäche. Unerwarteterweise entwickeln viele Patienten auch Kardiomyopathie und Myopathie aufgrund der Akkumulation toxischer Polyglucosan-Körper (einer weniger verzweigten Form von Glykogen) in Herz- und Skelettmuskulatur.

Um die Rolle von LUBAC im Glykogenstoffwechsel zu erforschen, generierten wir *Ripk1*$^{\beta\text{-}KO}$-Mäuse, denen HOIP, der katalytische Kern von LUBAC, in Herz- und Skelettmuskelzellen fehlt. Diese Mäuse waren lebensfähig und zeigten keine auffälligen Phänotypen. Histologische Analysen zeigten jedoch eine Polyglucosan-Akkumulation im Herzen, was die Hypothese stärkt, dass LUBAC den Glykogenstoffwechsel durch einen unbekannten Mechanismus reguliert. Unsere vorläufigen Ergebnisse deuten darauf hin, dass LUBAC die Autophagie regulieren könnte, da ATG16L1, ein wichtiger Gerüstprotein für die LC3-Lipidation, in *Ripk1*$^{\beta\text{-}KO}$-Herzen signifikant herunterreguliert war. Der genaue Mechanismus, durch den LUBAC den Glykogenstoffwechsel steuert, bedarf weiterer Untersuchungen.

Zusammenfassend ergab meine Arbeit, dass β-Zellen die TNF-vermittelten Zelltodpfade auf eine alternative Weise regulieren, die von klassischen Kontrollpunkten unabhängig ist. Während erhöhte cFLIP-Spiegel eine wichtige Rolle bei dieser Resistenz spielen könnten, sind wahrscheinlich auch andere molekulare Mechanismen beteiligt, die weiterer Untersuchungen bedürfen. Darüber hinaus scheint LUBAC, ein kritischer Kontrollpunkt in der TNF-Signalübertragung, den Glykogenstoffwechsel zu regulieren, möglicherweise durch die Förderung der autophagie-vermittelten Entfernung von Polyglucosan-Körpern.

Abbreviations of units

%	percent
°C	Degree Celsius
Bp	base pair
G, mg, µg, ng	gram, milligram, microgram, nanogram
h, min, sec	hours, minutes, seconds
kDa	kilo Dalton
l, ml, µl	liter, milliliter, microliter
M, mM, µM, nM pM	molar, millimolar, micromolar, nanomolar, picomolar
RCF	relative centrifugal force

Glossary

A

APAF-1: Apoptotic protease activating factor-1

ASC: Apoptosis-associated Speck-like Protein Containing a CARD

AIM2: Absent in melanoma 2

ATG9a: Autophagy-related 9A

ATF6: Activating transcription factor 6

ATP: Adenosine triphosphate

ALT: Alanine transaminase

AST: Aspartate aminotransferase

B

BCL-2: B-cell lymphoma 2

BCL_{XL}: B-cell lymphoma-extra large

BAD: Bcl-2-Antagonist-of-Cell-Death

BAK: Bcl-2 homologous antagonist killer

BAX: Apoptosis regulator BAX

BID: BH3 interacting-domain death agonist

C

CAD: Caspase-activated DNase

CX3CL1: Chemokine (C-X3-C motif) ligand 1

cIAP1/2: Cellular inhibitor of apoptosis protein-1/2

CYLD: Cylindromatosis

cFLIP: Fas-associated death domain-like IL-1β–converting enzyme inhibitory protein

CTLA-4: Cytotoxic T-lymphocyte associated protein 4

D

DAMP: Damage-associated molecular patterns

E

eIF2α: Eukaryotic Initiation Factor 2

ELAVL1: ELAV Like RNA Binding Protein 1

F

FADD: FAS-associated death domain protein

FIP200: Focal adhesion kinase family interacting protein of 200 kD

G

GSDMD: Gasdermin D

GSDME: Gasdermin E

GAD: Glutamic acid decarboxylase

GLUT2: Glucose transporter 2

GYS1/2: Glycogen synthase 1/2

GSK3: Glycogen synthase kinase 3

GP: Glycogen phosphorylase

G6Pase: Glucose 6-phosphatase

GBE: Glycogen branching enzyme

GAA: α-glucosidase

H

HMGB1: High mobility group box 1 protein

HOIL-1: Heme-oxidized IRP2 ubiquitin ligase 1

HOIP: HOIL-1 interacting protein

HLA: Human leukocyte antigen

HECT: Homologous to E6AP C-terminus

I

IL-1β: Interleukin-1

IL-18: Interleukin-18

IKKα/β: IkappaB kinase α/β

IKKε: IkappaB kinase ε

INS: Insulin

IL-2: Interleukin-2

IL-12: Interleukin-12

IL-4: Interleukin-4

IL-5: Interleukin-5

IL-13: Interleukin-13

IL-17: Interleukin-17

IL-10: Interleukin-10

IL-35: Interleukin-35

IL-21: Interleukin-21

IFNγ: Interferonγ

IRS: Insulin receptor substrate

IREα: Inositol-requiring enzyme-1α

iNOS: inducible nitric oxide synthases

J

JNK: c-Jun N-terminal kinase

K

L

LDH: Lactate dehydrogenase

LUBAC: Linear chain assembly complex

M

MOM: Mitochondrial outer membrane

MOMP: Mitochondrial outer membrane permeabilization

MCL-1: Myeloid cell leukemia-1

MAPK: Mitogen-activated protein kinase

MLKL: Mixed lineage kinase domain-like pseudokinase

MK2: Mitogen-activated protein kinase-activated protein kinase 2

MHC: Major histocompatibility complex

N

NRLP3: NLR family pyrin domain containing 1/ 3

NAIP: Neuronal apoptosis inhibitory protein

NLRC4: NOD-like receptor containing a caspase activating and recruitment domain 4

NINJ1: Ninjurin-1

NEMO: NF-kappa-B essential modulator

NF-κB: Nuclear factor 'kappa-light-chain-enhancer' of activated B-cells

NO: Nitric oxide

O

OTULIN: OTU deubiquitinase with linear linkage specificity

P

PUMA: p53 upregulated modulator of apoptosis

PTPN22: Protein tyrosine phosphatase non-receptor type 22

PERK: PKR-like endoplasmic reticulum kinase

PKA: Protein kinase A

Q

R

RIPK1: Receptor-interacting serine/threonine-protein kinase 1

RIPK3: Receptor-interacting serine/threonine-protein kinase 3

RelA: REL-associated protein

RNF146: Ring Finger Protein 146

RAG2: Recombination activating gene 2

RING: Really Interesting New Gene

S

SHARPIN: SHANK associated RH domain interactor

SERCA2B: Sarcoplasmic/endoplasmic reticulum Ca2+-ATPase 2B

T

TNF: Tumor necrosis factor

TNFR1: Tumor necrosis factor receptor 1

TRAIL: TNF-related apoptosis-inducing ligand

TRAILR1/2: TNF-related apoptosis-inducing ligand receptor ½

TRIF: Toll-interleukin 1 receptor domain (TIR)-containing adaptor inducing IFN-β

TLR3/4: Toll-like receptor 3/4

TRADD: TNFR1-associated death domain protein

TAB1: TGF-β activated kinase 1

TAK1/2: Transforming growth factor beta-activated kinase 1/2

TBK1: TANK-binding kinase 1

TAX1BP1: Tax1 binding protein

TNKS1: Tankyrase 1

TGF-β: Transforming growth factor β

U

V

W

X

XBP1: X-Box Binding Protein 1

Y

Z

ZBP1: Z-DNA binding protein

THE REGULATION OF TNF SIGNALING IN METABOLISM-RELATED DISEASES

GENERAL INTRODUCTION

In the general introduction of my thesis, I begin by reviewing the literature on the three most common programmed cell death modalities: apoptosis, necroptosis, and pyroptosis. The output of TNF signaling is normally prosurvival and proinflammatory gene activation. However, it can also induce cell death. Given the cytotoxic nature of TNF signaling, I focus on the molecular checkpoints that regulate TNF signaling to maintain a balance between survival and death. At the conclusion of the chapter, I raise key questions about the regulation of cell death mechanisms from my perspective.

1. Programmed cell death

Death is inevitable for all living organisms, from cells to individuals. Today, it is widely accepted that cell death is crucial for maintaining homeostasis by removing damaged or nonfunctional cells and eliminating pathogens during infections. Moreover, cell death is essential for normal morphogenesis during developmental stages [1]. However, cell survival and death require a fine balance. While excessive cell death is linked to inflammatory and autoimmune diseases, resistance to cell death is a defining characteristic of cancer cells.

Historically, it was believed that cell death is an unregulated event that happens inevitably due to the death of damaged or nonfunctional cells [1]. In 1965, Hohn Kerr pioneered programmed cell death research by distinguishing the different types of cell death in rat liver injury [2]. In 1972, Kerr and colleagues used the term apoptosis for the first time [3]. They described the morphology of apoptotic cells as a “formation of small, roughly spherical or ovoid cytoplasmic fragments some of which contain pyknotic remnants of nuclei” [3]. Interestingly, the word "apoptosis" is derived from Greek, meaning "falling of the leaves from the trees," highlighting the programmed and orderly nature of this form of cell death [3].

Many other forms of programmed cell death (PCD) have been discovered in recent years. This includes necroptosis, pyroptosis, ferroptosis, cuproptosis, among many others [4]. They can be divided into two groups based on the leakage of cell contents into the extracellular space: non-lytic and lytic cell death [1]. Non-lytic cell death generally refers to apoptosis, as the recently identified forms of programmed cell death are mostly lytic. In the following sections of my thesis, I will focus on three cell death forms: apoptosis, necroptosis and pyroptosis. Therefore, these forms of cell death are discussed in detail below.

1.1. Apoptosis

Apoptosis is a caspase-dependent and non-lytic form of cell death that occurs inside the apoptotic blebs. Caspases are cysteine proteases that cleave their targets after specific aspartic acid residues [5]. During apoptosis, they coordinate the dismantling of the cells by cleaving specific targets. Since there is no leakage of cell content to the extracellular space, this form of cell death is considered immunologically silent [4]. Apoptosis can be triggered intrinsically and extrinsically. Intrinsic apoptosis is triggered by the activation of intracellular stress sensors, such as those responding to DNA damage or endoplasmic reticulum stress [6]. The activation of intracellular sensors acts through MOM, resulting in its subsequent permeabilization, known as MOMP. MOMP leads to cytochrome c release which triggers the assembly of apoptosome, consisting of APAF1 and Caspase-9 [7]. Once Caspase-9 is activated through apoptosome formation, it cleaves effector caspases, Caspase-3/7. MOMP is the

critical event in intrinsic apoptosis, known as the "point of no return," and as such, it is tightly regulated by BCL-2 family proteins [8]. BCL-2 family proteins are divided into three groups: initiators, guardians, and executioners. In the case of cellular stress, initiators, such as PUMA, and BAD, inhibit the function of guardians [6]. Guardians are prosurvival proteins such as BCL-2, MCL-1, and BCL_{XL}. Additionally, initiators activate executioners, BAK and BAX. When activated, BAK and BAX accumulate in MOM and oligomerize to trigger MOMP (Figure GI-1). In contrast, extrinsic apoptosis is initiated by death receptors and their specific ligands, such as TNFR1/TNF, FAS/FASL (CD95/CD95L), and TRAILR1-2/TRAIL (Figure GI-1)[9]. During extrinsic apoptosis, initiator Caspase-8 can directly activate effector Caspase-3 or, depending on the cell type, cleave BID to trigger the intrinsic apoptosis pathway (Figure GI-1) [4]. In type I cells, Caspase-8 can directly cleave Caspase-3 to induce apoptosis [10]. Whereas type II cells require intermediate BID cleavage by Caspase-8 that acts as a bridge between extrinsic and intrinsic apoptosis. Truncated BID (tBID) then translocates to the MOM and leads to MOMP in cooperation with BAK and BAX. Active Caspase-3 cleaves many downstream targets to trigger apoptotic blebbing, chromatin condensation and DNA degradation [11]. Active Caspase-3 cleaves CAD to release the active component iCAD. iCAD leads to DNA degradation and chromatin condensation in the nucleus. Active Caspase-3 also cleaves Gelsolin, a protein that nucleates actin polymerization. Once cleaved, Gelsolin then breaks down actin filaments, leading to loss of cell integrity and disruption of signal transduction within the cell. At the final step, apoptotic cells are engulfed by macrophages, a process also known as efferocytosis [12]. At this step, apoptotic cells send “find me” and “eat me” signals to macrophages. “Find me” signals include DAMPS and some chemokines such as CX3CL1. Phosphatidylserine (PS) is one of the best-characterized “eat me” signals. Normally, it is found in the inner cell membrane; however, its exposure to the surface of the membrane indicates apoptosis and “eat me” signal to the macrophages.

Due to its highly regulated nature, apoptosis has been considered as immunologically silent. However, this view has been challenged by recent findings [13]. It has been shown that apoptotic cell death can switch to pyroptosis through cleavage of GSDME via Caspase-3, suggesting that apoptosis can also be immunogenic under certain circumstances [13–15].

1.2. Necroptosis

Necroptosis is a lytic form of cell death which can trigger inflammation. Although the observation of a non-apoptotic form of cell death via death receptors dates back to the 1990s, the term “necroptosis” was used for the first time in 2005 [16–18]. The authors emphasize that this form of cell death is induced by death receptors when the caspases are inhibited [16]. In the same study, the authors identified Necrostatin-1s (Nec-1s) through a chemical library

screening as an inhibitor of necroptosis [16]. Nec-1s was shown to be an inhibitor of RIPK1, suggesting that necroptosis is regulated by kinases [19]. Later on, it was shown that phosphorylated RIPK1 interacts with RIPK3 via their RHIM domain. This interaction triggers the oligomerization of RIPK1 and RIPK3, and autophosphorylation of RIPK3 [20–22]. In 2012, the final piece of the puzzle was identified as MLKL, which is responsible for necroptotic pore formation after being phosphorylated by RIPK3 (Figure GI-1) [23,24]. Necroptosis can be triggered by death receptors, TNFR1, FAS (CD95) and TRAIL upon their engagement with their respective ligands. TRIF is an RHIM-containing-adaptor protein which acts downstream of TLR3/4 [25]. Therefore, activation of TLR3/4 can induce necroptosis since TRIF can directly interact with RIPK3 to induce necroptosis (Figure GI-1) [25]. More recently, another RHIM-containing protein, ZBP1 was shown to induce necroptosis (Figure GI-1) [26,27].

1.3. Pyroptosis

Pyroptosis is a lytic form of cell death that is dependent on caspase activation. The first observation of pyroptosis dates back to the 1980s [28]. Although many reports observed that exposure of macrophages to bacteria triggers cell death, the term "pyroptosis" was first used in 2001, differentiating it from apoptosis [29,30]. Pyroptosis is derived from the Greek words “pyro,” meaning “fever,” and “tosis,” meaning “falling”, emphasizing the inflammatory nature of this form of cell death [29]**.** Inflammasomes were discovered as platforms that lead to Caspase-1 activation and subsequent IL-1β and IL-18 cleavage [31]. NRLP3 is the most studied inflammasome. It was first discovered due to the gain of function mutations in patients leading to an autoinflammatory disease called cryopyrin-associated periodic syndrome (CAPS). Later on, it was shown that NRLP3 can also form inflammasome leading to Caspase-1 activation and pyroptosis (Figure GI-1) [32]. NRLP3 inflammasome consists of NRLP3 which acts as a sensor, ASC which acts as an adaptor and Caspase-1. It was shown that NRLP3 can be activated by a wide range of stimuli such as ATP, cholesterol crystals, ceramides, etc. [33]. Canonical inflammasomes activate Caspase-1 through an assembled complex which requires signal recognition by cytoplasmic sensors such as NRLP1/3, AIM2, NAIP–NLRC4. In the non-canonical inflammasome pathway, Caspase-11 in mice and Caspase-4/5 in humans can be directly activated by LPS [34]. GSDMD, the final piece of the puzzle, was discovered in 2015. It was demonstrated that GSDMD cleavage by Caspase-1 triggers its oligomerization and leads to pore formation (Figure GI-1) [36]. Recently, it has been demonstrated that in addition to Caspase-1/4/5/11, Caspase-8 activation via extrinsic apoptosis pathways can also lead to GSDMD cleavage [37–39].

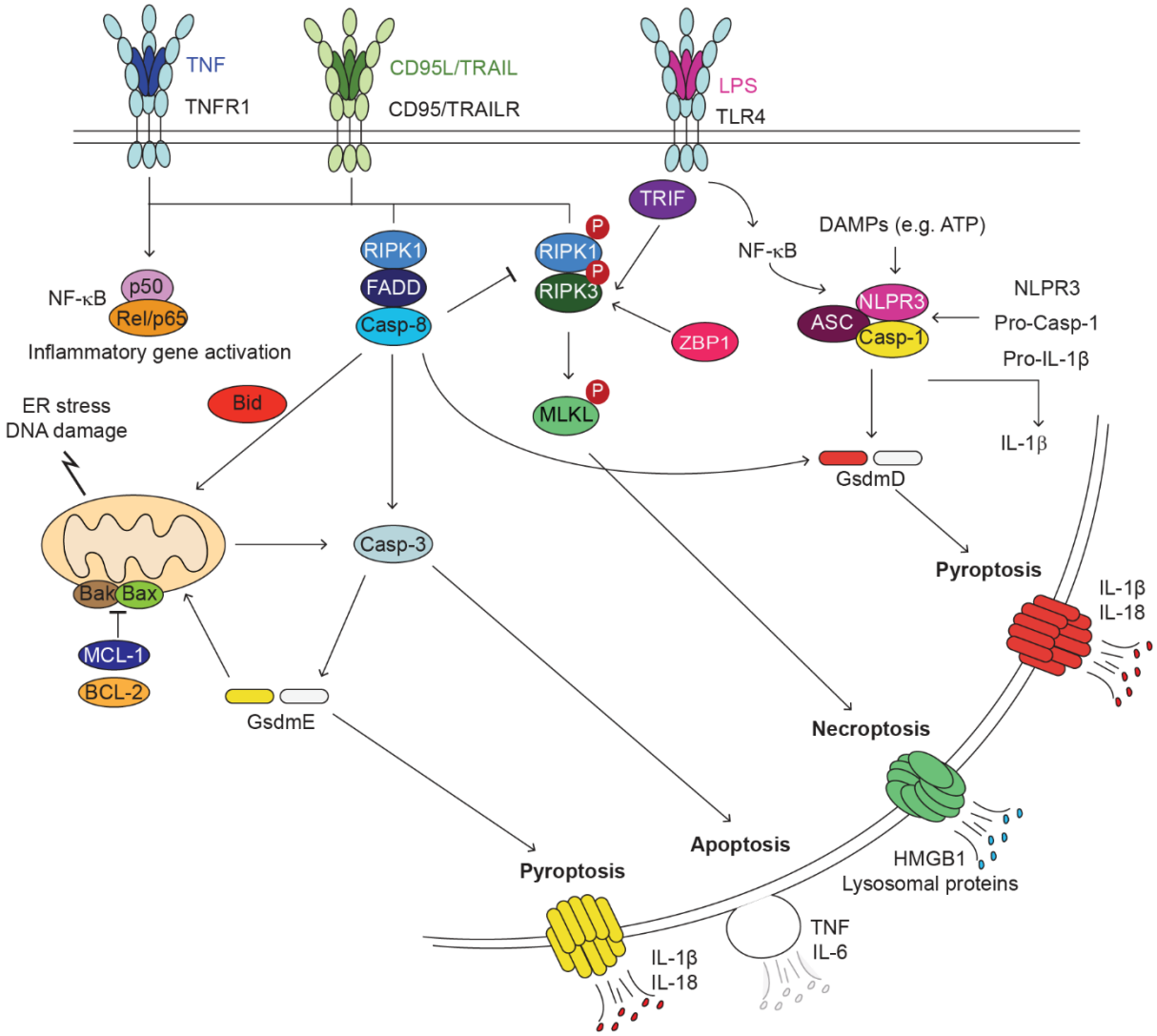

Figure GI-1. Overview of different cell death pathways. ER stress and DNA damage can lead to intrinsic apoptosis via permeabilization of MOM by BAK and BAX which eventually leads to Caspase-3 activation. Antiapoptotic proteins, including BCL-2 and MCL-1, inhibit BAK and BAX. Extrinsic apoptosis is triggered by death receptors including TNFR1 and FAS/TRAILR. The engagement of TNFR1 with TNF primarily leads to inflammatory gene activation by NF-κB and under certain conditions can induce apoptosis and necroptosis. On the contrary, when FAS and TRAILR engage with their respective ligands the primary response is apoptosis via Caspase-8 activity. When Caspase-8 activity is inhibited, RIPK1 and RIPK3 interaction leads to RIPK3 activation by autophosphorylation. Activated RIPK3 phosphorylate and activate MLKL which leads to necroptotic pore formation in the cell membrane. In addition to RIPK1, TRIF and ZBP1 can also activate RIPK3 to trigger necroptosis. LPS recognition by TLR4 upregulates pyroptotic proteins such as NRLP3 and IL-1β, a step known as priming. The activation of NRLP3 by DAMPs activates Caspase-1. Caspase-1 cleaves GSDMD which mediates the formation of pyroptotic pores in the cell membrane. GSDMD can also be cleaved by Caspase-8 to initiate pyroptosis. Downstream intrinsic and extrinsic apoptosis, GSDME can be cleaved by Caspase-3 to trigger pyroptosis. Adapted from [35].

This facilitates the release of proinflammatory cytokines, IL-1β and IL-18 (Figure GI-1). Upon its cleavage, GSDMD was shown to cause damage in the outer and inner membranes of mitochondria to facilitate pyroptosis [40]. Downstream of pore formation by GSDMD, NINJ1

mediates plasma membrane rupture (PMR), leading to the release of large proteins such as LDH and HMGB1, which act as DAMPs [41]. These components collectively contribute to the inflammatory nature of pyroptosis. GSDME is another member of the Gasdermin family. Interestingly, GSDME can be cleaved by Caspase-3 downstream apoptosis induction [14,15] (Figure GI-1). Cleavage of GSDME mediates pyroptotic pores and release of DAMPs. Furthermore, once cleaved, GSDME permeabilizes the mitochondrial membrane, enhancing the intrinsic apoptosis pathway by facilitating cytochrome c release [42]. These findings challenged the notion that apoptosis is inherently a non-inflammatory form of cell death.

2. Death receptor (DR)-induced cell death

DRs belong to the TNFR superfamily and are characterized by their cytoplasmic death domain. Because of this domain, binding to their respective ligands can trigger cell death, specifically apoptosis and necroptosis [43]. DRs induce two main signals, inflammatory gene activation and cell death. TNFR1 mainly induces gene activation by the formation of a membrane-bound complex, known as complex I which leads to inflammatory gene activation by NF-κB and MAPK pathways (Figure GI-2). However, it can also induce cell death through the formation of a secondary cytosolic complex. On the contrary, FAS (CD95) and TRAILR1-2 induce primarily cell death through the formation of a membrane-bound complex, called DISC (Figure GI-2). This complex can disassociate from the receptor and give rise to a cytoplasmic complex which can trigger the activation via NF-κB and MAPK pathways (Figure GI-2). Hence, while the main signaling output of TNFR1 is prosurvival and proinflammatory, CD95 and TRAILR1-2 mainly induce cell death.

3. TNF signaling: A fine balance between life and death

TNF is a proinflammatory cytokine which plays an essential role in host defense against pathogens [44]. It has two cellular receptors, TNFR1 and TNFR2. Although both TNFR1 and TNFR2 can induce proinflammatory gene activation, only TNFR1 can exert cytotoxic activities since it bears a cytoplasmic death domain [43]. Due to its cytotoxic potential, TNF-TNFR1 signaling is tightly regulated by molecular brakes, known as checkpoints of TNF signaling [45]. These checkpoints are crucial to maintain the balance between cell survival and death in response to TNF.

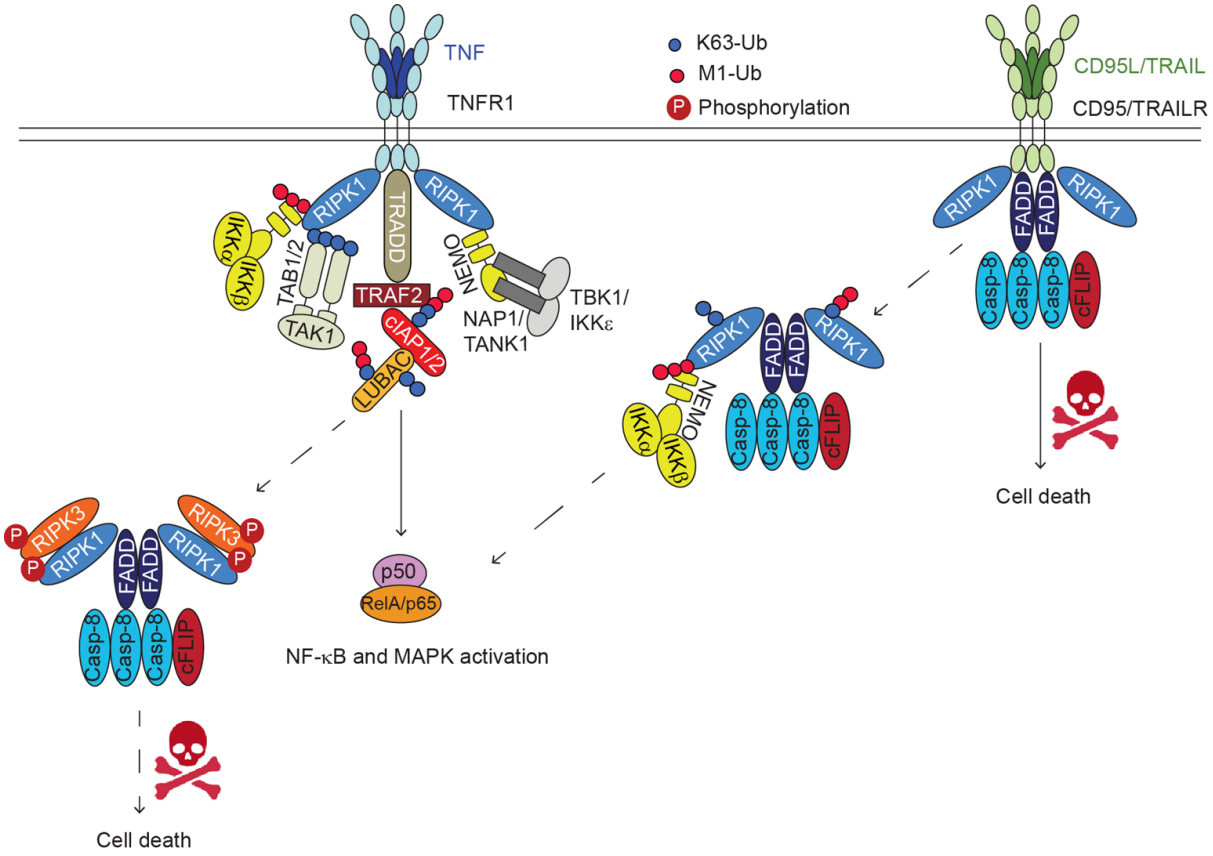

Figure GI-2. Signaling Pathways Activated by Death Receptors. Death receptors induce two main signals, proinflammatory gene activation and cell death. Binding of TNF to TNFR1 triggers the formation of Complex I which includes RIPK1, E3 ligases such as cIAPs and LUBAC, and kinases such as IKK and TAK1 complex. This complex leads to inflammatory gene activation by NF-κB and MAPK pathways. However, dissociation of this complex from the receptor can also lead to cell death. In contrast, CD95 and TRAILR1-2 mainly induce cell death through the formation of a complex which includes FADD, Caspase-8, and cFLIP. Dissociation of this complex from the receptor can lead to activation of NF-κB and MAPK pathways. Dashed arrows represent secondary signaling outputs.

3.1. TNF-induced proinflammatory gene activation

The binding of TNF to TNFR1 triggers the trimerization of the receptor and leads to a membrane-bound complex formation, known as Complex I of TNFR1 signaling (Figure GI-3). TRADD and RIPK1 bind to the receptor and serve as adaptor proteins [46]. Subsequently, TRAF2 and E3 ligases, cIAP1/2 and LUBAC (consists of HOIL-1, HOIP and SHARPIN) are recruited to the complex [47,48]. cIAP1/2 and LUBAC generate ubiquitin chains on their substrates such as RIPK1 and stabilize the complex. Ubiquitin chains serve as scaffolds for kinases to be recruited to the complex. The generation of K63 chains on RIPK1 and other substrates by cIAP1/2 is important for the recruitment of TAB1 and TAK1/2 which then induces the activation of MAPK pathway [49]. K63 chains are also important for the recruitment of LUBAC to the complex. LUBAC generates linear (M1) chains which allows the recruitment of NEMO

(adaptor protein, also known as IKKγ) [50]. NEMO brings the kinases IKKα/β and IKKε/TBK1 to the complex. Due to the close proximity between TAK1 and IKK complex, TAK1 phosphorylates and activates IKKα/β. In turn, IKKα/β phosphorylates and targets IκB (the inhibitor of NF-κB) for proteasomal degradation. After release from their inhibitor, p50/p65 dimers migrate to the nucleus to induce gene activation [45]. The post-translational modification cascade in the complex ensures the proinflammatory and prosurvival gene activation in response to TNF.

3.2. TNF-induced cell death

Under physiological conditions, several factors orchestrate the stabilization and optimal activation of complex I, resulting in gene activation. Post-translational modifications not only ensure effective signal transduction but also serve as checkpoints in TNFR1 signaling (Figure GI-3). A defect in any of the checkpoints causes RIPK1 autophosphorylation and disassociation from complex I [51]. This leads to the formation of a cytosolic complex, known as complex II of TNFR1 signalling. Complex II contains RIPK1 to which FADD is recruited [52,53]. FADD brings Caspase-8 to the complex which, upon recruitment-mediated activation, initiates apoptosis. When the activity of Caspase-8 is inhibited, RIPK1 recruits RIPK3 via its RHIM domain [20–22]. This interaction triggers autophosphorylation and activation of RIPK3. Activated RIPK3 subsequently phosphorylates and, thereby, activates the pseudokinase MLKL which triggers necroptosis by forming pores in the membrane [23,24]. Thus, the kinase activities of both RIPK1 and RIPK3 are required for TNF-induced necroptosis [20–22]. Notably, in the absence of RIPK1, RIPK3 can still be activated by ZBP1 to induce necroptosis [26,27]. In recent years, GSDMD was shown to be cleaved by Caspase-8 while GSDME is cleaved by Caspase-3 [14,15]. Therefore, TNF can induce three distinct cell death modalities namely, apoptosis, necroptosis and pyroptosis.

3.3. Checkpoints of TNF-induced cell death

Certain pathogens can hijack proinflammatory gene activation by inhibiting key kinases, such as TAK1 and IKKs, that drive NF-κB and MAPK activation [54–57]. Since these kinases act as checkpoints, their inhibition triggers TNF-induced cell death. Therefore, from an evolutionary point of view, these checkpoints in TNF signaling seem to serve as backup mechanisms to ensure proper host defense. While these non-redundant checkpoints are advantageous in controlling pathogen invasion, mutations that disrupt them can be detrimental to the host [58]. Indeed, mutations that impair these checkpoints are sufficient to cause inflammatory diseases in humans (summarized in Table GI-1). Mouse models have been invaluable in elucidating the role of these checkpoints in the regulation of TNF-induced cell death. Interestingly, mutations that inhibit these molecular brakes in mice lead to embryonic lethality due to

excessive cell death, as discussed in the following sections and summarized in Table GI-2. Thus, it is clear that TNF-induced cell death checkpoints serve as essential safeguards of physiological inflammation in both mice and humans and are therefore tightly regulated.

3.3.1. RIPK1: The master regulator of TNF-induced cell death

RIPK1 acts as a molecular switch which regulates cell fate within TNF signaling. Paradoxically, the scaffold function of RIPK1 enables cell survival and facilitates signal transduction, whereas its kinase function induces cell death. This was discovered by the finding that loss of RIPK1 leads to postnatal lethality in mice between days 1 and 3, as a result of uncontrolled apoptosis and necroptosis [59]. The deficiency of RIPK1 is rescued by blocking both apoptosis and necroptosis by the additional deletion of Caspase-8 and RIPK3, respectively [60,61]. Activation of necroptosis in the absence of RIPK1 was later described to be caused by other RHIM domain-containing proteins, ZBP1 and TRIF [26,27]. Therefore, concomitant deletion of ZBP1 and TRIF restored the viability of mice lacking RIPK1 and Casepase-8 (*Ripk1*$^{-/-}$*Casp8*$^{-/-}$*Zbp1*$^{-/-}$*Trif*$^{-/-}$ mice).

In contrast to its scaffold activity, the kinase activity of RIPK1 induces TNF-induced necroptosis and apoptosis [62,63]. Therefore, the kinase activity of RIPK1 is tightly regulated by ubiquitination and phosphorylation-dependent checkpoints in TNF signaling [45,64]. Additionally, NF-κB activation, Caspase-8-dependent cleavage events and lysosomal degradation act as checkpoints of TNF signaling. Importantly, several secondary checkpoints were identified to limit cell death when the cells are already committed to die (explained in detail in Box GI-1 at the end of this chapter).

3.3.2. Ubiquitination-dependent checkpoints

Ubiquitination is a post-translational event regulating various cellular processes from cell cycle to inflammatory signaling [65]. It is an enzymatic process which requires three sequential steps which are initiation, conjugation, and ligation. In the first step, ubiquitin is attached to an E1 ubiquitin-activating enzyme in an ATP-dependent manner. The ubiquitin is then transferred to an E2-ubiquitin conjugating enzyme. In the final step, ubiquitin is attached to the lysine residue of the target protein by an E3 ubiquitin ligase [66]. Monoubiquitination is a common cellular process that functions as a signal for various activities, including endocytosis and subcellular localization. Polyubiquitin chains can be attached to seven lysine residues—K7, K11, K27, K29, K33, K48, and K63—as well as a target protein's N-terminal methionine (M1). These ubiquitin chains can form in homotypic, heterotypic, or branched structures [65]. Different configurations of ubiquitin chains are recognized by specific "reader" proteins, which interpret the signals and trigger distinct cellular outcomes. This intricate signaling system is collectively known as the "ubiquitin code" [67].

Ubiquitination plays a key role in determining the signaling outcomes of TNF signaling. The E3 ligases cIAP1 and cIAP2 attach K63-linked polyubiquitin chains to target proteins such as RIPK1 and promote cell survival by enabling NF-κB and MAPK activation (Figure GI-3) [47,68]. Crucially, the recruitment of cIAP1/2 to the TNF receptor complex acts as a checkpoint [69]. When this recruitment is impaired, RIPK1 undergoes autophosphorylation, dissociates from complex I, and triggers cell death pathways. Mice lacking either cIAP1 or cIAP2 are viable and display no significant abnormalities [70,71]. However, the combined deficiency of both cIAP1 and cIAP2 leads to embryonic lethality at day E10.5, indicating functional redundancy between the two [72]. The additional deletion of TNFR1 rescued the embryonic lethality only to birth. Similarly, a recent study showed that blockade of cell death by additional deletion of Caspase-8 and MLKL rescues embryonic lethality, but mice survive only until birth [73]. These findings indicate that cIAP1 and cIAP2 are crucial for perinatal survival, with functions extending beyond cell death regulation.

LUBAC is the only known E3 ligase that can conjugate linear ubiquitin (M1) chains (Figure GI-3) [74]. Importantly, it plays an important role in cell fate decisions[75]. LUBAC generates M1 chains on its targets including RIPK1, TRADD and TNFR1 and stabilizes the complex [76]. Similar to cIAP1/2, it promotes cell survival by enabling NF-κB and MAPK activation while preventing cell death. It is composed of three subunits: HOIP, HOIL-1 and SHARPIN. HOIP is the main catalytic component of LUBAC, and its deficiency causes embryonic lethality at day E10.5 due to death of endothelial cells [75]. The additional deletion of Caspase-8 and MLKL rescues embryonic lethality, and pups survive until 4-5 weeks of age [77]. Although HOIL-1 is not the main catalytic component, it is important for the stability of LUBAC. Therefore, HOIL-1 deficiency phenocopies HOIP deficiency [77]. Chronic proliferative dermatitis mutation (*Cpdm*) mice bear a mutation in their *Sharpin* gene which causes destabilization of LUBAC. These mice develop dermatitis, multi-organ inflammation, splenomegaly, and loss of Payer´s patches in the gut [78]. It was later shown that the main driver of this phenotype is TNFR1-induced cell death since the deletion of TNF significantly delays the onset of the disease [79–82]. Moreover, the disease is prevented by the inhibition of RIPK1 kinase activity or additional deletion of Caspase-8 and MLKL [63,77].

Importantly, the balance between E3 ligases and deubiquitinases (DUBs) is crucial to enable gene activation and prevent cell death. The binding of A20 to linear chains protects their degradation by DUBs [76]. In contrast, CYLD and OTULIN cleave M1 chains to suppress NF-κB activation and disassemble complex I [83]. The loss of OTULIN leads to embryonic lethality [84]. Likewise, an inactivating mutation in OTULIN (C129A) causes embryonic lethality in mice at E10.5 which resembles LUBAC deficiency [85]. These findings suggest that the balance

between E3 ligases and DUBs is critical for cell fate decisions in TNF signaling.

3.3.3. Phosphorylation-dependent checkpoints

The phosphorylation of RIPK1 by TAK1, IKKα/β, and TBK1/IKKε exert prosurvival functions by inhibiting the autophosphorylation of RIPK1 (Figure GI-3) [9]. TAK1/TAB2/TAB3 are recruited to K63 chains, which are generated by cIAP1/2. Upon their recruitment, TAK1 phosphorylates itself and downstream targets to activate the MAPK pathway. Moreover, TAK1-mediated phosphorylation of RIPK1 promotes cell survival [86]. NEMO is an adaptor protein that preferentially binds to M1 chains generated by LUBAC. NEMO brings IKKα/β to the complex I. The close proximity between K63 and M1 chains enables the TAK1-mediated activation of IKKα/β. Besides activating the NF-κB pathway, IKKα/β also phosphorylates RIPK1 to prevent its autophosphorylation [87]. NEMO also acts as an adaptor for TBK1/IKKε recruitment. The phosphorylation of RIPK1 by TBK1 is also shown to prevent cell death by inhibiting RIPK1 autophosphorylation [50]. Therefore, the concerted action of kinases within complex I not only enables effective gene activation by NF-κB and MAPK pathway but also inhibits RIPK1-dependent cell death.

The critical nature of this phosphorylation cascade is revealed by the embryonic lethality observed with the loss of key components. The deficiency of TAK1 causes embryonic lethality at day E10 [88]. The deficiency of adaptor protein NEMO causes embryonic lethality at day E12.5 due to massive apoptosis in the liver [89]. Similarly, the deficiencies of kinases that are recruited to NEMO cause embryonic lethality due to liver degeneration. The deficiency of IKKα/β causes embryonic lethality due to aberrant apoptosis in the liver [90,91]. Likewise, TBK1 deficiency also causes embryonic lethality at E14.5 due to uncontrolled liver apoptosis [92].

3.3.4. NF-κB activation-dependent checkpoint

The NF-κB activation is the first identified checkpoint of TNF signaling [93]. It involves the transcriptional and translational upregulation of prosurvival genes such as A20, cIAPs and cFLIP [45]. Indeed, RelA (p65) deficiency causes embryonic lethality due to massive apoptosis in the liver [94]. Importantly, cycloheximide (CHX) which is a widely used apoptotic sensitizer of TNF- or TRAIL-induced cell death, blocks translational upregulation of NF-κB-target genes. Therefore, it depletes short-lived prosurvival proteins such as cFLIP [95]. cFLIP is a critical regulator of Caspase-8 by limiting its activation. Therefore, sustaining the levels of cFLIP and other prosurvival proteins through NF-κB-induced gene activation is an important checkpoint in TNF signaling (Figure GI-3).

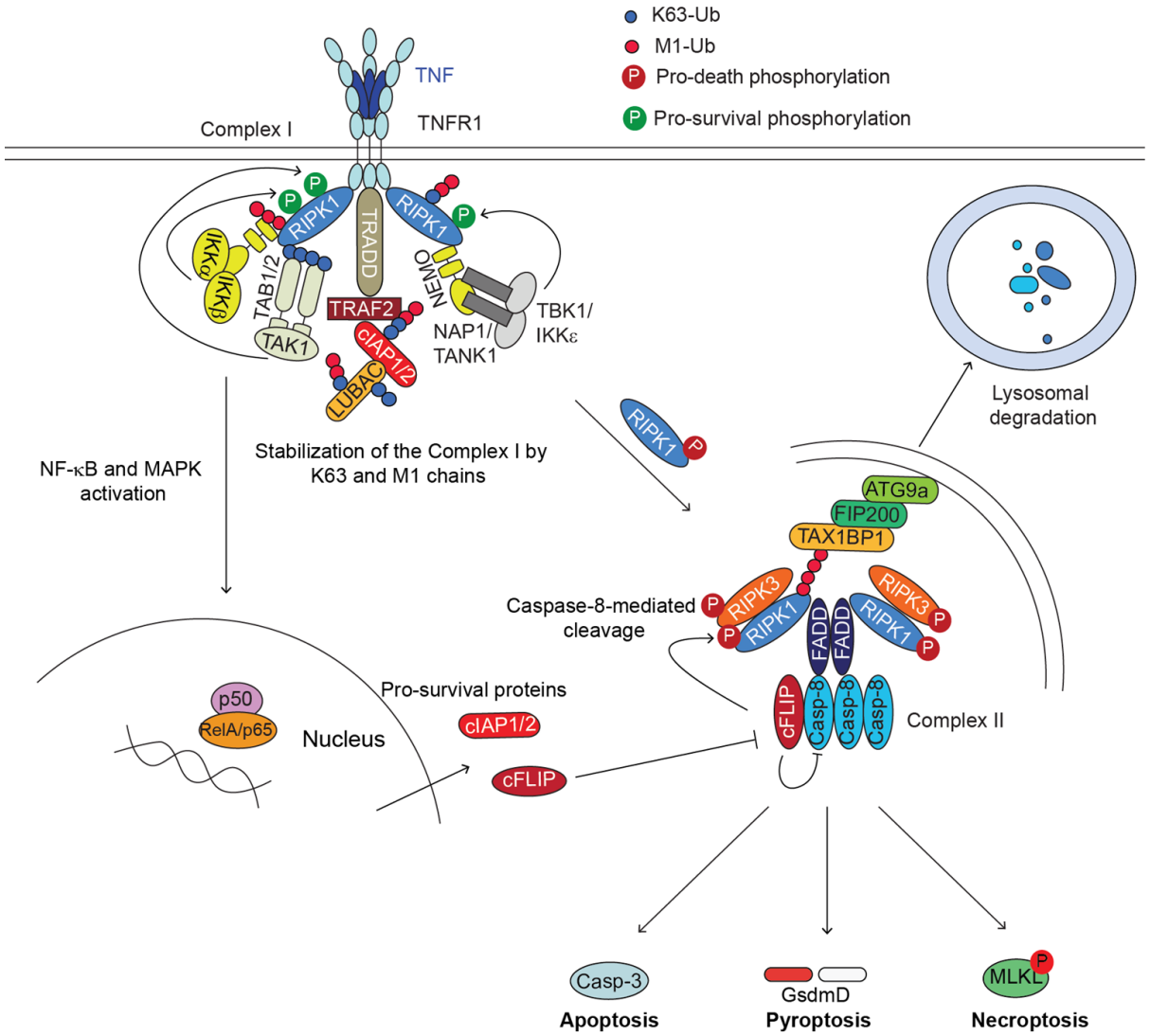

Figure GI-3. The checkpoints regulating life and death in TNF signaling. The binding of TNF to TNFR1 triggers the formation of a membrane-bound complex, known as Complex I of TNFR1. cIAP1/2 conjugates K63 chains on its targets, including RIPK1. This allows the recruitment of LUBAC to the complex which generates M1 chains on the complex components, including RIPK1. Ubiquitination events act as a checkpoint and stabilize the complex. TAK1/TAB2/TAB3 complex is recruited to K63 chains. This causes autophosphorylation of TAK1 which then phosphorylates downstream targets to activate the MAPK pathway. NEMO is an adaptor protein that is recruited to linear chains which brings along IKKα/β. The proximity between K63 and M1 chains enables TAK1 to phosphorylate IKKα/β. IKKα/β then activate the downstream NF-κB pathway. NEMO also acts as an adaptor for TBK1/IKKε and brings them to the complex. TAK1, IKKα/β and TBK1/IKKε phosphorylate RIPK1 to inhibit its autophosphorylation. Importantly, all these phosphorylation events act as checkpoints. In case of an impairment in the ubiquitination or phosphorylation events, RIPK1 autophosphorylates itself and disassociates from complex I to initiate cell death. NF-κB activation upregulates prosurvival proteins such as cFLIP to limit Caspase-8 activation. Once Complex II is formed, Caspase-8 cleaves RIPK1 to terminate the cell death signal, both apoptosis and necroptosis. Finally, via an unconventional autophagy pathway Complex II and active Caspase-8 are targeted for lysosomal degradation to limit

the cytotoxic potential of Complex II. The formation of Complex II can lead to three different cell death modalities. Active Caspase-8 can cleave Caspase-3 to initiate apoptosis or GSDMD to initiate pyroptosis. When Caspase-8 activity is inhibited, activated RIPK3 phosphorylates MLKL to induce necroptosis.

3.3.5. Caspase-8-dependent checkpoint

Caspase-8 belongs to aspartate-specific cysteine protease which is essential for the initiation of extrinsic apoptosis in response to death ligands [96]. Caspase-8 is typically present in cells in its inactive zymogen form (pro-Caspase-8), and its activation requires autoproteolytic cleavage. FADD is the only identified adaptor protein for Caspase-8. The binding of pro-Caspase-8 to FADD triggers its oligomerization and proximity-driven autoproteolytic cleavage. Importantly, the full activation of Caspase-8 requires two-sequential autoproteolytic cleavage. The deficiency of Caspase-8 causes embryonic lethality due to aberrant necroptosis [97–99]. The embryonic lethality caused by Caspase-8 deficiency can be rescued by additional deletion of RIPK3 or MLKL [98,100]. Later on, it was shown that Caspase-8 cleaves and inactivates RIPK1 to terminate cell death signals (Figure GI-3). Indeed, mice bearing an uncleavable form of RIPK1 (*Ripk1*^{D325A}) die embryonically due to aberrant cell death [101]. Therefore, cleavage of RIPK1 by Caspase-8 is an important checkpoint within TNF signaling.

cFLIP is another important checkpoint which regulates the activity of Caspase-8 (Figure GI-3, Box GI-1). cFLIP shares significant homology with Caspase-8 by being its catalytically inactive homolog [96]. Although it has different isoforms that are generated by alternative splicing, the most common isoform is cFLIP$_L$. cFLIP has dual functions in the regulation of Caspase-8. It is reported to both activate and inhibit Caspase-8 function [96,102]. cFLIP is also recruited to the FADD-Caspase-8 complex. Importantly, Caspase-8 has a higher affinity to cFLIP than itself. Heterodimerization of cFLIP and Caspase-8 rearranges the catalytic site of Caspase-8 and facilitates its first autoproteolytic cleavage. Thus, cFLIP-Caspase-8 heterodimers are essential to block necroptosis (Figure GI-3). Whereas Caspase-8 homodimers are required for full activation of Caspase-8 and thereby for apoptosis. Indeed, cFLIP deficiency causes embryonic lethality which is mediated by uncontrolled apoptosis and necroptosis. Therefore, cFLIP deficiency can be rescued by blocking both apoptosis and necroptosis by additional deletion of RIPK3 and FADD [103].

3.3.6. Lysosomal degradation-dependent checkpoints

A recently identified checkpoint is mediated by a selective autophagy pathway which mediates the removal of Complex II from cytoplasm (Figure GI-3) [45,104]. In this pathway, the linear chains on cytosolic RIPK1 act as a recognition signal for the selective autophagy receptor, TAX1BP1. This initiates the autophagosome formation that encapsulates Complex II by bringing

additional proteins such as FIP200 and ATG9A. Once encapsulated, Complex II and active Caspase-8 are targeted for lysosomal degradation to limit TNF-induced apoptosis. Indeed, ATG9A deficiency causes embryonic lethality due to apoptosis of fetal liver hematopoietic cells [104]. Several other degradation-dependent checkpoints were identified as secondary mechanisms to limit TNF-induced cell death (see Box GI-1).

Box GI-1. Secondary mechanism to limit TNF-induced cell death

Several other mechanisms are identified which limit cell death when the cells are already committed to die. MK2 phosphorylates RIPK1 when one of the checkpoints is inhibited to limit the cytotoxic potential of RIPK1. Indeed, it has been shown that MK2 inhibition along with cIAP depletion sensitizes cells to death [105]. Moreover, mice were more sensitive to TNF shock when administered along with an MK2 inhibitor [106]. The K48 ubiquitination of RIPK1 by cIAP1 was shown to limit cell death by targeting RIPK1 to proteasomal degradation. Importantly, when the UBA domain of cIAP1 is mutated, RIPK1 accumulates in the cytoplasm and sensitizes cells to TNF-induced cell death [69]. Recently, PARylation of Complex II was shown as a secondary mechanism to limit TNF-induced cell death [107]. TNKS1 PARylates Complex II, facilitating the recruitment of RNF146, which adds K48-linked ubiquitin chains to target Complex II for proteasomal degradation. The deficiency of tankyrases sensitizes cells to TNF-induced cell death. cFLIP also serves as a Caspase-8 substrate besides being its key regulator. It has been shown that the cleavage of cFLIP at the D377 site is crucial for limiting TNF-induced apoptosis and necroptosis [102]. Cells expressing an uncleavable form of cFLIP (D377A) show increased sensitivity to TNF-induced cell death by favoring the formation of complex II. Furthermore, *Cflip*^{D377A} mice show increased susceptibility to SARS-CoV infection, impaired wound healing, and an exacerbated SHARPIN-deficient phenotype.

Table GI-1. Phenotypes of the patients with mutations in the checkpoints of TNF signaling.

	Gene	Protein	Mutation	Phenotype	Refs
RIPK1 deficiency	*RIPK1*	RIPK1	Homozygous, loss-of-function mutations	Immunodeficiency, recurrent infections, Intestinal inflammation	108,109
Ubiquitination-dependent	*RNF31*	HOIP	Homozygous, loss-of-function mutations	Autoinflammation and immunodeficiency	110,111
	RBCK1	HOIL-1	Various mutations in different domains	Polyglucosan body accumulation in muscle and heart with/out immunodeficiency: PGBM1	112–119
	SHARPIN	SHARPIN	Homozygous, loss-of-function mutations	Autoinflammation and immunodeficiency	120
	OTULIN	OTULIN	Homozygous, loss of function	Recurrent fever, neutrophilic panniculitis, systemic inflammation: ORAS	121–124
	OTULIN	OTULIN	Heterozygous variants	Late-onset ORAS	125
Kinase-dependent	*IKBKG*	NEMO	Loss of function	Incontinentia pigmenti and immunodeficiency	126
	IKBKG	NEMO	C-terminal deletion	Skin and intestine inflammation, ectodermal dysplasia, immunodeficiency	127
	IKBKG	NEMO	Exon 5 deletion	Severe autoinflammatory syndrome: NDAS	128,129
	TBK1	TBK1	Homozygous, loss of function	Chronic and systemic inflammation	130
NF-κB activation	*RELA*	RELA (p65)	Haploinsufficiency	Chronic mucocutaneous ulceration	131
Caspase-8 dependent	*CASP8*	Caspase-8	Homozygous, loss of function	Very early onset inflammatory bowel disease	132
	CASP8	Caspase-8	Homozygous, loss of function	Autoimmune lymphoproliferative syndrome	133
	RIPK1	RIPK1	Heterozygous mutations at the cleavage site by Caspase-8	Early-onset periodic fever Lymphadenopathy	134

Adapted from [58].

Table GI-2. Phenotypes of mice with constitutive deficiencies in the checkpoints of TNF signaling.

	Gene	Phenotype	Phenotype	Rescue	Refs
RIPK1 deficiency	*Ripk1*$^{-/-}$	Perinatal lethality	Multiorgan cell death and inflammation	*Casp8*$^{-/-}$*Ripk3*$^{-/-}$ *Tradd*$^{-/-}$*Ripk3*$^{-/-}$ *Tnfr1*$^{-/-}$*-Ripk3*$^{-/-}$ *Casp8*$^{-/-}$*Zbp1*$^{-/-}$*Trif*$^{-/-}$	60,61,26,27
Ubiquitination-dependent	*Ciap1/2*$^{-/-}$	Embryonic lethality (E10.5)	Cardiovascular defects	*Casp8*$^{-/-}$*Mlkl*$^{-/-}$	73
	Hoip$^{-/-}$	Embryonic lethality (E10.5)	Endothelial cell death	*Casp8*$^{-/-}$*Mlkl*$^{-/-}$	75,77
	Hoil1$^{-/-}$	Embryonic lethality (E10.5)	Endothelial cell death	*Casp8*$^{-/-}$*Mlkl*$^{-/-}$	75,77
	Otulin^{C129A}	Embryonic lethality (E10.5)	Endothelial cell death	*Casp8*$^{-/-}$*Ripk3*$^{-/-}$*Ripk1*$^{+/-}$	85
Kinase-dependent	*Tak1*$^{-/-}$	Embryonic lethality (E10)	Abnormal neural tube	-	88
	Nemo$^{-/-}$	Embryonic lethality (E12.5)	Liver degeneration	-	89
	Ikk1/2$^{-/-}$	Embryonic lethality (E12)	Liver degeneration	-	90,91
	Tbk1$^{-/-}$	Embryonic lethality (E14.5)	Liver degeneration	*Ripk1*^{D138N} *Tnf*$^{-/-}$ *Tnfr1*$^{-/-}$	92,135
NF-κB activation	*Rela*$^{-/-}$	Embryonic lethality (E15-16)	Liver degeneration	*Tnf*$^{-/-}$	94
Caspase-8 dependent	*Casp8*$^{-/-}$	Embryonic lethality (E10.5)	Vascular, cardiac and hematopoietic defects	*Ripk3*$^{-/-}$ *Mlkl*$^{-/-}$	97–99
	Ripk1^{D325A}	Embryonic lethality (E10.5)	Abnormal yolk sac vascularization	*Fadd*$^{-/-}$*Mlkl*$^{-/-}$	101
	Cflip$^{-/-}$	Embryonic lethality (E10.5)	Vascular and cardiac defects	*Fadd*$^{-/-}$*Ripk3*$^{-/-}$	103,136
Unconventional autophagy	*Atg9a*$^{-/-}$	Embryonic lethality (E14.5)	Liver hematopoietic cell death	-	104

Outstanding questions

Are TNF signaling checkpoints universally active in all cell types, or can cells selectively deactivate some to prevent cell death?

Why some cell types are sensitive to TNF-induced cell death while others are not? Which mechanisms make a cell type resistant to TNF-induced cell death?

Can cells compensate for the loss of specific checkpoints by overactivating others? For instance, could high cFLIP expression counteract the inhibition of ubiquitin- or kinase-dependent checkpoints?

Most cell death studies have been conducted in highly proliferative cell types, such as intestinal epithelial cells. Could it be that TNF or death receptor signaling is regulated differently in cell types with low proliferative activity, such as pancreatic β-cells?

4. References

1. Newton, K., Strasser, A., Kayagaki, N. & Dixit, V. M. Cell death. *Cell* **187**, 235–256 (2024).
2. Kerr, J. F. A histochemical study of hypertrophy and ischaemic injury of rat liver with special reference to changes in lysosomes. *J. Pathol. Bacteriol.* **90**, 419–435 (1965).
3. Kerr, J. F., Wyllie, A. H. & Currie, A. R. Apoptosis: a basic biological phenomenon with wide-ranging implications in tissue kinetics. *Br. J. Cancer* **26**, 239–257 (1972).
4. Park, W. *et al.* Diversity and complexity of cell death: a historical review. *Exp. Mol. Med.* **55**, 1573–1594 (2023).
5. Van Opdenbosch, N. & Lamkanfi, M. Caspases in cell death, inflammation, and disease. *Immunity* **50**, 1352–1364 (2019).
6. Czabotar, P. E. & Garcia-Saez, A. J. Mechanisms of BCL-2 family proteins in mitochondrial apoptosis. *Nat. Rev. Mol. Cell Biol.* **24**, 732–748 (2023).
7. Kaloni, D., Diepstraten, S. T., Strasser, A. & Kelly, G. L. BCL-2 protein family: attractive targets for cancer therapy. *Apoptosis* **28**, 20–38 (2023).
8. Dadsena, S., King, L. E. & García-Sáez, A. J. Apoptosis regulation at the mitochondria membrane level. *Biochim. Biophys. Acta Biomembr.* **1863**, 183716 (2021).
9. Peltzer, N. & Walczak, H. Cell death and inflammation--a vital but dangerous liaison. *Trends Immunol.* **40**, 387–402 (2019).
10. Kantari, C. & Walczak, H. Caspase-8 and bid: caught in the act between death receptors and mitochondria. *Biochim. Biophys. Acta* **1813**, 558–563 (2011).
11. Elmore, S. Apoptosis: a review of programmed cell death. *Toxicol. Pathol.* **35**, 495–516 (2007).
12. Ge, Y., Huang, M. & Yao, Y.-M. Efferocytosis and Its Role in Inflammatory Disorders. *Front Cell Dev Biol* **10**, 839248 (2022).
13. Bock, F. J. & Riley, J. S. When cell death goes wrong: inflammatory outcomes of failed apoptosis and mitotic cell death. *Cell Death Differ.* **30**, 293–303 (2023).
14. Rogers, C. *et al.* Cleavage of DFNA5 by caspase-3 during apoptosis mediates progression to secondary necrotic/pyroptotic cell death. *Nat. Commun.* **8**, 14128 (2017).
15. Wang, Y. *et al.* Chemotherapy drugs induce pyroptosis through caspase-3 cleavage of a gasdermin. *Nature* **547**, 99–103 (2017).
16. Degterev, A. *et al.* Chemical inhibitor of nonapoptotic cell death with therapeutic potential for ischemic brain injury. *Nat. Chem. Biol.* **1**, 112–119 (2005).
17. Vercammen, D. *et al.* Dual signaling of the Fas receptor: initiation of both apoptotic and necrotic cell death pathways. *J. Exp. Med.* **188**, 919–930 (1998).
18. Matsumura, H. *et al.* Necrotic death pathway in Fas receptor signaling. *J. Cell Biol.* **151**, 1247–1256 (2000).
19. Degterev, A. *et al.* Identification of RIP1 kinase as a specific cellular target of necrostatins. *Nat. Chem. Biol.* **4**, 313–321 (2008).
20. Cho, Y. S. *et al.* Phosphorylation-driven assembly of the RIP1-RIP3 complex regulates programmed necrosis and virus-induced inflammation. *Cell* **137**, 1112–1123 (2009).
21. He, S. *et al.* Receptor interacting protein kinase-3 determines cellular necrotic response to TNF-alpha. *Cell* **137**, 1100–1111 (2009).
22. Zhang, D.-W. *et al.* RIP3, an energy metabolism regulator that switches TNF-induced cell death from apoptosis to necrosis. *Science* **325**, 332–336 (2009).
23. Zhao, J. *et al.* Mixed lineage kinase domain-like is a key receptor interacting protein 3 downstream component of TNF-induced necrosis. *Proc. Natl. Acad. Sci. U. S. A.* **109**, 5322–5327 (2012).
24. Sun, L. *et al.* Mixed lineage kinase domain-like protein mediates necrosis signaling downstream of RIP3 kinase. *Cell* **148**, 213–227 (2012).
25. Kaiser, W. J. *et al.* Toll-like receptor 3-mediated necrosis via TRIF, RIP3, and MLKL. *J. Biol. Chem.* **288**, 31268–31279 (2013).
26. Lin, J. *et al.* RIPK1 counteracts ZBP1-mediated necroptosis to inhibit inflammation. *Nature* **540**, 124–128 (2016).

27. Newton, K. *et al.* RIPK1 inhibits ZBP1-driven necroptosis during development. *Nature* **540**, 129–133 (2016).
28. Friedlander, A. M. Macrophages are sensitive to anthrax lethal toxin through an acid-dependent process. *J. Biol. Chem.* **261**, 7123–7126 (1986).
29. D'Souza, C. A. & Heitman, J. Dismantling the Cryptococcus coat. *Trends Microbiol.* **9**, 112–113 (2001).
30. Zychlinsky, A., Prevost, M. C. & Sansonetti, P. J. Shigella flexneri induces apoptosis in infected macrophages. *Nature* **358**, 167–169 (1992).
31. Martinon, F., Burns, K. & Tschopp, J. The inflammasome: a molecular platform triggering activation of inflammatory caspases and processing of proIL-beta. *Mol. Cell* **10**, 417–426 (2002).
32. Agostini, L. *et al.* NALP3 forms an IL-1beta-processing inflammasome with increased activity in Muckle-Wells autoinflammatory disorder. *Immunity* **20**, 319–325 (2004).
33. Swanson, K. V., Deng, M. & Ting, J. P.-Y. The NLRP3 inflammasome: molecular activation and regulation to therapeutics. *Nat. Rev. Immunol.* **19**, 477–489 (2019).
34. Kayagaki, N. *et al.* Non-canonical inflammasome activation targets caspase-11. *Nature* **479**, 117–121 (2011).
35. Veli, Ö. & Peltzer, N. Life and Death of Pancreatic β-cells. in *Encyclopedia of Cell Biology (Second Edition)* (eds. Bradshaw, R. A., Hart, G. W. & Stahl, P. D.) 19–29 (Academic Press, Oxford, 2023).
36. Broz, P. & Dixit, V. M. Inflammasomes: mechanism of assembly, regulation and signalling. *Nat. Rev. Immunol.* **16**, 407–420 (2016).
37. Chen, K. W. *et al.* Extrinsic and intrinsic apoptosis activate pannexin-1 to drive NLRP3 inflammasome assembly. *EMBO J.* **38**, e101638 (2019).
38. Orning, P. *et al.* Pathogen blockade of TAK1 triggers caspase-8-dependent cleavage of gasdermin D and cell death. *Science* **362**, 1064–1069 (2018).
39. Sarhan, J. *et al.* Caspase-8 induces cleavage of gasdermin D to elicit pyroptosis during Yersinia infection. *Proc. Natl. Acad. Sci. U. S. A.* **115**, E10888–E10897 (2018).
40. Miao, R. *et al.* Gasdermin D permeabilization of mitochondrial inner and outer membranes accelerates and enhances pyroptosis. *Immunity* **56**, 2523–2541.e8 (2023).
41. Kayagaki, N. *et al.* NINJ1 mediates plasma membrane rupture during lytic cell death. *Nature* **591**, 131–136 (2021).
42. Rogers, C. *et al.* Gasdermin pores permeabilize mitochondria to augment caspase-3 activation during apoptosis and inflammasome activation. *Nat. Commun.* **10**, 1689 (2019).
43. Walczak, H. Death receptor-ligand systems in cancer, cell death, and inflammation. *Cold Spring Harb. Perspect. Biol.* **5**, a008698 (2013).
44. Arias, A. A. *et al.* Tuberculosis in otherwise healthy adults with inherited TNF deficiency. *Nature* (2024) doi:10.1038/s41586-024-07866-3.
45. Huyghe, J., Priem, D. & Bertrand, M. J. M. Cell death checkpoints in the TNF pathway. *Trends Immunol.* **44**, 628–643 (2023).
46. Hsu, H., Huang, J., Shu, H. B., Baichwal, V. & Goeddel, D. V. TNF-dependent recruitment of the protein kinase RIP to the TNF receptor-1 signaling complex. *Immunity* **4**, 387–396 (1996).
47. Mahoney, D. J. *et al.* Both cIAP1 and cIAP2 regulate TNFalpha-mediated NF-kappaB activation. *Proc. Natl. Acad. Sci. U. S. A.* **105**, 11778–11783 (2008).
48. Haas, T. L. *et al.* Recruitment of the linear ubiquitin chain assembly complex stabilizes the TNF-R1 signaling complex and is required for TNF-mediated gene induction. *Mol. Cell* **36**, 831–844 (2009).
49. Emmerich, C. H. *et al.* Activation of the canonical IKK complex by K63/M1-linked hybrid ubiquitin chains. *Proc. Natl. Acad. Sci. U. S. A.* **110**, 15247–15252 (2013).
50. Lafont, E. *et al.* TBK1 and IKKε prevent TNF-induced cell death by RIPK1 phosphorylation. *Nat. Cell Biol.* **20**, 1389–1399 (2018).
51. Annibaldi, A. & Meier, P. Checkpoints in TNF-Induced Cell Death: Implications in Inflammation and Cancer. *Trends Mol. Med.* **24**, 49–65 (2018).
52. Feoktistova, M., Geserick, P. & Leverkus, M. Ripoptosome Analysis by Caspase-8

Coimmunoprecipitation. *Cold Spring Harb. Protoc.* **2016**, db.prot087403 (2016).
53. Micheau, O. & Tschopp, J. Induction of TNF receptor I-mediated apoptosis via two sequential signaling complexes. *Cell* **114**, 181–190 (2003).
54. Mukherjee, S. *et al.* Yersinia YopJ acetylates and inhibits kinase activation by blocking phosphorylation. *Science* **312**, 1211–1214 (2006).
55. Mittal, R., Peak-Chew, S.-Y. & McMahon, H. T. Acetylation of MEK2 and I kappa B kinase (IKK) activation loop residues by YopJ inhibits signaling. *Proc. Natl. Acad. Sci. U. S. A.* **103**, 18574–18579 (2006).
56. Haase, R., Richter, K., Pfaffinger, G., Courtois, G. & Ruckdeschel, K. Yersinia outer protein P suppresses TGF-beta-activated kinase-1 activity to impair innate immune signaling in Yersinia enterocolitica-infected cells. *J. Immunol.* **175**, 8209–8217 (2005).
57. Paquette, N. *Serine/threonine Acetylation of TGFbeta-Activated Kinase (TAK1) by Yersinia Pestis YopJ Inhibits Innate Immune Signaling*.
58. van Loo, G. & Bertrand, M. J. M. Death by TNF: a road to inflammation. *Nat. Rev. Immunol.* **23**, 289–303 (2023).
59. Kelliher, M. A. *et al.* The death domain kinase RIP mediates the TNF-induced NF-kappaB signal. *Immunity* **8**, 297–303 (1998).
60. Rickard, J. A. *et al.* RIPK1 regulates RIPK3-MLKL-driven systemic inflammation and emergency hematopoiesis. *Cell* **157**, 1175–1188 (2014).
61. Dillon, C. P. *et al.* RIPK1 blocks early postnatal lethality mediated by caspase-8 and RIPK3. *Cell* **157**, 1189–1202 (2014).
62. Polykratis, A. *et al.* Cutting edge: RIPK1 Kinase inactive mice are viable and protected from TNF-induced necroptosis in vivo. *J. Immunol.* **193**, 1539–1543 (2014).
63. Berger, S. B. *et al.* Cutting Edge: RIP1 kinase activity is dispensable for normal development but is a key regulator of inflammation in SHARPIN-deficient mice. *J. Immunol.* **192**, 5476–5480 (2014).
64. Peltzer, N., Darding, M. & Walczak, H. Holding RIPK1 on the ubiquitin leash in TNFR1 signaling. *Trends Cell Biol.* **26**, 445–461 (2016).
65. Damgaard, R. B. The ubiquitin system: from cell signalling to disease biology and new therapeutic opportunities. *Cell Death Differ.* **28**, 423–426 (2021).
66. Guo, H. J., Rahimi, N. & Tadi, P. *Biochemistry, Ubiquitination*. (StatPearls Publishing, 2023).
67. Dikic, I. & Schulman, B. A. An expanded lexicon for the ubiquitin code. *Nat. Rev. Mol. Cell Biol.* **24**, 273–287 (2023).
68. Bertrand, M. J. M. *et al.* cIAP1 and cIAP2 facilitate cancer cell survival by functioning as E3 ligases that promote RIP1 ubiquitination. *Mol. Cell* **30**, 689–700 (2008).
69. Annibaldi, A. *et al.* Ubiquitin-Mediated Regulation of RIPK1 Kinase Activity Independent of IKK and MK2. *Mol. Cell* **69**, 566–580.e5 (2018).
70. Conze, D. B. *et al.* Posttranscriptional downregulation of c-IAP2 by the ubiquitin protein ligase c-IAP1 in vivo. *Mol. Cell. Biol.* **25**, 3348–3356 (2005).
71. Conte, D. *et al.* Inhibitor of apoptosis protein cIAP2 is essential for lipopolysaccharide-induced macrophage survival. *Mol. Cell. Biol.* **26**, 699–708 (2006).
72. Moulin, M. *et al.* IAPs limit activation of RIP kinases by TNF receptor 1 during development. *EMBO J.* **31**, 1679–1691 (2012).
73. Zhang, J. *et al.* Ubiquitin Ligases cIAP1 and cIAP2 Limit Cell Death to Prevent Inflammation. *Cell Rep.* **27**, 2679–2689.e3 (2019).
74. Kirisako, T. *et al.* A ubiquitin ligase complex assembles linear polyubiquitin chains. *EMBO J.* **25**, 4877–4887 (2006).
75. Peltzer, N. *et al.* HOIP deficiency causes embryonic lethality by aberrant TNFR1-mediated endothelial cell death. *Cell Rep.* **9**, 153–165 (2014).
76. Draber, P. *et al.* LUBAC-Recruited CYLD and A20 Regulate Gene Activation and Cell Death by Exerting Opposing Effects on Linear Ubiquitin in Signaling Complexes. *Cell Rep.* **13**, 2258–2272 (2015).
77. Peltzer, N. *et al.* LUBAC is essential for embryogenesis by preventing cell death and enabling

haematopoiesis. *Nature* **557**, 112–117 (2018).
78. HogenEsch, H. *et al.* A spontaneous mutation characterized by chronic proliferative dermatitis in C57BL mice. *Am. J. Pathol.* **143**, 972–982 (1993).
79. Rickard, J. A. *et al.* TNFR1-dependent cell death drives inflammation in Sharpin-deficient mice. *Elife* **3**, (2014).
80. Gerlach, B. *et al.* Linear ubiquitination prevents inflammation and regulates immune signalling. *Nature* **471**, 591–596 (2011).
81. Ikeda, F. *et al.* SHARPIN forms a linear ubiquitin ligase complex regulating NF-κB activity and apoptosis. *Nature* **471**, 637–641 (2011).
82. Tokunaga, F. *et al.* SHARPIN is a component of the NF-κB-activating linear ubiquitin chain assembly complex. *Nature* **471**, 633–636 (2011).
83. Takiuchi, T. *et al.* Suppression of LUBAC-mediated linear ubiquitination by a specific interaction between LUBAC and the deubiquitinases CYLD and OTULIN. *Genes Cells* **19**, 254–272 (2014).
84. Rivkin, E. *et al.* The linear ubiquitin-specific deubiquitinase gumby regulates angiogenesis. *Nature* **498**, 318–324 (2013).
85. Heger, K. *et al.* OTULIN limits cell death and inflammation by deubiquitinating LUBAC. *Nature* **559**, 120–124 (2018).
86. Geng, J. *et al.* Regulation of RIPK1 activation by TAK1-mediated phosphorylation dictates apoptosis and necroptosis. *Nat. Commun.* **8**, 359 (2017).
87. Dondelinger, Y. *et al.* NF-κB-Independent Role of IKKα/IKKβ in Preventing RIPK1 Kinase-Dependent Apoptotic and Necroptotic Cell Death during TNF Signaling. *Mol. Cell* **60**, 63–76 (2015).
88. Shim, J.-H. *et al.* TAK1, but not TAB1 or TAB2, plays an essential role in multiple signaling pathways in vivo. *Genes Dev.* **19**, 2668–2681 (2005).
89. Schmidt-Supprian, M. *et al.* NEMO/IKK gamma-deficient mice model incontinentia pigmenti. *Mol. Cell* **5**, 981–992 (2000).
90. Tanaka, M. *et al.* Embryonic lethality, liver degeneration, and impaired NF-kappa B activation in IKK-beta-deficient mice. *Immunity* **10**, 421–429 (1999).
91. Li, Z. W. *et al.* The IKKbeta subunit of IkappaB kinase (IKK) is essential for nuclear factor kappaB activation and prevention of apoptosis. *J. Exp. Med.* **189**, 1839–1845 (1999).
92. Bonnard, M. *et al.* Deficiency of T2K leads to apoptotic liver degeneration and impaired NF-kappaB-dependent gene transcription. *EMBO J.* **19**, 4976–4985 (2000).
93. Van Antwerp, D. J., Martin, S. J., Kafri, T., Green, D. R. & Verma, I. M. Suppression of TNF-alpha-induced apoptosis by NF-kappaB. *Science* **274**, 787–789 (1996).
94. Beg, A. A., Sha, W. C., Bronson, R. T., Ghosh, S. & Baltimore, D. Embryonic lethality and liver degeneration in mice lacking the RelA component of NF-kappa B. *Nature* **376**, 167–170 (1995).
95. Kreuz, S., Siegmund, D., Scheurich, P. & Wajant, H. NF-kappaB inducers upregulate cFLIP, a cycloheximide-sensitive inhibitor of death receptor signaling. *Mol. Cell. Biol.* **21**, 3964–3973 (2001).
96. Tummers, B. & Green, D. R. Caspase-8: regulating life and death. *Immunol. Rev.* **277**, 76–89 (2017).
97. Oberst, A. *et al.* Catalytic activity of the caspase-8–FLIPL complex inhibits RIPK3-dependent necrosis. *Nature* **471**, 363–367 (2011).
98. Kaiser, W. J. *et al.* RIP3 mediates the embryonic lethality of caspase-8-deficient mice. *Nature* **471**, 368–372 (2011).
99. Varfolomeev, E. E. *et al.* Targeted disruption of the mouse Caspase 8 gene ablates cell death induction by the TNF receptors, Fas/Apo1, and DR3 and is lethal prenatally. *Immunity* **9**, 267–276 (1998).
100. Alvarez-Diaz, S. *et al.* The Pseudokinase MLKL and the Kinase RIPK3 Have Distinct Roles in Autoimmune Disease Caused by Loss of Death-Receptor-Induced Apoptosis. *Immunity* **45**, 513–526 (2016).
101. Newton, K. *et al.* Cleavage of RIPK1 by caspase-8 is crucial for limiting apoptosis and necroptosis. *Nature* **574**, 428–431 (2019).
102. Martinez Lagunas, K. *et al.* Cleavage of cFLIP restrains cell death during viral infection and tissue

injury and favors tissue repair. *Sci Adv* **9**, eadg2829 (2023).
103. Dillon, C. P. *et al.* Survival function of the FADD-CASPASE-8-cFLIP(L) complex. *Cell Rep.* **1**, 401–407 (2012).
104. Huyghe, J. *et al.* ATG9A prevents TNF cytotoxicity by an unconventional lysosomal targeting pathway. *Science* **378**, 1201–1207 (2022).
105. Jaco, I. *et al.* MK2 Phosphorylates RIPK1 to Prevent TNF-Induced Cell Death. *Mol. Cell* **66**, 698–710.e5 (2017).
106. Dondelinger, Y. *et al.* MK2 phosphorylation of RIPK1 regulates TNF-mediated cell death. *Nat. Cell Biol.* **19**, 1237–1247 (2017).
107. Liu, L. *et al.* Tankyrase-mediated ADP-ribosylation is a regulator of TNF-induced death. *Sci Adv* **8**, eabh2332 (2022).
108. Li, Y. *et al.* Human RIPK1 deficiency causes combined immunodeficiency and inflammatory bowel diseases. *Proc. Natl. Acad. Sci. U. S. A.* **116**, 970–975 (2019).
109. Cuchet-Lourenço, D. *et al.* Biallelic RIPK1 mutations in humans cause severe immunodeficiency, arthritis, and intestinal inflammation. *Science* **361**, 810–813 (2018).
110. Oda, H. *et al.* Second Case of HOIP Deficiency Expands Clinical Features and Defines Inflammatory Transcriptome Regulated by LUBAC. *Front. Immunol.* **10**, 479 (2019).
111. Boisson, B. *et al.* Human HOIP and LUBAC deficiency underlies autoinflammation, immunodeficiency, amylopectinosis, and lymphangiectasia. *J. Exp. Med.* **212**, 939–951 (2015).
112. Boisson, B. *et al.* Immunodeficiency, autoinflammation and amylopectinosis in humans with inherited HOIL-1 and LUBAC deficiency. *Nat. Immunol.* **13**, 1178–1186 (2012).
113. Krenn, M. *et al.* Mutations outside the N-terminal part of RBCK1 may cause polyglucosan body myopathy with immunological dysfunction: expanding the genotype–phenotype spectrum. *J. Neurol.* **265**, 394–401 (2018).
114. Chen, L. *et al.* Polyglucosan body myopathy 1 may cause cognitive impairment: a case report from China. *BMC Musculoskelet. Disord.* **22**, 35 (2021).
115. Nilsson, J. *et al.* Polyglucosan body myopathy caused by defective ubiquitin ligase RBCK1. *Ann. Neurol.* **74**, 914–919 (2013).
116. Nitschke, S. *et al.* Glycogen synthase downregulation rescues the amylopectinosis of murine RBCK1 deficiency. *Brain* **145**, 2361–2377 (2022).
117. AlAnzi, T., Al Harbi, F., AlGhamdi, A. & Mohamed, S. A novel variant of RBCK1 gene causes mild polyglucosan myopathy. *Neurosciences* **27**, 45–49 (2022).
118. Wang, K. *et al.* Whole-genome DNA/RNA sequencing identifies truncating mutations in RBCK1 in a novel Mendelian disease with neuromuscular and cardiac involvement. *Genome Med.* **5**, 67 (2013).
119. RBCK1-related disease: a rare multisystem disorder with polyglucosan storage, autoinflammation, recurrent infections, skeletal and cardiac myopathy - four additional patients and a review of the current literature. *J. Inherit. Metab. Dis.* **43**, 1002–1013.
120. Oda, H. *et al.* Biallelic human SHARPIN loss of function induces autoinflammation and immunodeficiency. *Nat. Immunol.* **25**, 764–777 (2024).
121. Damgaard, R. B. *et al.* The deubiquitinase OTULIN is an essential negative regulator of inflammation and autoimmunity. *Cell* **166**, 1215–1230.e20 (2016).
122. Zhou, Q. *et al.* Biallelic hypomorphic mutations in a linear deubiquitinase define otulipenia, an early-onset autoinflammatory disease. *Proc. Natl. Acad. Sci. U. S. A.* **113**, 10127–10132 (2016).
123. Damgaard, R. B. *et al.* OTULIN deficiency in ORAS causes cell type-specific LUBAC degradation, dysregulated TNF signalling and cell death. *EMBO Mol. Med.* **11**, e9324 (2019).
124. Nabavi, M. *et al.* Auto-inflammation in a patient with a novel homozygous OTULIN mutation. *J. Clin. Immunol.* **39**, 138–141 (2019).
125. Zinngrebe, J. *et al.* Compound heterozygous variants in OTULIN are associated with fulminant atypical late-onset ORAS. *EMBO Mol. Med.* **14**, e14901 (2022).
126. Smahi, A. *et al.* Genomic rearrangement in NEMO impairs NF-kappaB activation and is a cause of incontinentia pigmenti. The International Incontinentia Pigmenti (IP) Consortium. *Nature* **405**, 466–

472 (2000).
127. Zilberman-Rudenko, J. *et al.* Recruitment of A20 by the C-terminal domain of NEMO suppresses NF-κB activation and autoinflammatory disease. *Proc. Natl. Acad. Sci. U. S. A.* **113**, 1612–1617 (2016).
128. Lee, Y. *et al.* Genetically programmed alternative splicing of NEMO mediates an autoinflammatory disease phenotype. *J. Clin. Invest.* **132**, (2022).
129. de Jesus, A. A. *et al.* Distinct interferon signatures and cytokine patterns define additional systemic autoinflammatory diseases. *J. Clin. Invest.* **130**, 1669–1682 (2020).
130. Taft, J. *et al.* Human TBK1 deficiency leads to autoinflammation driven by TNF-induced cell death. *Cell* **184**, 4447–4463.e20 (2021).
131. Badran, Y. R. *et al.* Human RELA haploinsufficiency results in autosomal-dominant chronic mucocutaneous ulceration. *J. Exp. Med.* **214**, 1937–1947 (2017).
132. Lehle, A. S. *et al.* Intestinal inflammation and dysregulated immunity in patients with inherited caspase-8 deficiency. *Gastroenterology* **156**, 275–278 (2019).
133. Chun, H. J. *et al.* Pleiotropic defects in lymphocyte activation caused by caspase-8 mutations lead to human immunodeficiency. *Nature* **419**, 395–399 (2002).
134. Lalaoui, N. *et al.* Mutations that prevent caspase cleavage of RIPK1 cause autoinflammatory disease. *Nature* **577**, 103–108 (2020).
135. Xu, D. *et al.* TBK1 Suppresses RIPK1-Driven Apoptosis and Inflammation during Development and in Aging. *Cell* **174**, 1477–1491.e19 (2018).
136. Yeh, W. C. *et al.* Requirement for Casper (c-FLIP) in regulation of death receptor-induced apoptosis and embryonic development. *Immunity* **12**, 633–642 (2000).

CHAPTER I

Understanding the Role of RIPK1 in β-cell Homeostasis and during Diabetes

In this chapter of my thesis, I begin with an introduction to diabetes and the molecular mechanisms that lead to β-cell loss. The results are presented as a published article (Veli et al., 2024, Mol. Met.), where we demonstrate that β-cells regulate TNF-induced cell death signaling in a distinct manner, independent of RIPK1 and other major checkpoints. At the end of the chapter, I will discuss perspectives and raise key questions that emerged from this project.

1. Introduction

1.1. Overview of Pancreatic Functions and Hormonal Regulation

The pancreas is an abdominal glandular organ with dual functions. The exocrine pancreas comprises acinar and ductal cells which produce digestive enzymes. The endocrine pancreas is composed of the Islets of Langerhans, which are crucial for regulating blood glucose levels (Figure CI-1) [1]. Pancreatic islets consist of four cell types, β-cells (75-80 %), α-cells (10-15 %), δ-cells (5 %), and ε-cells (1 %) [2,3]. β-cells secrete insulin which stimulates glucose uptake by other organs such as the liver and adipose tissue, thereby lowering the blood glucose back to normal range. α-cells secrete glucagon when blood glucose is below normal range. Glucagon stimulates the release of glucose from the liver into the bloodstream through a process known as glycogenolysis in response to low blood glucose levels. Hence, insulin and glucagon have counteracting effects on blood glucose levels and function synergistically to maintain normoglycemia. δ-cells secrete somatostatin in response to high blood glucose that provides a local inhibitory effect on insulin and glucagon secretion. ε-cells secrete two antagonistic hormones, ghrelin and obestatin to control appetite. While ghrelin, known as the hunger hormone, inhibits insulin secretion, obestatin reduces appetite and enhances glucose-stimulated insulin secretion (Figure CI-1) [2,3]. In summary, the cells within the pancreatic islets work in concert to regulate glucose metabolism and maintain blood glucose homeostasis.

1.2. Diabetes Mellitus

Diabetes Mellitus originates from the Greek word diabetes, meaning "to pass through," and the Latin word mellitus, meaning "honey" [4]**.** According to the World Health Organization (WHO), “Diabetes mellitus is a chronic disease that occurs either when the pancreas does not produce enough insulin or when the body cannot effectively use the insulin it produces. This leads to elevated levels of blood glucose (hyperglycemia), which over time can cause serious damage to many of the body's systems, especially the nerves and blood vessels” [5]. Diabetes can be grossly divided into Type 1 Diabetes (T1D) and Type 2 Diabetes (T2D) which are explained in detail below.

1.2.1. Type 1 Diabetes (T1D)

1.2.1.1. Etiology of T1D

Type 1 diabetes (T1D) is a chronic autoimmune disease which is caused by the immune destruction of pancreatic β-cells [6]. Therefore, T1D is characterized by elevated blood glucose levels (hyperglycemia) due to the loss of insulin secreting β-cells. There is currently no available cure for T1D, and the patients need life-long insulin injections. Therefore,

understanding the exact mechanisms dictating β-cell demise responsible for eliciting or propagating immune responses during T1D represents an urgent medical need.

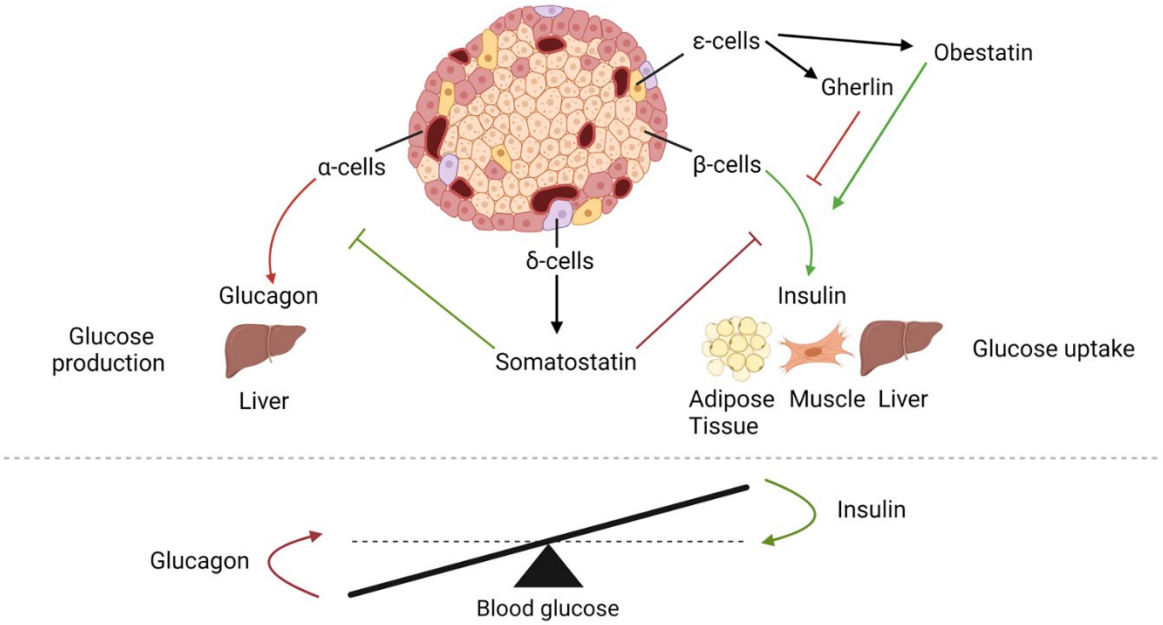

Figure CI-1. Different cell types in pancreatic islets and hormonal release. Pancreatic islets are composed of four different cell types. β-cells secrete insulin which stimulates glucose uptake by the other organs to lower the blood glucose. α-cells secrete glucagon which promotes glucose secretion by the liver to increase the blood glucose levels. Somatostatin is secreted by δ-cells to inhibit insulin and glucagon secretion. ε-cells secrete ghrelin and obestatin which have antagonistic functions on insulin secretion and appetite control. Green and red arrows indicate the means to lower or increase blood glucose. Adapted from [2].

The progression of T1D can be divided into three stages [6,7]. At the first stage, autoantibodies can be found in the patients´ blood indicating that immune tolerance to β-cells is broken. Therefore, the β-cell mass starts to decline due to autoimmunity despite the patients still maintaining normoglycemia. At the second stage, although the patients have hyperglycemia, they do not show any symptoms. The symptoms, like thirst and frequent urination, weight loss, start to appear only at the third stage when the patients lose 80 % of their functional β-cells mass. Therefore, the patients are generally diagnosed with T1D at this stage. It is a significant medical need to understand disease etiology in order to develop effective early-stage diagnostic tools.

Genome-wide association studies (GWAS) and single nucleotide polymorphisms (SNP) profiling have been powerful tools to identify causal variants and genes for T1D [7]. The HLA region on chromosome 6 shows the strongest association with the genetic risk of T1D,

accounting for 30-50% of the risk. In particular, individuals heterozygous for DR3-DQ2 and DR4-DQ8 haplotypes are at the highest risk for developing T1D [8]. In addition to the HLA region, more than 50 non-HLA loci or genes were identified as candidate genes. Among those genes, INS, PTPN22, CTLA-4 show the strongest association. It is important to note that predominance of identified non-HLA genes are related to immune or cytokine signaling. Although it is widely accepted that genetic predisposition plays a role in the development of T1D, studies have shown that monozygotic twins have a 30-70% concordance rate for the disease. Moreover, some individuals with high-risk alleles never develop the disease. This suggests that the disease cannot be attributed solely to genetic predisposition. Several environmental factors, such as diet, viruses, vitamin D deficiency were suggested to play a role in triggering the immune reaction towards β-cells [9]. The complex interplay between genetics and environmental factors that trigger the onset of T1D has yet to be fully understood.

Box CI-1. Mouse models for Type 1 Diabetes

Non-obese diabetic (NOD) mice have been one of the most frequently used mouse models in T1D research due to similarities in the disease pathogenesis with human autoimmune diabetes [10]. Indeed, studying this strain considerably contributed to our understanding of T1D pathology. NOD strain is a spontaneous and polygenic model for T1D. The most important factor contributing to T1D in NOD mice is MHC (synonym of HLA across vertebrates) loci. Besides MHC loci, non-MHC genes such as idd locus, CTLA-4, IL-2 are known to be susceptibility genes in NOD mice [11]. The incidence of diabetes is higher in NOD females than males. The females start to develop diabetes spontaneously between 10-14 weeks of age. They develop full blown diabetes around 30 weeks of age. NOD.*scid* strain is a derivative of NOD strain with RAG2 deficiency. Since this strain lacks T and B cells, it is particularly useful to study the relative contribution of different T and B cell subsets via adoptive transfer [12]. Another widely used model in T1D research is the double transgenic RIP-mOVA model. RIP-mOVA mice express ovalbumin specifically in β-cells. In the T-cell transfer model, T-cells from OT-I TCR-transgenic mice, which recognize ovalbumin peptides, are injected (i.v.) into RIP-mOVA mice. The advantage of this model compared to NOD mice is the shorter time frame for the development of disease, 16 weeks after the adoptive transfer [12,13]. Multiple low dose streptozotocin (MLDSTZ) is a widely used pharmacological model to induce experimental diabetes. Streptozotocin (STZ) is selectively toxic for β-cells. It enters cells via the GLUT2 receptor which is abundantly expressed on β-cell membrane and induces oxidative stress, leading to β-cell damage. It mediates release of antigens from β-cells such as GAD and triggers an immune reaction towards β-cells [12]. This model is advantageous for studying the effects of a specific mutation or chemical in synchronized groups over short time frames.

1.2.1.2. Immunopathology of T1D

The connection between the immune system and T1D was first suggested in 1974 by identification of HLA antigens in patients´ blood [14]. Today it is widely accepted that the immune system is fundamentally involved in T1D pathogenesis. Insulitis is one of the hallmarks of T1D. It is characterized by the mono-nuclear immune cell infiltration to pancreatic islets. The predominant cell type in insulitic lesions is $CD8^+$ cells. However, there are also other cell types such as $CD4^+$ T cells, B cells, macrophages [15]. It is important to note that insulitis affects islets to varying degrees in both mice and humans, with insulitis observed in approximately 30% of islets [16,17].

It is thought that the innate immune system plays a role in the early stages of the disease. Dendritic cells in islet and pancreatic lymph nodes play an essential role in the recruitment and activation of autoreactive T-cells and thereby initiating the disease (Figure CI-2) [18]. Macrophages constitute 80% of the immune cell population in islets and they are suggested to play a key role in the initiation and destruction of the β-cells [16,19]. Indeed, when the tissue-resident macrophages were depleted in NOD mice, the incidence of diabetes was significantly reduced (see Box CI-1 for the mouse models of T1D). It has been shown that depletion of macrophages reduced the entry of other leukocytes to islets [20]. Another mode that macrophages contribute to diabetes onset and progression is partly due to their ability to secrete proinflammatory cytokines such as IL-1β and TNF. These cytokines are known to have cytotoxic effects on β-cells [16]. The role of neutrophils and natural killer (NK) cells in T1D pathology is not fully understood. Neutrophils may contribute to T1D pathology by secreting proinflammatory cytokines and recruiting other immune cells [16]. NK cells are also implicated in T1D; however, their exact role remains unclear due to the diversity of NK cell populations [16,21].

The role of the adaptive immune system in T1D diabetes has been extensively studied. In genetically predisposed individuals' autoantibodies appear between the ages of 1 and 5 years. Although the autoantibodies are not believed to be pathogenic, B cells play an important role in T1D pathogenesis (Figure CI-2). It has been demonstrated that NOD mice lacking B cells have a lower incidence of developing T1D [22,23]. NOD mice which have B cells that cannot secrete antibodies but can present antigens showed a significant increase in diabetes incidence [24]. NOD mice with B cells that are unable to uptake antigens through their Ig receptor recognition were shown to have a delayed onset of T1D whereas NOD mice that bear engineered B cells to selectively recognize insulin have an accelerated diabetes [25,26]. These results suggest that B cells contribute to T1D pathogenesis primarily through their antigen presentation function.

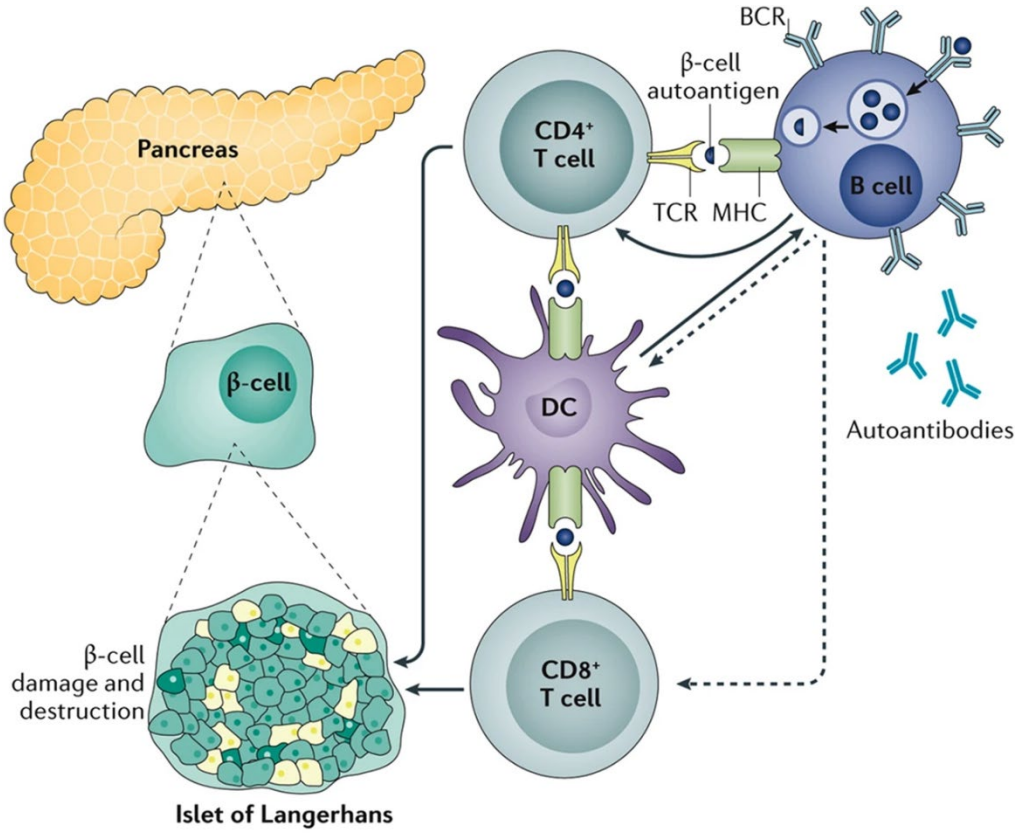

Figure CI-2. A simple overview of different immune cell type interactions in T1D. Dendritic cells and B cells activate β-cell specific-CD4⁺ and CD8⁺ T cells via antigen presentation. Moreover, B cells produce autoantigens β-cell specific autoantibodies which can be used as diagnostic markers [6]. Adapted from [6].

Box CI-2. Differentiation of effector CD4⁺ T cells

CD4⁺ T cells, also known as T helper cells, play a crucial role in orchestrating the immune responses. After their activation by antigen-presenting cells such as dendritic cells or B cells, they can differentiate into different T helper subsets, mainly T-helper 1 (Th1), T-helper 2 (Th2), T-helper 17 (Th17), T-regulatory (Tregs) and follicular helper T cell (Tfh) [27]. This lineage-specific differentiation depends on different cytokines and costimulatory molecules. Th1 differentiation requires IL-12, and they secrete IFNγ upon their differentiation. They play an important role in body defense against intracellular organisms. Th2 cells require IL-4 for their differentiation and once differentiated they secrete IL-4, IL-5, and IL-13. Their function is important in defense against extracellular organisms such as parasites. Th17 cells require IL-6 and TGF-β and they secrete IL-17 upon their differentiation. They play an important role against extracellular pathogens, particularly in epithelial and mucosal barriers such as gut. T regulatory cells (Tregs) require IL-2 and TGF-β for their differentiation. Once differentiated,

Tregs secrete anti-inflammatory cytokines IL-10, IL-35 and TGF-β. Tregs are essential for peripheral immune tolerance and preventing autoimmunity. Follicular helper T (Tfh) cells require IL-6 and IL-21 for their differentiation. They secrete IL-21 which is important for B cell stimulation. Tfh cells play a critical role in germinal centers by contributing to the high-affinity antibody production of B cells. Moreover, they play a crucial role in memory B cell formation.

$CD4^+$ T cells play an important role in T1D pathogenesis (Figure CI-2). The differentiation of effector $CD4^+$ T cell subsets is explained in Box CI-2. Indeed, NOD mice deficient in $CD4^+$ were protected from autoimmune diabetes [28]. Moreover, treatment with CD4-depleting or non-depleting antibodies in NOD mice prevented diabetes onset [29,30]**.** It was initially thought that T1D is a Th1-mediated pathology given the cytotoxic effects of IFNγ on β-cells. However, in recent years there have been contradicting reports about the role of Th1 cells in T1D pathology. While some studies put Th1 cells and IFN-γ in the center of T1D pathogenesis, some reported no or minimal effect [31–34]. In more recent studies, Th17 cells are suggested to play a role in T1D pathogenesis. It has been shown that IL-17 is upregulated both in mice and men in the early stages of T1D [35,36]. However, mechanistic studies carried out with mice suggested that Th17 cells can play a protective role. Segmented filamentous bacteria (SFB) is known to induce Th17 differentiation [37]. NOD mice colonized with SFB were shown to be protected compared to the uncolonized mice [38]. Distinctively, cells which produce both IFN-γ and IL-17 were identified in the islets of T1D patients [39]. Several other reports also confirmed the presence of IFN-γ and IL-17, also called Th1/Th17 cells [40,41]. The contribution of Th1/Th17 to disease pathogenesis warrants further investigation. T1D pathogenesis is associated with T regulatory cell dysfunction. The depletion of Tregs in mice leads to autoimmunity towards β-cells. Moreover, FOXP3 (transcriptional factor for Treg differentiation) mutations lead to T1D in humans [42]. The role of follicular helper T (Tfh) cells has been also studied in T1D [43]. It has been shown that newly diagnosed patients have higher circulating Tfh cells and IL-21 [44–46]. In summary, whilst it is clear that $CD4^+$ T cells play a crucial role in T1D pathogenesis, the contribution of different subsets remains to be elucidated.

$CD8^+$ cells, also known as cytotoxic T cells, are pivotal in the destruction of β-cells due to their capacity to directly induce cell death via perforin and granzyme. Indeed, cytotoxic T cells are the most abundant cell type in insulitic lesions [16]. Autoreactive $CD8^+$ cells can be found in patients´ pancreas and blood [16]. NOD.*scid* mice treated with $CD8^+$ non-depleting antibody following splenocyte transfer from NOD mice prevented diabetes onset, suggesting that $CD8^+$ cells are required for disease onset and progression [47]. Studies suggest that the β-cells destruction by cytotoxic T cells is mostly dependent on perforin and granzymes and do not require FAS-FASL interaction [48].

1.2.2. Type 2 Diabetes (T2D)

1.2.2.1. Etiology of T2D

Type 2 diabetes (T2D) is the most prevalent type of diabetes which represents 90% of all diabetic cases. It is caused by the body's inability to respond properly to insulin and the impaired secretion of insulin by β-cells [49]. Although genetic predisposition can play a role, it is widely accepted that T2D is mostly associated with lifestyle. Obesity, unhealthy diet, and low physical activity are among the most important risk factors for the disease. In fact, obesity increases the risk of T2D by 90-fold and a predominance of the patients are obese or overweight [50]. Genome-wide association studies (GWAS) reported more than 100 genetic variants associated with T2D. However, the identified variants increase the risk only by 10-20 % [49]. Moreover, these variants are common amongst non-diabetic individuals, carried by 54 % of the population. This evidence emphasizes the importance of lifestyle and environmental factors in the pathogenesis of T2D.

1.2.2.2. Pathophysiology of T2D

The first pillar of T2D is the gradual impairment of insulin secretion from pancreatic islets due to long-term insulin resistance in skeletal muscles, liver, and adipose tissue [49]. There are many molecular pathways that converge and contribute to insulin resistance. One of these mechanisms is mitochondrial dysfunction. It has been shown in mice and man that obesity leads to mitochondrial dysfunction in multiple organs such as adipose tissue, liver, and muscle. Mitochondrial dysfunction in adipose tissue impairs the secretion of adiponectin, a crucial adipokine with insulin-sensitizing and anti-inflammatory effects [51]. In other tissues such as muscle, mitochondrial dysfunction gives rise to reactive oxygen species (ROS) which in turn activate redox-sensitive serine kinases. These kinases phosphorylate IRS protein and induce insulin resistance (Figure CI-3). Low-grade chronic inflammation is one of the hallmarks of obesity and metabolic syndrome. It is well-established that proinflammatory cytokines such as IL-6 and TNF are increased in adipose tissue, livers and serums of individuals and mice with insulin resistance [52]. Proinflammatory cytokines are shown to cause insulin resistance by activating the downstream kinases such as IKK and MAP kinases which in turn phosphorylates IRS protein, inducing insulin resistance [52,53]. Suppressors of cytokine signaling (SOCS) are cytokine-inducible proteins and they provide a negative feedback loop to cease cytokine signaling [54]. However, these proteins are also shown to inhibit insulin function by phosphorylating IRS [55]. Dysregulated lipid metabolism also contributes to inflammation. It has been shown that FFAs (free fatty acids) can activate TLR4 and NLRP3 which lead to insulin resistance [56,57]. Unfolded protein response (UPR) is also suggested to contribute to insulin resistance. It has been demonstrated that in the adipose tissue of individuals with T2D, there

is an increase in the ER-stress related proteins, namely XBP1, IRE1α [58]. In turn, these proteins activate JNK, which phosphorylates IRS (Figure CI-3, Box CI-3). Obesity and insulin resistance have been shown to increase β-cell mass to compensate the increased secretory demand [61]. Increased demand for insulin secretion puts β-cells under stress such as ROS production, ER stress, activation of inflammatory pathways as explained above. Over time, this results in β-cell exhaustion and a gradual decline in their secretory capacity. Eventually, chronic stress causes the death of β-cells, resulting in a decline in β-cell mass and progression to type 2 diabetes.

Box CI-3. Endoplasmic reticulum (ER) stress

The endoplasmic reticulum (ER) is the organelle responsible for synthesizing and folding secretory proteins. ER stress arises when there is an accumulation of unfolded or misfolded proteins [59]. In response to ER stress, unfolded protein response (UPR) is initiated by the cells to restore homeostasis. There are three sensors in the ER lumen to sense and respond to ER stress by activating UPR. IRE1α, PERK and ATF6 [59,60]. When IRE1 is activated by ER stress, it induces the alternative splicing of XBP1, a transcription factor for proteins that increase ER folding capacity and degrade misfolded proteins. When activated, PERK phosphorylates eIF2α which is essential for 80S ribosome. Therefore, PERK activation slows down the protein translation. ATF6 is another sensor that monitors the ER lumen. Once the ER stress is detected, traffic to the Golgi apparatus will be cleaved by specific proteases. The cleaved fragment then acts as a transcriptional factor to upregulate the expression of proteins that overlap with those activated by XBP1. Activation of UPR activates both cytoprotective and pro-apoptotic pathways simultaneously. However, if cellular homeostasis cannot be restored, pro-apoptotic pathways prevail, leading to cell death.

1.3. The role NF-κB activation and proinflammatory cytokines in diabetes

Inflammation is a protective and prosurvival mechanism against infections and tissue damage. It includes a series of events, vasodilatation, recruitment of the immune cells to the infection or tissue injury sites. NF-κB activation is the central regulator of proinflammatory gene expression. It can be activated downstream many pathways including pattern recognition receptors (PRR) that directly recognize motifs from the pathogen such as LPS or viral RNA. Activation of PRRs leads to recruitment and activation of IKK complex which in turn phosphorylates and targets IκB for degradation (Figure CI-4). The degradation of IκB allows the translocation of the NF-κB complex to the nucleus to induce inflammatory gene activation. NF-κB can also be activated through cytokines such as TNF and IL-1β (Figure CI-4). Under normal circumstances, inflammation should be resolved in a timely manner once the insult is cleared.

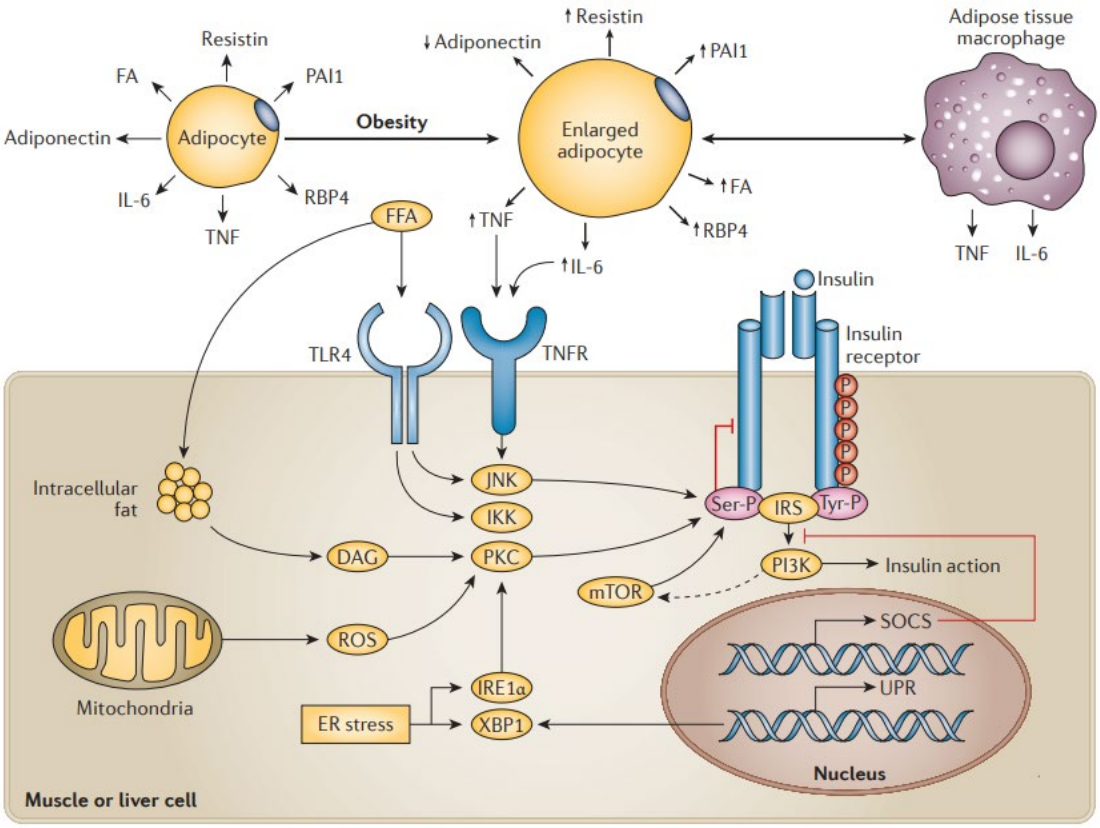

Figure CI-3. Mechanisms of insulin resistance. Due to obesity, enlarged adipocytes secrete FFAs and proinflammatory cytokines. The inflammation and cell death in the adipose tissue cause recruitment of macrophages that secrete proinflammatory cytokines such as TNF and IL-6. Leakage of FFAs and low-grade inflammation contributes to insulin resistance in other cells such as liver and muscle by leading to phosphorylation of IRS and inhibiting insulin signaling. Moreover, ROS production by mitochondria and ER stress are also shown to contribute to insulin resistance by leading to phosphorylation by IRS. Adapted from [49].

Deregulated inflammation and sustained NF-κB activation is associated with autoimmune and autoinflammatory diseases. Activation of NF-κB by PRRs and cytokines is believed to be the main driver of insulitis [62]**.** It has been shown that the conditional and specific inhibition of NF-κB by tetracycline-induced expression of the negative dominant form of IκB protects mice from MLDSTZ-induced diabetes. Moreover, the primary pancreatic islets were protected from IL-1β + IFNγ-induced cell death (Box CI-4) [63]. Similarly, other studies showed that blockade of NF-κB protected β-cells from cell death in vitro [64,65]. In contrast, another study done by using NOD mice showed that constitutive inhibition of NF-κB accelerates the disease outcome [66]. The precise role of NF-κB activation in β-cell loss is yet to be fully elucidated. However, current findings suggest that the contribution of NF-κB may vary depending on the different stages of the disease as well as the T1D model that is used.

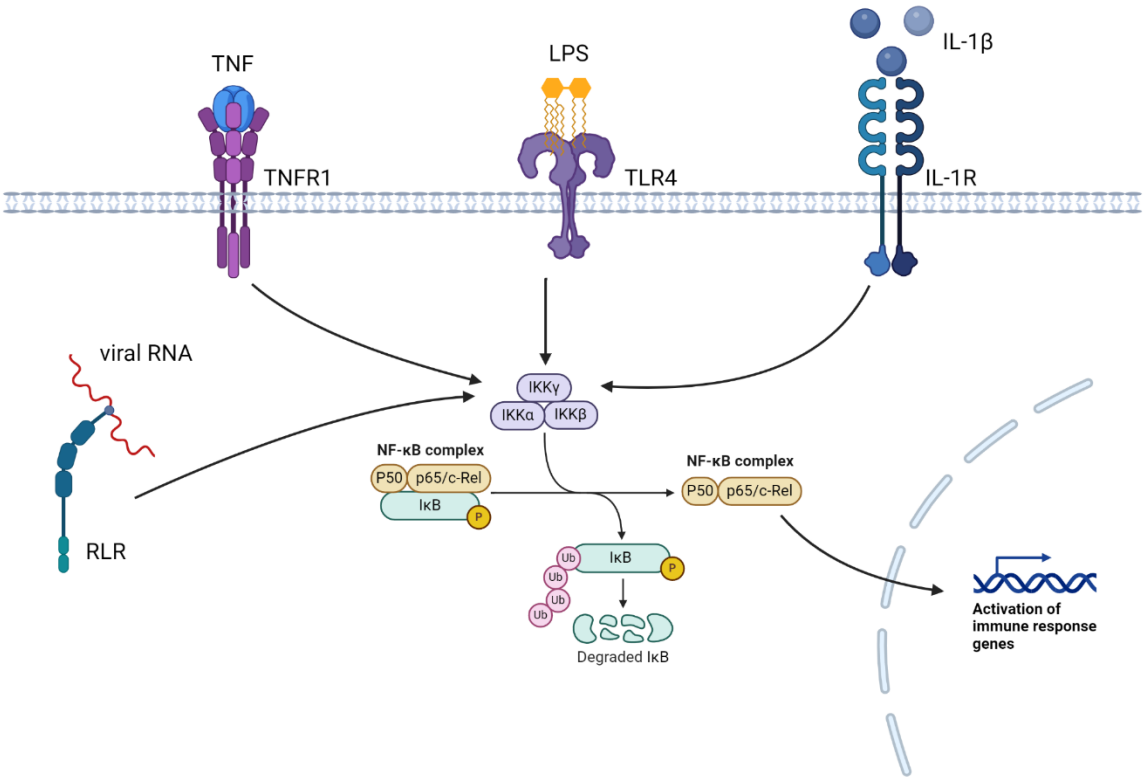

Figure CI-4. NF-κB activation in response to cytokines and PRRs. The activation of pattern recognition receptors (PRRs) or cytokine receptors such as TNFR1 leads to the recruitment and activation of the IKK (IKKγ, IKKα, IKKβ) complex, which in turn phosphorylates IκB. Once phosphorylated, IκB is degraded, allowing NF-κB (p50, p65, c-Rel) to translocate to the nucleus and initiate inflammatory gene transcription. Created with BioRender.

IL-1β is a potent proinflammatory cytokine. Therefore, it has been hypothesized that IL-1β antagonism may preserve functional β-cell mass in T1D. Indeed, the studies in mice showed that inhibition of IL-1β delays the onset of diabetes [67,68]. However, the IL-1R antagonism in clinical trials showed only a modest amelioration compared to healthy controls [69]. TNF is another proinflammatory cytokine associated with β-cell loss in mice and man [70,71]. Moreover, a TNF-neutralizing antibody, Golimumab, preserved β-cell function in newly diagnosed T1D patients [72].

The role of proinflammatory cytokines has been extensively studied in T2D. Research has demonstrated that IL-1β plays a significant role in low-grade inflammation. Inhibition of IL-1β has been shown to improve glucose homeostasis and reduce inflammation in obese mouse models. Moreover, treatment with IL-1β-neutralizing antibodies is shown to improve glycemic control and β-cell function in T2D patients [73]. While TNF neutralization improved glucose metabolism in obese mouse models, studies in humans have not shown similar beneficial effects [74–76].

Box CI-4. Cytokine-induced cell death: the Achilles heel of β-cells

Proinflammatory cytokine cocktail (IL-1β + IFNγ + TNF) is a potent inducer of cell death in β-cells. It is believed that the immune cells that infiltrate into islets during diabetes secrete these cytokines which contribute to β-cell demise. Although the exact mechanisms by which cytokines induce β-cell death are not fully understood, it is known that ER stress play a key role [77]. Due to their secretory nature, β-cells are susceptible to ER stress. Exposure of human, mouse and rat β-cells to cytokines leads to ER stress via different mechanisms [78]. It has been shown that NO production by iNOS contributes to ER-stress in rat cells via SERCA2B (calcium pump) depletion. Whereas in murine cells, ER stress was only partially dependent on NO [77]. Interestingly, although NO production is also induced in human β-cells, cytokine-induced cell death is found to be independent of NO. In human β-cells, upon exposure to cytokines, IRE1α phosphorylates JNK which plays an apoptotic role [77]. The contribution of extrinsic cell death machinery to cytokine-induced β-cell death is not well characterized.

1.4. The role of TNF-induced cell death in diabetes

Despite being driven by distinct mechanisms, the key overlap between T1D and T2D is the death of insulin-secreting β-cells. This eventually leads to a reduction in total β-cell mass and poor glycemic control [2]. Apoptosis is believed to be the main form of cell death that leads to β-cell demise. Indeed, β-cell specific Caspase-8 loss protected mice from MLDSTZ and high-fat diet (HFD)-induced diabetes [79]. Similarly, the loss of Caspase-3 protected the mice from MLDSTZ-induced diabetes and lymphocyte infiltration to the islets (insulitis) [80]. In recent years, it has been shown that the activation of Caspase-3/8 can lead to another form of programmed cell death called pyroptosis via the cleavage of Gasdermins [81,82]. Given that proptosis is a highly inflammatory form of cell death, it is tempting to speculate that it contributes to β-cell demise during diabetes. However, little is known if pyroptosis occurs in β-cell and if they have the machinery to undergo pyroptotic cell death.

Necroptosis is another highly inflammatory mode of cell death. The contribution of necroptosis to diabetes is controversial. In a transplantation model, RIPK3-deficient islets were as sensitive to T-cell killing as wild-type islets [83]. Similarly, mice bearing kinase inactive RIPK1 were not MLDSTZ-induced diabetes [84,85]. In contrast, constitutive RIPK3 deficiency protected mice from MLDSTZ-induced diabetes, suggesting a potential role for necroptosis [86] The kinase activities of both RIPK1 and RIPK3 are essential for TNF-induced necroptosis. Therefore, the discrepancy between our findings and those of Contreras et al. may be due to necroptosis-independent roles of RIPK3 in inflammation, which warrants further investigation.

2. Aims of the study

TNF is a proinflammatory cytokine associated with β-cell death and dysfunction in diabetes. It has been shown that the loss of TNFR1 or administration of TNF-neutralizing antibodies delayed onset of hyperglycemia in NOD mice [87,88]. In a small pilot study, a TNF-blocking antibody, Etanercept, lowered the A1C (glycosylated hemoglobin) levels and increased insulin production in a cohort of 11 newly diagnosed T1D patients [89]. In a recent study with a larger cohort of patients, a monoclonal TNF antibody, Golimumab, increased the endogenous production of insulin, improving glucose metabolism [72]. Similarly, mice lacking TNF were shown to be protected from obesity and insulin resistance [90]. Despite the prominent role of TNF in the pathogenesis of diabetes, the mechanisms of TNF-induced cell death are not well characterized.

RIPK1 is a molecular switch between life and death within TNF signalling. The kinase function of RIPK1 is essential for TNF-induced necroptosis and partially apoptosis [91–93]. In contrast, the scaffolding activity of RIPK1 is prosurvival and crucial for limiting cell death. The deficiency of RIPK1 leads to perinatal lethality in mice and it is essential for the survival of many cell types including intestinal epithelial cells, keratinocytes, etc [94,95]. The contribution of RIPK1 kinase activity and necroptosis to β-cell loss during diabetes remained controversial [83,84,86]. Moreover, the role of RIPK1 scaffolding function in β-cell homeostasis and during diabetes remains to be elucidated.

During my PhD, I aimed to characterize mechanisms of TNF-induced apoptosis and necroptosis in β-cells. In order to do so, I used *Ripk1*^{D138N} mice which are resistant to TNF-induced necroptosis. We created two additional mouse models, *Ripk1*$^{β\text{-}KO,}$ and *Hoip*$^{β\text{-}KO}$ mice, to inhibit important checkpoints of TNF signaling in β-cells. These mouse models and our detailed ex vivo analysis led to a better understanding of TNF signaling in β-cells. I present the results of this project in the following section, demonstrating that β-cells have a distinct way of regulating TNF signaling and are mostly resistant to TNF-induced cell death.

3. References

1. Pandol, S. J. *Anatomy*. (Morgan & Claypool Life Sciences, 2010).
2. Veli, Ö. & Peltzer, N. Life and Death of Pancreatic β-cells. in *Encyclopedia of Cell Biology (Second Edition)* (eds. Bradshaw, R. A., Hart, G. W. & Stahl, P. D.) 19–29 (Academic Press, Oxford, 2023).
3. Da Silva Xavier, G. The Cells of the Islets of Langerhans. *J. Clin. Med. Res.* **7**, (2018).
4. Sapra, A. & Bhandari, P. Diabetes. in *StatPearls* (StatPearls Publishing, Treasure Island (FL), 2023).
5. Diabetes. https://www.who.int/news-room/fact-sheets/detail/diabetes.
6. Katsarou, A. *et al.* Type 1 diabetes mellitus. *Nat Rev Dis Primers* **3**, 17016 (2017).
7. Pociot, F. & Lernmark, Å. Genetic risk factors for type 1 diabetes. *Lancet* **387**, 2331–2339 (2016).
8. Insel, R. A. *et al.* Staging presymptomatic type 1 diabetes: a scientific statement of JDRF, the Endocrine Society, and the American Diabetes Association. *Diabetes Care* **38**, 1964–1974 (2015).
9. Butalia, S., Kaplan, G. G., Khokhar, B. & Rabi, D. M. Environmental Risk Factors and Type 1 Diabetes: Past, Present, and Future. *Can J Diabetes* **40**, 586–593 (2016).
10. Chaparro, R. J. & Dilorenzo, T. P. An update on the use of NOD mice to study autoimmune (Type 1) diabetes. *Expert Rev. Clin. Immunol.* **6**, 939–955 (2010).
11. Mullen, Y. Development of the Nonobese Diabetic Mouse and Contribution of Animal Models for Understanding Type 1 Diabetes. *Pancreas* **46**, 455–466 (2017).
12. Van Belle, T. L., Taylor, P. & von Herrath, M. G. Mouse Models for Type 1 Diabetes. *Drug Discov. Today Dis. Models* **6**, 41–45 (2009).
13. Clough, L. E. *et al.* Release from regulatory T cell-mediated suppression during the onset of tissue-specific autoimmunity is associated with elevated IL-21. *J. Immunol.* **180**, 5393–5401 (2008).
14. Nerup, J. *et al.* HL-A antigens and diabetes mellitus. *Lancet* **2**, 864–866 (1974).
15. Gomez-Tourino, I., Arif, S., Eichmann, M. & Peakman, M. T cells in type 1 diabetes: Instructors, regulators and effectors: A comprehensive review. *J. Autoimmun.* **66**, 7–16 (2016).
16. Herold, K. C. *et al.* The immunology of type 1 diabetes. *Nat. Rev. Immunol.* **24**, 435–451 (2024).
17. Pugliese, A. Insulitis in the pathogenesis of type 1 diabetes. *Pediatr. Diabetes* **17 Suppl 22**, 31–36 (2016).
18. Ferris, S. T. *et al.* A minor subset of Batf3-dependent antigen-presenting cells in islets of Langerhans is essential for the development of autoimmune diabetes. *Immunity* **41**, 657–669 (2014).
19. Citro, A., Campo, F., Dugnani, E. & Piemonti, L. Innate Immunity Mediated Inflammation and Beta Cell Function: Neighbors or Enemies? *Front. Endocrinol.* **11**, 606332 (2020).
20. Carrero, J. A. *et al.* Resident macrophages of pancreatic islets have a seminal role in the initiation of autoimmune diabetes of NOD mice. *Proc. Natl. Acad. Sci. U. S. A.* **114**, E10418–E10427 (2017).
21. Gardner, G. & Fraker, C. A. Natural Killer Cells as Key Mediators in Type I Diabetes Immunopathology. *Front. Immunol.* **12**, 722979 (2021).
22. Akashi, T. *et al.* Direct evidence for the contribution of B cells to the progression of insulitis and the development of diabetes in non-obese diabetic mice. *Int. Immunol.* **9**, 1159–1164 (1997).
23. Hu, C.-Y. *et al.* Treatment with CD20-specific antibody prevents and reverses autoimmune diabetes in mice. *J. Clin. Invest.* **117**, 3857–3867 (2007).
24. Wong, F. S. *et al.* Investigation of the role of B-cells in type 1 diabetes in the NOD mouse. *Diabetes* **53**, 2581–2587 (2004).
25. Silveira, P. A. *et al.* The preferential ability of B lymphocytes to act as diabetogenic APC in NOD mice depends on expression of self-antigen-specific immunoglobulin receptors. *Eur. J. Immunol.* **32**, 3657–3666 (2002).
26. Hulbert, C., Riseili, B., Rojas, M. & Thomas, J. W. Cutting edge: B cell specificity contributes to the outcome of diabetes in nonobese diabetic Mice1. *J. Immunol.* **167**, 5535–5538 (2001).
27. Luckheeram, R. V., Zhou, R., Verma, A. D. & Xia, B. $CD4^+$T cells: differentiation and functions. *Clin. Dev. Immunol.* **2012**, 925135 (2012).
28. Wang, Y., Hao, L., Gill, R. G. & Lafferty, K. J. Autoimmune diabetes in NOD mouse is L3T4 T-

lymphocyte dependent. *Diabetes* **36**, 535–538 (1987).
29. Shizuru, J. A., Taylor-Edwards, C., Banks, B. A., Gregory, A. K. & Fathman, C. G. Immunotherapy of the nonobese diabetic mouse: treatment with an antibody to T-helper lymphocytes. *Science* **240**, 659–662 (1988).
30. Hutchings, P., O'Reilly, L., Parish, N. M., Waldmann, H. & Cooke, A. The use of a non-depleting anti-CD4 monoclonal antibody to re-establish tolerance to beta cells in NOD mice. *Eur. J. Immunol.* **22**, 1913–1918 (1992).
31. Katz, J. D., Benoist, C. & Mathis, D. T helper cell subsets in insulin-dependent diabetes. *Science* **268**, 1185–1188 (1995).
32. Wang, B. *et al.* Interferon-gamma impacts at multiple points during the progression of autoimmune diabetes. *Proc. Natl. Acad. Sci. U. S. A.* **94**, 13844–13849 (1997).
33. Anderson, J. T., Cornelius, J. G., Jarpe, A. J., Winter, W. E. & Peck, A. B. Insulin-Dependent Diabetes in the Nod Mouse Model II. β Cell Destruction in Autoimmune Diabetes is a TH2 and not A TH1 Mediated Event. *Autoimmunity* **15**, 113–122 (1993).
34. *Index Medicus*. (U.S. Department of Health, Education, and Welfare, Public Health Service, National Institutes of Health, National Library of Medicine, 2003).
35. Li, C.-R., Mueller, E. E. & Bradley, L. M. Islet antigen-specific Th17 cells can induce TNF-α-dependent autoimmune diabetes. *J. Immunol.* **192**, 1425–1432 (2014).
36. Marwaha, A. K. *et al.* Cutting edge: Increased IL-17-secreting T cells in children with new-onset type 1 diabetes. *J. Immunol.* **185**, 3814–3818 (2010).
37. Ivanov, I. I. *et al.* Induction of intestinal Th17 cells by segmented filamentous bacteria. *Cell* **139**, 485–498 (2009).
38. Kriegel, M. A. *et al.* Naturally transmitted segmented filamentous bacteria segregate with diabetes protection in nonobese diabetic mice. *Proc. Natl. Acad. Sci. U. S. A.* **108**, 11548–11553 (2011).
39. Reinert-Hartwall, L. *et al.* Th1/Th17 plasticity is a marker of advanced β cell autoimmunity and impaired glucose tolerance in humans. *J. Immunol.* **194**, 68–75 (2015).
40. Lau, K. *et al.* Inhibition of type 1 diabetes correlated to a Lactobacillus johnsonii N6.2-mediated Th17 bias. *J. Immunol.* **186**, 3538–3546 (2011).
41. Nikoopour, E. *et al.* Th17 polarized cells from nonobese diabetic mice following mycobacterial adjuvant immunotherapy delay type 1 diabetes. *J. Immunol.* **184**, 4779–4788 (2010).
42. Hwang, J. L. *et al.* FOXP3 mutations causing early-onset insulin-requiring diabetes but without other features of immune dysregulation, polyendocrinopathy, enteropathy, X-linked syndrome. *Pediatr. Diabetes* **19**, 388–392 (2018).
43. Watts, D. *et al.* Transient Depletion of Foxp3+ Regulatory T Cells Selectively Promotes Aggressive β Cell Autoimmunity in Genetically Susceptible DEREG Mice. *Front. Immunol.* **12**, 720133 (2021).
44. Kenefeck, R. *et al.* Follicular helper T cell signature in type 1 diabetes. *J. Clin. Invest.* **125**, 292–303 (2015).
45. Ferreira, R. C. *et al.* IL-21 production by CD4+ effector T cells and frequency of circulating follicular helper T cells are increased in type 1 diabetes patients. *Diabetologia* **58**, 781–790 (2015).
46. Viisanen, T. *et al.* Circulating CXCR5+PD-1+ICOS+ Follicular T Helper Cells Are Increased Close to the Diagnosis of Type 1 Diabetes in Children With Multiple Autoantibodies. *Diabetes* **66**, 437–447 (2016).
47. Phillips, J. M. *et al.* Type 1 diabetes development requires both CD4+ and CD8+ T cells and can be reversed by non-depleting antibodies targeting both T cell populations. *Rev. Diabet. Stud.* **6**, 97–103 (2009).
48. Dudek, N. L. *et al.* Cytotoxic T-cells from T-cell receptor transgenic NOD8.3 mice destroy beta-cells via the perforin and Fas pathways. *Diabetes* **55**, 2412–2418 (2006).
49. DeFronzo, R. A. *et al.* Type 2 diabetes mellitus. *Nat Rev Dis Primers* **1**, 15019 (2015).
50. Reed, J., Bain, S. & Kanamarlapudi, V. A Review of Current Trends with Type 2 Diabetes Epidemiology, Aetiology, Pathogenesis, Treatments and Future Perspectives. *Diabetes Metab. Syndr. Obes.* **14**, 3567–3602 (2021).
51. Wang, C.-H., Wang, C.-C., Huang, H.-C. & Wei, Y.-H. Mitochondrial dysfunction leads to

impairment of insulin sensitivity and adiponectin secretion in adipocytes. *FEBS J.* **280**, 1039–1050 (2013).
52. de Alvaro, C., Teruel, T., Hernandez, R. & Lorenzo, M. Tumor necrosis factor alpha produces insulin resistance in skeletal muscle by activation of inhibitor kappaB kinase in a p38 MAPK-dependent manner. *J. Biol. Chem.* **279**, 17070–17078 (2004).
53. Arkan, M. C. *et al.* IKK-beta links inflammation to obesity-induced insulin resistance. *Nat. Med.* **11**, 191–198 (2005).
54. Alexander, W. S. Suppressors of cytokine signalling (SOCS) in the immune system. *Nat. Rev. Immunol.* **2**, 410–416 (2002).
55. Howard, J. K. & Flier, J. S. Attenuation of leptin and insulin signaling by SOCS proteins. *Trends Endocrinol. Metab.* **17**, 365–371 (2006).
56. Shi, H. *et al.* TLR4 links innate immunity and fatty acid-induced insulin resistance. *J. Clin. Invest.* **116**, 3015–3025 (2006).
57. Wen, H. *et al.* Fatty acid-induced NLRP3-ASC inflammasome activation interferes with insulin signaling. *Nat. Immunol.* **12**, 408–415 (2011).
58. Boden, G. *et al.* Increase in Endoplasmic Reticulum Stress–Related Proteins and Genes in Adipose Tissue of Obese, Insulin-Resistant Individuals. *Diabetes* **57**, 2438–2444 (2008).
59. Chen, X., Shi, C., He, M., Xiong, S. & Xia, X. Endoplasmic reticulum stress: molecular mechanism and therapeutic targets. *Signal Transduct Target Ther* **8**, 352 (2023).
60. Corazzari, M., Gagliardi, M., Fimia, G. M. & Piacentini, M. Endoplasmic reticulum stress, unfolded protein response, and cancer cell fate. *Front. Oncol.* **7**, 78 (2017).
61. Chen, C., Cohrs, C. M., Stertmann, J., Bozsak, R. & Speier, S. Human beta cell mass and function in diabetes: Recent advances in knowledge and technologies to understand disease pathogenesis. *Mol. Metab.* **6**, 943–957 (2017).
62. Eizirik, D. L., Colli, M. L. & Ortis, F. The role of inflammation in insulitis and beta-cell loss in type 1 diabetes. *Nat. Rev. Endocrinol.* **5**, 219–226 (2009).
63. Eldor, R. *et al.* Conditional and specific NF-κB blockade protects pancreatic beta cells from diabetogenic agents. *Proceedings of the National Academy of Sciences* **103**, 5072–5077 (2006).
64. Heimberg, H. *et al.* Inhibition of cytokine-induced NF-kappaB activation by adenovirus-mediated expression of a NF-kappaB super-repressor prevents beta-cell apoptosis. *Diabetes* **50**, 2219–2224 (2001).
65. Giannoukakis, N., Rudert, W. A., Trucco, M. & Robbins, P. D. Protection of human islets from the effects of interleukin-1beta by adenoviral gene transfer of an Ikappa B repressor. *J. Biol. Chem.* **275**, 36509–36513 (2000).
66. Kim, S. *et al.* NF-κB prevents β cell death and autoimmune diabetes in NOD mice. *Proceedings of the National Academy of Sciences* **104**, 1913–1918 (2007).
67. Thomas, H. E. *et al.* IL-1 receptor deficiency slows progression to diabetes in the NOD mouse. *Diabetes* **53**, 113–121 (2004).
68. Schulze, F. *et al.* Inhibition of IL-1beta improves Glycaemia in a Mouse Model for Gestational Diabetes. *Sci. Rep.* **10**, 3035 (2020).
69. Cabrera, S. M. *et al.* Interleukin-1 antagonism moderates the inflammatory state associated with Type 1 diabetes during clinical trials conducted at disease onset. *Eur. J. Immunol.* **46**, 1030–1046 (2016).
70. Tai, N., Wong, F. S. & Wen, L. The role of the innate immune system in destruction of pancreatic beta cells in NOD mice and humans with type I diabetes. *J. Autoimmun.* **71**, 26–34 (2016).
71. Kim, H.-E. *et al.* Tumour necrosis factor-alpha-induced glucose-stimulated insulin secretion inhibition in INS-1 cells is ascribed to a reduction of the glucose-stimulated Ca2+ influx. *J. Endocrinol.* **198**, 549–560 (2008).
72. Quattrin, T. *et al.* Golimumab and Beta-Cell Function in Youth with New-Onset Type 1 Diabetes. *N. Engl. J. Med.* **383**, 2007–2017 (2020).
73. Sloan-Lancaster, J. *et al.* Double-blind, randomized study evaluating the glycemic and anti-inflammatory effects of subcutaneous LY2189102, a neutralizing IL-1β antibody, in patients with

type 2 diabetes. *Diabetes Care* **36**, 2239–2246 (2013).
74. Wascher, T. C. *et al.* Chronic TNF-α Neutralization Does Not Improve Insulin Resistance or Endothelial Function in 'Healthy' Men with Metabolic Syndrome. *Molecular Medicine* **17**, 189–193 (2011).
75. Hotamisligil, G. S., Arner, P., Caro, J. F., Atkinson, R. L. & Spiegelman, B. M. Increased adipose tissue expression of tumor necrosis factor-alpha in human obesity and insulin resistance. *J. Clin. Invest.* **95**, 2409–2415 (1995).
76. Borst, S. E. & Bagby, G. J. Neutralization of tumor necrosis factor reverses age-induced impairment of insulin responsiveness in skeletal muscle of Sprague-Dawley rats. *Metabolism* **51**, 1061–1064 (2002).
77. Brozzi, F. *et al.* Cytokines induce endoplasmic reticulum stress in human, rat and mouse beta cells via different mechanisms. *Diabetologia* **58**, 2307–2316 (2015).
78. Meyerovich, K., Ortis, F., Allagnat, F. & Cardozo, A. K. Endoplasmic reticulum stress and the unfolded protein response in pancreatic islet inflammation. *J. Mol. Endocrinol.* **57**, R1–R17 (2016).
79. Liadis, N. *et al.* Distinct in vivo roles of caspase-8 in beta-cells in physiological and diabetes models. *Diabetes* **56**, 2302–2311 (2007).
80. Liadis, N. *et al.* Caspase-3-Dependent β-Cell Apoptosis in the Initiation of Autoimmune Diabetes Mellitus. *Mol. Cell. Biol.* **25**, 3620–3629 (2005).
81. Demarco, B. *et al.* Caspase-8-dependent gasdermin D cleavage promotes antimicrobial defense but confers susceptibility to TNF-induced lethality. *Sci Adv* **6**, (2020).
82. Rogers, C. *et al.* Cleavage of DFNA5 by caspase-3 during apoptosis mediates progression to secondary necrotic/pyroptotic cell death. *Nat. Commun.* **8**, 14128 (2017).
83. Zhao, Y. *et al.* Autoreactive T cells induce necrosis and not BCL-2-regulated or death receptor-mediated apoptosis or RIPK3-dependent necroptosis of transplanted islets in a mouse model of type 1 diabetes. *Diabetologia* **58**, 140–148 (2015).
84. Takiishi, T. *et al.* Inhibition of RIPK1 kinase does not affect diabetes development: β-Cells survive RIPK1 activation. *Mol Metab* **69**, 101681 (2023).
85. Veli, Ö. *et al.* RIPK1 is dispensable for cell death regulation in β-cells during hyperglycemia. *Mol Metab* **87**, 101988 (2024).
86. Contreras, C. J. *et al.* RIPK1 and RIPK3 regulate TNFα-induced β-cell death in concert with caspase activity. *Mol Metab* **65**, 101582 (2022).
87. Yang, X. D. *et al.* Effect of tumor necrosis factor alpha on insulin-dependent diabetes mellitus in NOD mice. I. The early development of autoimmunity and the diabetogenic process. *J. Exp. Med.* **180**, 995–1004 (1994).
88. Kägi, D. *et al.* TNF receptor 1-dependent beta cell toxicity as an effector pathway in autoimmune diabetes. *J. Immunol.* **162**, 4598–4605 (1999).
89. Mastrandrea, L. *et al.* Etanercept treatment in children with new-onset type 1 diabetes: pilot randomized, placebo-controlled, double-blind study. *Diabetes Care* **32**, 1244–1249 (2009).
90. Uysal, K. T., Wiesbrock, S. M., Marino, M. W. & Hotamisligil, G. S. Protection from obesity-induced insulin resistance in mice lacking TNF-alpha function. *Nature* **389**, 610–614 (1997).
91. Peltzer, N. & Walczak, H. Cell death and inflammation--a vital but dangerous liaison. *Trends Immunol.* **40**, 387–402 (2019).
92. Polykratis, A. *et al.* Cutting edge: RIPK1 Kinase inactive mice are viable and protected from TNF-induced necroptosis in vivo. *J. Immunol.* **193**, 1539–1543 (2014).
93. Berger, S. B. *et al.* Cutting Edge: RIP1 kinase activity is dispensable for normal development but is a key regulator of inflammation in SHARPIN-deficient mice. *J. Immunol.* **192**, 5476–5480 (2014).
94. Dannappel, M. *et al.* RIPK1 maintains epithelial homeostasis by inhibiting apoptosis and necroptosis. *Nature* **513**, 90–94 (2014).
95. Kelliher, M. A. *et al.* The death domain kinase RIP mediates the TNF-induced NF-kappaB signal. *Immunity* **8**, 297–303 (1998).

4. Results

RIPK1 is dispensable for cell death regulation in β-cells during hyperglycemia

Önay Veli[1,2,3], Öykü Kaya[1,2,3], Ana B. Varanda[3,8], Ximena Hildebrandt[1,2,3], Peng Xiao[4], Yann Estornes[5,6], Matea Poggenberg[2], Yuan Wang[1,2,3], Manolis Pasparakis[3,7], Mathieu J.M. Bertrand[5,6], Henning Walczak[3,8], Alessandro Annibaldi[2], Alessandra K. Cardozo[4] and Nieves Peltzer[1,2,3]

[1]Department of Translational Genomics, Faculty of Medicine, University of Cologne, Cologne, Germany
[2]Centre for Molecular Medicine Cologne (CMMC), University of Cologne, Cologne, Germany
[3]Cologne Excellence Cluster on Cellular Stress Responses in Aging-Associated Diseases (CECAD), Cologne, Germany
[4]Inflammation and Cell Death Signalling group, Signal Transduction and Metabolism Laboratory, Université libre de Bruxelles, Brussels, Belgium
[5]VIB Center for Inflammation Research, 9052 Ghent, Belgium
[6]Department of Biomedical Molecular Biology, Ghent University, 9052 Ghent, Belgium.
[7]Institute for Genetics, University of Cologne, Cologne, Germany
[8]Institute of Biochemistry I, Medical Faculty, University of Cologne, 50931 Cologne, Germany

Correspondence: Nieves Peltzer, m.peltzer@uni-koeln.de

Published in Molecular Metabolism on 14th of July 2024.

https://doi.org/10.1016/j.molmet.2024.101988

Abstract

Objective: Receptor-interacting protein kinase 1 (RIPK1) orchestrates the decision between cell survival and cell death in response to tumor necrosis factor (TNF) and other cytokines. Whereas the scaffolding function of RIPK1 is crucial to prevent TNF-induced apoptosis and necroptosis, its kinase activity is required for necroptosis and partially for apoptosis. Although TNF is a proinflammatory cytokine associated with β-cell loss in diabetes, the mechanism by which TNF induces β-cell demise remains unclear.

Methods: Here, we dissected the contribution of RIPK1 scaffold versus kinase functions to β-cell death regulation using mice lacking RIPK1 specifically in β-cells (*Ripk1*$^{\beta\text{-}KO}$ mice) or expressing a kinase-dead version of RIPK1 (*Ripk1*^{D138N} mice), respectively. These mice were challenged with streptozotocin, a model of autoimmune diabetes. Moreover, *Ripk1*$^{\beta\text{-}KO}$ mice were further challenged with a high-fat diet to induce hyperglycemia. For mechanistic studies, pancreatic islets were subjected to various killing and sensitising agents.

Results: Inhibition of RIPK1 kinase activity (*Ripk1*^{D138N} mice) did not affect the onset and progression of hyperglycemia in a type 1 diabetes model. Moreover, the absence of RIPK1 expression in β-cells did not affect normoglycemia under basal conditions or hyperglycemia under diabetic challenges. *Ex vivo*, primary pancreatic islets are not sensitised to TNF-induced apoptosis and necroptosis in the absence of RIPK1. Intriguingly, we found that pancreatic islets display high levels of the antiapoptotic cellular FLICE-inhibitory protein (cFLIP) and low levels of apoptosis (Caspase-8) and necroptosis (RIPK3) components. Cycloheximide treatment, which led to a reduction in cFLIP levels, rendered primary islets sensitive to TNF-induced cell death which was fully blocked by caspase inhibition.

Conclusion: Unlike in many other cell types (e.g., epithelial, and immune), RIPK1 is not required for cell death regulation in β-cells under physiological conditions or diabetic challenges. Moreover, *in vivo,* and *in vitro* evidence suggest that pancreatic β-cells do not undergo necroptosis but mainly caspase-dependent death in response to TNF. Last, our results show that β-cells have a distinct mode of regulation of TNF-cytotoxicity that is independent of RIPK1 and that may be highly dependent on cFLIP.

Highlights

- RIPK1 scaffold and kinase activities are dispensable for β-cell survival.
- RIPK1 is not required for β-cell function and survival under streptozotocin challenge or high-fat diet feeding.
- Loss of major TNF checkpoints does not licence TNF to kill β-cells.
- Expression of high levels of cFLIP along with low levels of apoptotic and necroptotic proteins could represent the primary protective mechanism in β-cells.

1. Introduction

Diabetes represents a group of metabolic disorders characterized by hyperglycemia due to defects in insulin production, sensing or both[1]. Type 1 diabetes is caused by autoimmune reaction towards insulin-producing β-cells[1] whereas type 2 diabetes is caused by insulin resistance which eventually leads to β-cell failure[2]. Although caused by different mechanisms, the key overlap between type 1 and type 2 diabetes is β-cell death. TNF is a proinflammatory cytokine which can induce inflammatory gene activation or cell death. The binding of TNF to TNFR1 induces the formation of complex-I which includes various prosurvival proteins, which act as checkpoints of TNF signalling, such as RIPK1 and the E3 ligases, cIAP1/2 and LUBAC[3]. This enables optimal gene activation by the NF-κB and MAPK pathways. Under certain conditions, for example, when any of these checkpoints are inhibited, RIPK1, via its kinase activity, autophosphorylates itself and induces the formation of complex-II. This complex can lead to apoptosis via Caspase-8. cFLIP (*CFLAR*) is a direct substrate and regulator of Caspase-8. It regulates levels of apoptosis by restraining the full activation of Caspase-8[4]. Yet, the cFLIP/Caspase-8 heterodimer still bears sufficient activity to prevent another type of cell death called necroptosis[5]. When the activity of Caspase-8 is fully inhibited or absent, phosphorylated RIPK1 induces necroptosis via RIPK3 and MLKL[3,6]. In contrast to its kinase activity, the scaffolding function of RIPK1 is essential to limit cell death since loss of RIPK1 promotes both apoptosis and necroptosis leading to postnatal lethality in mice[7–9]. Hence, RIPK1 serves as a molecular switch regulating cell fate within TNF signalling and, as such, is tightly regulated[10].

TNF has been associated with β-cell loss and dysfunction[11,12]. Treatment with TNF-blocking monoclonal antibody in a cohort of 84 new-onset type 1 diabetes patients resulted in improved glucose metabolism[13]. Similarly, TNF blockade improved glucose metabolism and insulin resistance in rodent obesity models[14–16]. The mechanism of TNF-induced cell death is not fully characterised in β-cells despite the prominent role of TNF in diabetes pathogenesis[11,12]. In particular, the respective contribution of death receptor-induced apoptosis and necroptosis as

well as the implication of RIPK1 function in type 1 diabetes are unclear. Gene variants of RIPK1 are associated with metabolic syndrome in humans, and RIPK1 depletion, but not the inhibition of its kinase activity, was shown to protect from metabolic syndrome in mice[17,18]. On the contrary, Necrostatin-1s, a RIP1 kinase inhibitor, was shown to protect from metabolic syndrome[19]. To date, the role of RIPK1 scaffolding function in β-cells and diabetes remains unknown.

In the present study, we evaluated the role of RIPK1 in β-cell homeostasis by dissecting the contribution of its kinase versus scaffolding function under diabetic conditions. In line with previous reports, we show that the kinase activity of RIPK1 does not contribute to diabetes pathology. Crucially, our results demonstrate that β-cell survival is not affected by RIPK1 deficiency under basal conditions or upon diabetic challenges. Consequently, we conclude that β-cells are protected from the cytotoxic effect of TNF in the absence of RIPK1 possibly through high levels of anti-apoptotic cFLIP expression and poor expression of Caspase-8 and RIPK3.

2. Research Design and Methods

2.1. Mice

Ripk1$^{\beta\text{-}KO}$ and *Hoip*$^{\beta\text{-}KO}$ mice were generated by crossing *Ripk1*$^{fl/fl}$ (Dannappel et al., 2014) and *Hoip*$^{fl/fl20}$, respectively, with B6(Cg)-Ins1tm1.1(cre)Thor/J (Thorens et al., 2015) mice kindly gifted by Hans Stauss (UCL, London, UK). *Ripk1*^{D138N} mice were previously described (Polykratis et al., 2014). FFPE samples from *Ripk3/Caspase-8* double knockout (DKO) and *Cflar;VillinCre-ERT2* mice were provided by Henning Walczak and Alessandro Annibaldi, respectively[21–23]. Mice were maintained in SPF animal facilities of CECAD research center. All experimental procedures were approved by local authorities (Landesamt für Natur, Umwelt und Verbraucherschutz Nordrhein-Westfalen) in Germany. The blood glucose levels and weight of *Ripk1*$^{\beta\text{-}KO}$ and *Hoip*$^{\beta\text{-}KO}$ mice were monitored weekly starting from 8 weeks of age. For this analysis, only female mice were utilized. The blood glucose was measured by using Adia Diabetes kit. For the Glucose Tolerance test (GTT), mice were orally administered with glucose at the dose of 2g/kg (Sigma-Aldrich, G8769) after 6 hours of fasting. For Insulin Tolerance Test (ITT), mice were injected intraperitoneally 0,75 U/kg after 6 hours of fasting. For multiple low-dose Streptozotocin (MLDSTZ) model, male mice were injected either with citrate buffer, pH 4.5 or STZ with the dose of 50 mg/kg (Sigma-Aldrich, S0130) for 5 consecutive days. The mice were sacrificed at the experimental endpoint (20 days after the first injection) unless they reached the termination criteria (e.g. 20 % loss of the initial weight or blood glucose > 600). For diet-induced obesity, the mice were fed with either a standard diet (10% kcal fat, Research Diets Inc, D12450B) or a high-fat diet (60% kcal fat, Research

Diets Inc, D12492) for 20 weeks at the Inflammatory Research Center from UGent-VIB (SPF animal facility) according to institutional, national, and European animal regulations. A second cohort of 16-weeks of high fat diet feeding experiment was performed in CECAD ivRF. The mice were fed with either a standard diet (10% kcal fat, Research Diets Inc, D12450J) or a high-fat diet (60% kcal fat, Research Diets Inc, D12492). Only male mice were utilized for diet-induced obesity experiments.

2.2. Histological analysis, immunohistochemistry (IHC) and Immunofluorescence (IF)

Following the tissue harvest, the pancreas was fixed overnight in a 10% neutral buffered formalin solution and paraffin embedded. For insulin (1:6400 diluted in Animal-Free Blocker, VEC-SP-5035, Vector Laboratories, C.S. C279) and CD45 (1:100, Thermofischer, 14-0451-82) IHC, antigen retrieval was done by using citrate buffer, pH 6 (Sigma-Aldrich, C9999) in pancreas sections (5 µM) by maintaining sub-boiling conditions in microwave for 5 mins. For Caspase-8 (1:200, ALX-804-447-C100) and cFLIP (1:100, ab8421) IHC, antigen retrieval was done by using Tris-EDTA buffer, pH 9.5, in pancreas, spleen and colon sections by maintaining sub-boiling conditions in microwave for 10 mins. The sections were incubated with BLOXALL Endogenous Blocking Solution (VEC-SP-6000, Vector Laboratories) to block endogenous peroxidases. This is followed by 30 mins incubation with Animal-Free Blocker (VEC-SP-5035, Vector Laboratories). Following overnight incubation at 4^{o}C with primary antibodies, sections were washed with TBS-T (pH 7.6, 0.5 % Tween) 3 times for 10 mins. Sections were incubated with immPRESS® HRP Goat Anti-Rabbit IgG Polymer Detection Kit, Peroxidase (MP-7451, Vector Laboratories) for 30 mins. Following 3 times 10 mins washes, the colour was developed by using HIGHDEF® DAB Chromogen/Substrate Set (ENZ-ACC105-0200, Enzo). The slides were scanned by slidescanner (Hamamatsu S360). The insulin+ area was calculated by using QuPath0.4.0. For IF stainings, after antigen retrieval as described above, the sections were incubated with Animal-Free Blocker (VEC-SP-5035, Vector Laboratories) for 1 hour at RT. For insulin-glucagon staining, primary antibodies insulin (1:100,5330-0104G, Bio-Rad) and glucagon (1:100, C.S. 2760) were incubated overnight at 4^{o}C, followed by washes as described above. The secondary antibodies (1:300, SA5-10094, Invitrogen and A-11011, Invitrogen) were used for insulin and glucagon respectively. After washes as described above, sections were counterstained with DAPI and mounted. For cl. Casp-3 staining, following the antigen retrieval as described above, sections were permeabilized with 0.2% triton in Animal-Free Blocker. The rest of the protocol was performed as described above using cl. Casp-3 antibody (1:50, C.S. 9661) and secondary antibody (1:300, A-11011, Invitrogen). The images were acquired by using STELLARIS 5 Confocal

Microscope (Leica). The images were quantified by using FIJI and positive cells were counted manually. For cFLIP staining, antigen retrieval was done with Tris-EDTA buffer, pH 9.5. cFLIP antibody (1:100, ab8421) and the secondary antibody (1:300, A-1108, Invitrogen) was used as described above. The images were acquired by using STELLARIS 5 Confocal Microscope (Leica). The images were analyzed by QuPath0.4.0 using positive cell count command. Three different threshold values were set to detect different levels of fluorescence intensity.

2.3. Islet isolation, viability assay

For islet isolation, pancreas was digested in a water bath at 37 °C. Pancreatic islets were separated using density gradient (Histopaque-1077; Sigma Aldrich), followed by handpicking under microscope. Islets were cultured as described in[18]. The concentration of cytokines in the cocktail was used as follows: mTNF, 1000 U/mL (410-MT-025, R&D Systems), mIFN-γ,1000 U/mL (315-05-100ug, Peprotech) and hIL-1β, 50 U/mL (201-LB-005, R&D Systems). TNF stimulation in primary islets was done using mTNF, 1000 U/mL (410-MT-025, R&D Systems). The final concentration of zVAD, Z-IETD-FMK and Smac mimetics were 50 μM, 50 μM and 5 μM, respectively (Selleck Chemicals). The final concentration of cycloheximide was 5 μg/mL (Merck, C7698-1G). The cell death in islets were determined by using propidium iodide (PI, 5 μg/mL, Sigma-Aldrich) and Hoechst 33342 (HO, 5 μg/mL, Sigma-Aldrich). Cell death levels in islets were assessed by two independent researchers and one of the researchers was not aware of the treatment conditions as performed in Takiishi et al[18].

2.4. Western blot and ELISA

For western blot analysis, islets from *Ripk1*$^{\beta\text{-}KO}$ and control littermates were lysed in 30 mM Tris-Hcl, pH 7.5, 150 mM NaCl, 10 % glycerol, 1 % Triton X-100, 2 mM EDTA supplemented with PhosSTOP and cOmplete™, Mini Protease Inhibitor Cocktail (Roche). The denatured lysates were run using precast protein gels (4568084, Bio-rad) followed by transfer to the membrane (1704158, Bio-Rad). The membrane was incubated overnight at 4^{o}C with the primary RIPK1 antibody (BD, 610459), p-IκB (C.S. 9246), p-p65 (C.S. 3033), NF-κB p65 (C.S. 8242), total IκB (C.S. 9242), RIPK3 (ab62344), cFLIP (ab8421), cFLIP (C.S. 56343) Caspase-8 (MAB3429), insulin (BS-0862R). After the incubation with respective secondary antibody, color was developed using ECL (PerkinElmer, NEL103001EA). The serum insulin content of mice was quantified by insulin ELISA (Crystalchem, 90080). For qRT-PCR of the islets, RNA was extracted using Dynabeads™ mRNA DIRECT™ Purification Kit (61012). Reverse transcription was performed by using LunaScript RT SuperMix Kit (NEB #E3010) according to the manufacturer's protocol. For RT-PCR, Luna Universal qPCR Master Mix (NEB # M3003) was used. The primer sequences are as follow:

Target gene	Forward Primer (5´→3´)	Reverse Primer (5´→3´)
GAPDH	CTCCCACTCTTCCACCTTCG	GCCTCTCTTGCTCAGTGTCC
A20	CATGAAGCAAGAAGAACGGAAGA	GAGGCCCGGGCACATT
Fas	GCGGGTTCGTGAAACTGATAA	GCAAAATGGGCCTCCTTGATA
RIPK3	GAGATGGAAGACACGGCACT	GGTGGTGCTACCAAGGAGTT

2.5. scRNA-seq analysis of β-cells

For analysis of murine pancreatic islets expression, we utilized publicly available scRNA-seq data obtained from the National Center for Biotechnology Information (NCBI) Gene Expression Omnibus database under accession number GSE156175. Single-cell RNA sequencing of mouse islets exposed to proinflammatory cytokines[24]. Data Processing, quality control and normalization was performed as described in the original publication using R (R version 4.2.2) using the package Seurat (Version 4.2.0).

2.6. Tabula Muris analysis

The single-cell transcriptomic data used in this study was obtained from the FACS subset of Tabula Muris, a compendium of single-cell transcriptome data from male and female C57BL/6JN mice. The data was accessed from the Tabula Muris Consortium's public resource. The heatmaps were generated with the mean expression of each gene in specific cell types of each tissue. The Tabula Muris Consortium., Overall coordination., Logistical coordination. et al. Single-cell transcriptomics of 20 mouse organs creates a Tabula Muris. Nature 562, 367–372 (2018). https://doi.org/10.1038/s41586-018-0590-4

2.7. Statistical analysis

Data was represented as Means ± SD and statistical analyses were carried out using GraphPad Prism 10.1.2. (GraphPad Software Inc., San Diego, CA, USA). Unpaired two-tailed t-test was carried out to compare the means of two groups. 2-way ANOVA was used to compare the means of groups with more than one variable. If a multiple comparison test was used, it is clarified in the figure legend. A $p<0.05$ is considered statistically significant.

3. Results

3.1. Lack of RIPK1-kinase activity does not affect onset and progression of MLDSTZ-induced diabetes

The kinase activity of RIPK1 was shown to be necessary for TNF-induced necroptosis and under certain conditions apoptosis[25]. To test whether RIP1 kinase activity contributes to type 1 diabetes pathogenesis, we used RIPK1 kinase-inactive mice (*Ripk1*^{D138N}). *Ripk1*^{D138N} and WT mice were administered multiple low-dose streptozocin (MLDSTZ), and their blood glucose level was followed for 20 days (Fig. 1a). *Ripk1*^{D138N} mice presented normal onset and progression of hyperglycemia upon MLDSTZ treatment (Fig. 1a). At endpoint (20 days after the first injection or when the mice reached the termination criteria), we assessed islet composition by insulin-glucagon immunofluorescence (IF) staining and found that the β-cell (insulin-positive) or α-cell (glucagon-positive) ratio to total islet cells, and the total insulin-positive area were comparable between *Ripk1*^{D138N} and WT mice (Fig. 1b and Fig. S1a). Since the kinase activity of RIPK1 can also promote apoptosis, we performed cleaved Caspase-3 (cl. Casp-3) staining. However, we observed similar levels of cl. Casp-3 positive cells in islets of *Ripk1*^{D138N} and WT mice (Fig. 1c). We assessed insulitis upon MLDSTZ as described in Fig. S1b and did not observe any difference between the two genotypes (Fig. 1d). These data indicate that RIPK1 kinase-dependent cell death does not contribute to type 1 diabetes onset and progression.

3.2. RIPK1 deficiency in β-cells does not cause spontaneous metabolic disorder

To study the role of RIPK1 scaffolding survival function in pancreatic β-cells, we generated *Ripk1*$^{β\text{-}KO}$ mice (specific deletion of RIPK1 in β-cells). The deletion of RIPK1 was confirmed by Western blot from primary islets isolated from *Ripk1*$^{β\text{-}KO}$ and littermate controls (Fig. 2a).

Ripk1$^{β\text{-}KO}$ mice were normal weighed and presented normoglycemia throughout lifespan (Fig. 2b, c). Moreover, neither young (8 weeks old) nor adult (30 weeks old) mutant animals showed glucose intolerance in glucose tolerance test (GTT) assays (Fig. 2d, e). At 30 weeks of age, normal fed serum insulin levels in *Ripk1*$^{β\text{-}KO}$ mice were within normal range (Fig. 2f).

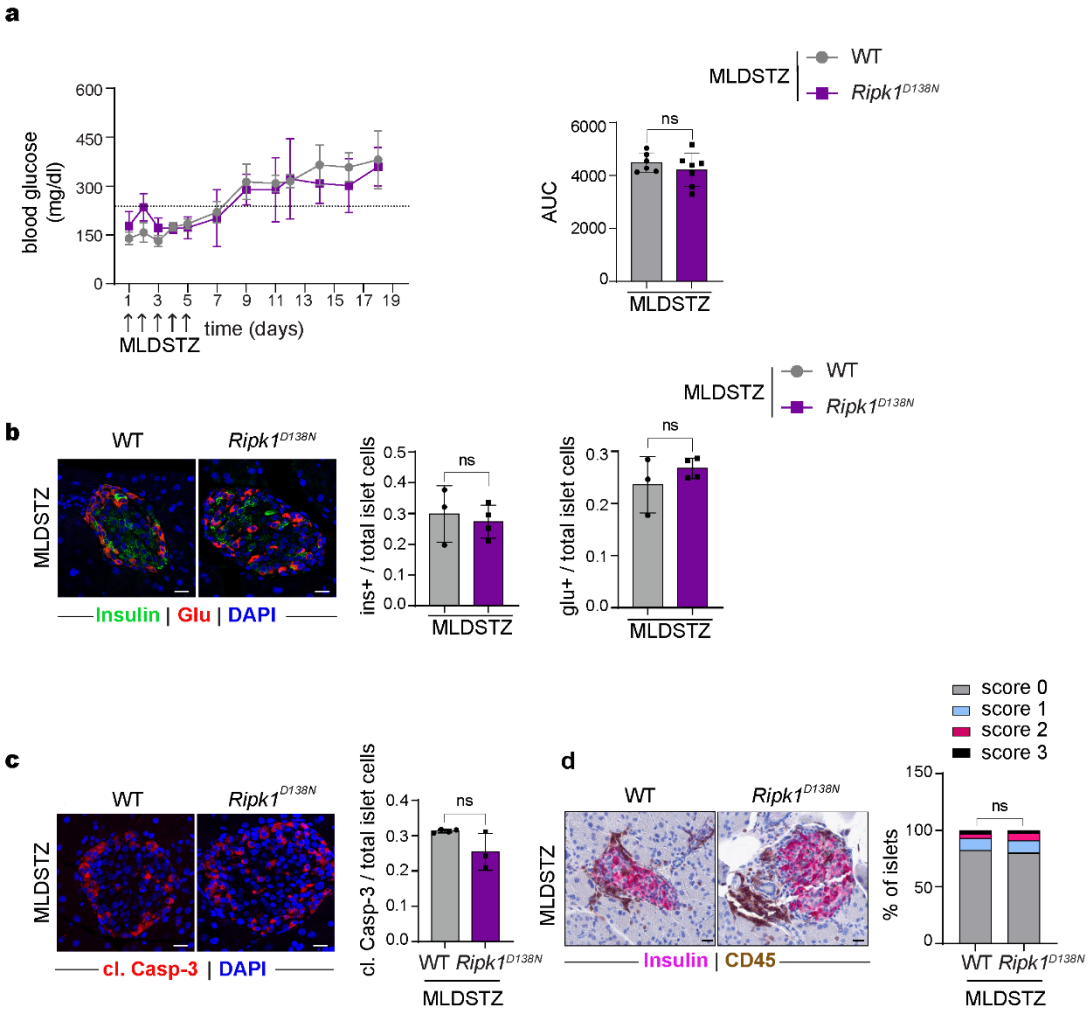

Figure 1. Kinase activity of RIPK1 does not affect type 1 diabetes onset and progression. *Ripk1*^{D138N} and WT controls were treated with MLDSTZ (50 mg/kg) for five consecutive days. **(a)** Fed-blood glucose levels were monitored over 20 days in (left) and area under the curve (AUC) was calculated (right) (n=6-7). **(b)** Representative images of insulin and glucagon IF (left) and quantification of insulin and glucagon positive cells in islets of MLDSTZ-treated *Ripk1*^{D138N} and WT controls (n=3-5 per group). **(c)** Representative images of cl. Casp-3 IF (left) and quantification of cl. Casp-3 positive cells in the islets of MLDSTZ-treated *Ripk1*^{D138N} and WT controls (n=3-5 per group). **(d)** Representative images of insulin-CD45 staining and insulitis were graded as score 0, score 1, score 2, score 3. The representative images of MLDSTZ are selected from score 2 for each genotype. The percentage of each score was calculated for each group (n=3-5 per group). Scale bars represent 20 μM. Means ± SD. Unpaired t-test (a, b, c). 2-way ANOVA with Tukey's multiple comparisons test (d).

Moreover, *Ripk1*$^{β\text{-}KO}$ mice displayed normal islet structure (Fig. 2g). To test whether β-cells have alternative mechanisms that protect them from loss of RIPK1, we deleted another key regulator of TNF signalling. HOIP is the main catalytic subunit of LUBAC, and its loss leads to cell death-dependent inflammation in cell types including endothelial cells and keratinocytes[20,26–28]. Deletion of HOIP in β-cells did not affect normal-fed blood glucose levels,

weight gain and glucose tolerance at different stages of life (Fig. S2a-d). Our results therefore suggest that RIPK1 and HOIP are dispensable for β-cell survival, development, and function in basal conditions.

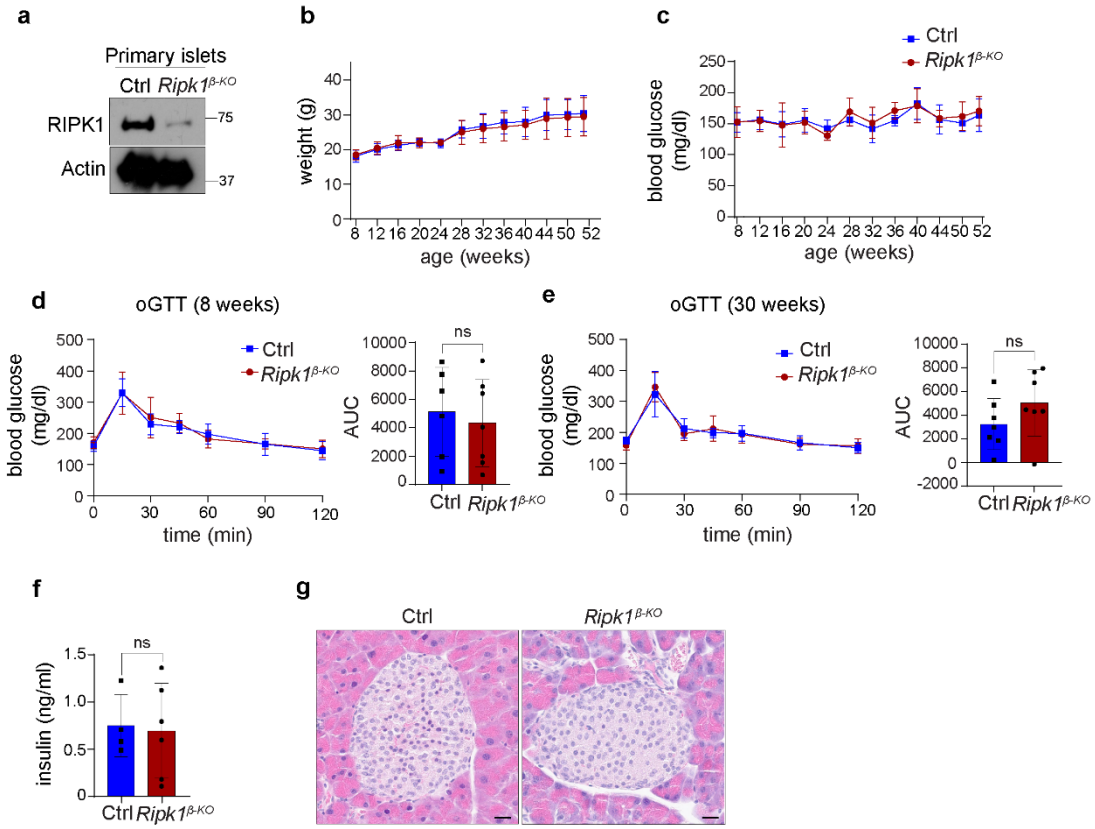

Figure 2. β-cell specific deletion of RIPK1 does not cause spontaneous metabolic disorder. (a) Deletion of RIPK1 is shown in primary islets from *Ripk1*$^{β\text{-}KO}$ and littermate controls by WB. **(b)** Body weight and **(c)** blood glucose was monitored weekly for 30 weeks in *Ripk1*$^{β\text{-}KO}$ and littermate controls (n=15 per group). **(d,e)** Oral GTT (oGTT) in 8 weeks-old mice **(d)** and in 30-weeks old **(e)** *Ripk1*$^{β\text{-}KO}$ and littermate controls. Area under curve (AUC) is shown on the right of each histogram (n=6-7 per group). **(f)** Fed serum insulin levels of 30-weeks old mice (n=4-6). **(g)** Representative images of pancreatic islets stained with H&E. Scale bar represents 20 µM. Means ± SD. Unpaired t-test (d,e,f).

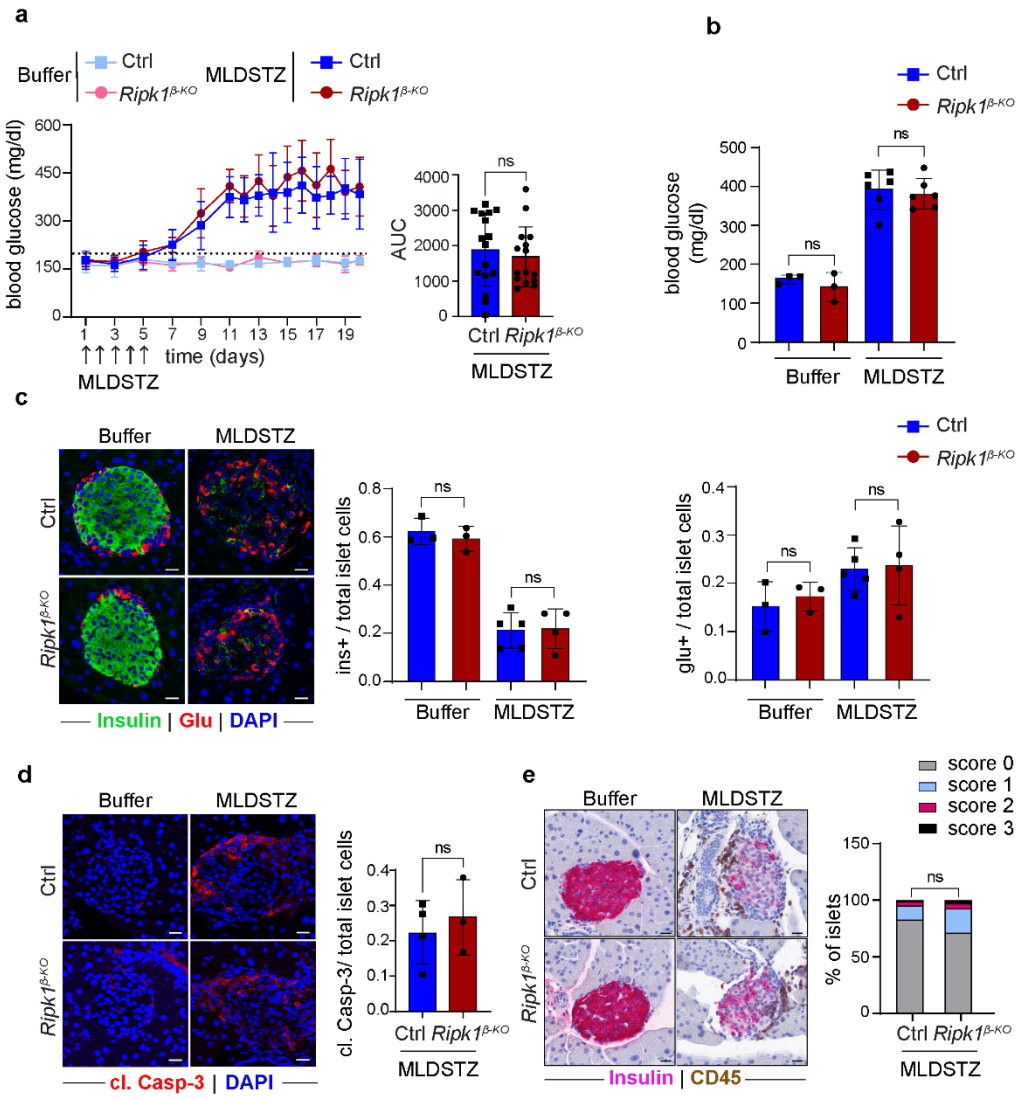

Figure 3. Type 1 diabetes onset and progression is not affected by loss of RIPK1 in β-cells. *Ripk1*$^{β\text{-}KO}$ and littermate controls were treated with citrate buffer or MLDSTZ. **(a)** Fed-blood glucose levels were monitored over 20 days in (left) and AUC was calculated (right) (n=15-16 per group for MLDSTZ, n=3 per group for buffer). **(b)** Fasting glucose levels at day 10 (n=7 per group for MLDSTZ, n=3 per group for buffer). **(c)** Representative images of insulin and glucagon IF (left) and quantification of insulin and glucagon positive cells in islets of buffer and MLDSTZ-treated *Ripk1*$^{β\text{-}KO}$ and littermate controls (n=3-5 per group). **(d)** Representative images of cl. Casp-3 IF (left) and quantification of cl. Casp-3 positive cells in the islets of MLDSTZ-treated *Ripk1*$^{β\text{-}KO}$ and littermate controls. **(e)** Representative images of insulin-CD45 staining and insulitis was graded as score 0, score 1, score 2, score 3. The representative images of MLDSTZ are selected from score 2 for each genotype. The percentage of each score was calculated for each group (n=3-5 per group). Scale bars represent 20 μM. Means ± SD. Unpaired t-test (a, b, c, d). 2-way ANOVA with Tukey's multiple comparisons test (e).

3.3. Loss of RIPK1 in β-cells does not affect onset and progression of MLDSTZ-induced diabetes

To test whether RIPK1 scaffolding function is required to limit β-cell death during type 1 diabetes, we challenged the mice with MLDSTZ. The onset and progression of hyperglycemia was comparable between *Ripk1*$^{β\text{-}KO}$ and littermate controls (Fig. 3a). Similarly, no difference was detected in blood glucose between *Hoip*$^{β\text{-}KO}$ mice and controls upon MLDSTZ (Fig. S2e). Fasting blood glucose levels, measured 10 days after the first STZ injection, were not affected by RIPK1 deficiency (Fig. 3b). The mice were sacrificed 20 days after the first injection or when they reached the endpoint criteria according to animal welfare. The insulin-glucagon staining showed decreased β-cell ratio to total islet cells upon MLDSTZ regardless of the presence of RIPK1 (Fig. 3c). Moreover, the insulin-positive area of MLDSTZ-treated *Ripk1*$^{β\text{-}KO}$ mice and littermate controls was similar (Fig. S3a). Since deficiency of RIPK1 induces apoptosis in certain cell types such as intestinal epithelial cells[29,30], we performed cl. Casp-3 staining to test whether loss of RIPK1 sensitised β-cells to apoptosis in response to MLDSTZ. Although we observed apoptosis induction upon MLDSTZ treatment, we failed to detect differences in cl. Casp-3 levels in *Ripk1*$^{β\text{-}KO}$ mice versus littermate controls (Fig. 3d). *Ripk1*$^{β\text{-}KO}$ mice presented similar insulitis scores to their littermates (Fig. 3e, S3b). Overall, our results indicate that RIPK1 scaffolding function, or HOIP, are not required for β-cell survival during MLDSTZ-induced diabetes.

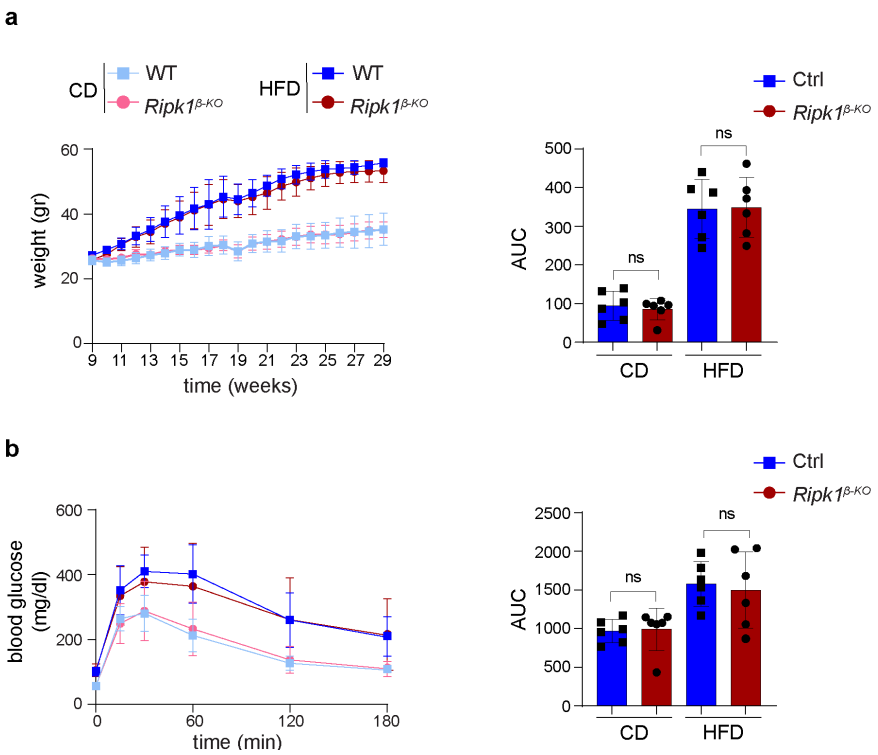

Figure 4. Hyperglycemia induced by HFD is not affected by RIPK1 deficiency in β-cells. *Ripk1$^{β-KO}$* and littermate controls were fed with CD or HFD for 20 weeks. **(a)** Weekly body weight measurements (left) and AUC was calculated (right). **(b)** Intraperitoneal GTT (i.p.GTT) was performed at 10 weeks after the start of diet (left) and AUC was calculated (right) (n=6 per group). Means ± SD. Unpaired t-test (a, b).

3.4. Hyperglycemia induced by high-fat diet is not affected by RIPK1 deficiency

To understand the role of RIPK1 in a model of hyperglycemia, we used diet-induced obesity. *Ripk1$^{β-KO}$* mice and littermate controls were fed a high-fat diet (HFD) for 20 weeks. No difference was observed in the weight gain between the two genotypes (Fig. 4a). Glucose tolerance test performed at 10 weeks of HFD feeding showed that *Ripk1$^{β-KO}$* mice were as glucose tolerant as their littermate controls (Fig. 4b). In a different cohort of mice, *Ripk1$^{β-KO}$* mice and littermate controls were fed with HFD for 16 weeks. In accordance with the previous cohort, we did not observe a difference between *Ripk1$^{β-KO}$* mice and littermate controls in terms of weight gain, glucose, and insulin tolerance at 16 weeks of HFD feeding (Fig. S4a-c). Our results suggest that deficiency of RIPK1 in β-cells does not affect diet-induced weight gain and hyperglycemia.

3.5. Resistance to TNF-induced cell death may be due to high cFLIP/Caspase-8 ratio and low RIPK3 expression

Next, we addressed whether β-cells lacking RIPK1 are sensitised to TNF-induced cell death *ex vivo*. We treated primary pancreatic islets with either TNF alone or in combination with Smac mimetics (S) to induce apoptosis by cIAP1/2 depletion or S+Zvad (Z) to induce necroptosis. Intriguingly, we found that pancreatic islets are resistant to TNF-induced apoptosis and necroptosis. Moreover, the deficiency of RIPK1 did not affect their sensitivity to TNF-induced apoptosis and necroptosis or to cytokine cocktail (TNF, IFNγ and IL-1β) (Fig. 5a). The observation that pancreatic islets are not sensitive to TNF-induced cell death raised the question whether they respond to TNF at all. Stimulation of primary islets isolated from *Ripk1$^{β-KO}$* mice and littermate controls with TNF, showed increased IκB and p65 phosphorylation and a mild increase in the expression of the NF-κB target genes, Fas and A20, suggesting that primary islets are responsive to TNF by activating NF-κB signaling pathway (Fig. S5a, b). It is important to note, that islets displayed a modest response to TNF, an observation that was previously reported[31]. Yet, there are no major differences in NF-κB activation in wildtype versus RIPK1-deficient islets. To better understand why RIPK1 does not act as a checkpoint in TNF-induced cell death, we analysed publicly available sc-RNA seq data of murine primary islets[24] (Fig. 5b and S5c). We found that islet cells express very low

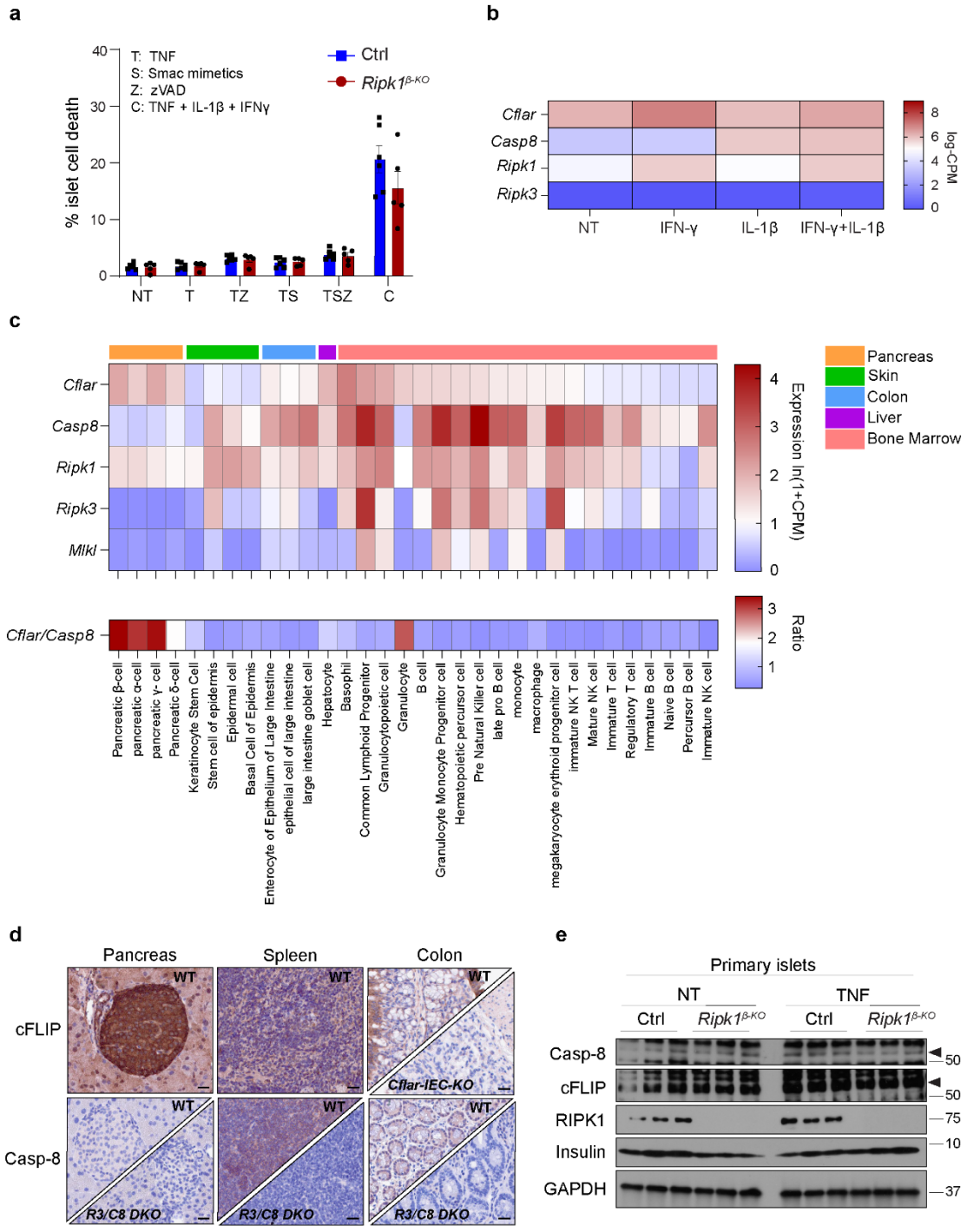

Figure 5. Pancreatic islets are not sensitive to TNF-induced cell death; potentially explained by lack of RIPK3 and high cFLIP expression. (a) Percentage of cell death in mouse primary islets isolated from *Ripk1*$^{\beta\text{-}KO}$ and littermate controls treated with TNF (T), TNF and zVAD (TZ), TNF and Smac mimetics (TS), TNF, Smac mimetics and zVAD (TSZ), Cocktail with IL-1β, TNF, IFNγ (C) for 24 hours (n=5-6 per group). **(b)** Gene expression profile of indicated genes from mouse β-cells treated with IL-1β, IFNγ, IL-1β + IFNγ for 6 hours or non-treated (NT). **(c)** Expression levels of indicated genes across different organs and cell types from the *Tabula Muris* dataset (upper panel). Ratio of cFLIP (*Cflar*) to Caspase-8 (*Casp8*) expression level in indicated organs and cell types **(d)** IHC staining of

Caspase-8 and cFLIP in pancreas, colon, and spleen. *R3/C8 DKO* stands for *Casp8/Ripk3* constitutive knockout (upper panel) and *Cflar-IEC-KO* (Cflar deletion in intestinal epithelial cells) (bottom right). Scale bars represent 20 μm. Chromogen (DAB) incubation was done equally in different tissues. **(e)** Primary islets isolated from *Ripk1*$^{\beta\text{-}KO}$ mice and littermate controls (n=3 per genotype) were stimulated with TNF for 24 h. The expression levels of indicated proteins were analyzed by western blotting.

to null levels of RIPK3 in non-treated conditions or upon stimulation with IFNγ and/or IL1β which may explain why pancreatic islets do not undergo necroptosis (Fig. 5b). Moreover, we found that β-cells express high levels of cFLIP and low levels of Caspase-8 under basal conditions (Fig. 5b). Next, we compared cFLIP and Caspase-8 expression in various tissues that are known to be affected by TNF-induced cell death upon deficiency of RIPK1, such as colon, skin, and bone marrow (Fig. 5c, upper panel). Among these tissues, islet cells have distinctively high cFLIP expression as compared to Caspase-8 and hence a high CFLAR/Caspase-8 ratio (Fig. 5c, lower panel). The same protein expression pattern was observed by cFLIP and Caspase-8 IHC stainings in pancreas, colon, and spleen (Fig. 5d and Fig S6a, b) and by Western blot of isolated pancreatic islets (Fig. 5e). This analysis revealed that islets express cFLIP under basal conditions but express very little, to undetectable, levels of Caspase-8 (Fig. 5d). While MLDSTZ treatment in mice resulted in overexpression of cFLIP and Caspase-8 (Fig. S6a, b), TNF stimulation did not cause gross changes in their expression (Fig. 5e), possibly explaining why there is cell death in MLDSTZ-treated islets as described above. No difference was observed in the expression levels of Caspase-8 and cFLIP between *Ripk1*$^{\beta\text{-}KO}$ mice and littermate controls (Fig. S6 a,b,c). Low expression of RIPK3 was also observed in these datasets and confirmed by western blot and qRT-PCR of pancreatic islets as compared to mouse embryonic fibroblasts (Fig. S6d, e). Taken together, low to null RIPK3 expression and high cFLIP to Caspase-8 ratio can be a plausible explanation for resistance of islet cells to TNF-induced extrinsic cell death.

3.6. Cycloheximide treatment sensitises pancreatic islets to TNF-induced cell death

Since we hypothesise that high cFLIP/Caspase-8 ratio protects β-cells to TNF-induced cell death, we tested whether cFLIP depletion by cycloheximide (CHX) treatment would, differently from smac mimetics (SM), render β-cells sensitive to TNF-induced cell death. CHX treatment efficiently reduced cFLIP protein levels after 24 hs (Fig. 6a). In line with cFLIP depletion, TNF plus CHX treatment, but not CHX alone, induced cell death in pancreatic islets (Fig. 6b,c) and as previously reported[32]. Notably, cell death was induced by TNF/CHX treatment but not by TNF/SM (Fig. 5a and 6b, c and S7).

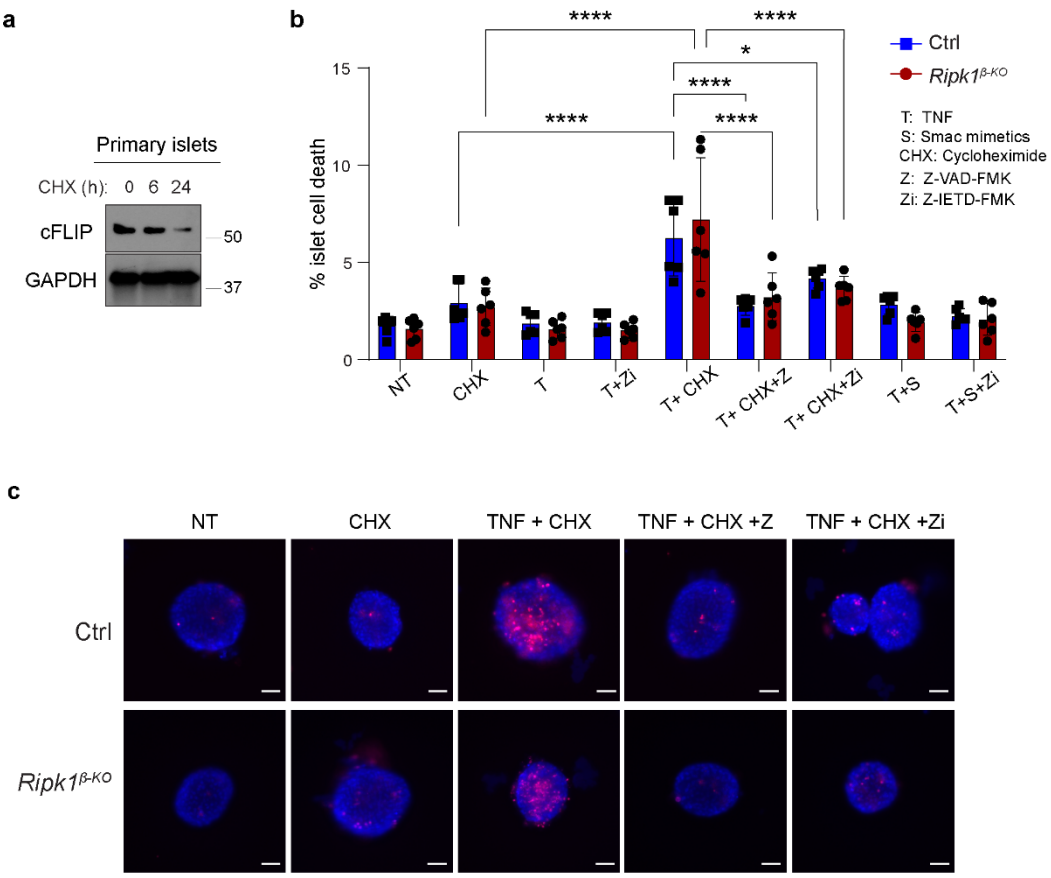

Figure 6. Cycloheximide treatment renders pancreatic islets sensitive to TNF-induced cell death, an implication of c-FLIP. (a) Primary islets were treated with CHX for 6h or 24 h and cFLIP levels were analyzed by western blotting. (b) Percentage of cell death in mouse primary islets isolated from *Ripk1*$^{\beta\text{-}KO}$ and littermate controls treated with the indicated conditions for 24h (n=6 per group). (c) Representative images of islets after 24h of treatment with the indicated conditions. Scale bars represent 100 µm. Means ± SD. 2-way ANOVA with Šídák's multiple comparisons test. *p<0.05, **p<0.01, ***p<0.001, ****p<0.0001

Moreover, TNF/CHX-induced cell death was completely prevented by the pan-caspase inhibitor zVAD or the Caspase-8 inhibitor, zIETD-fmk. This indicates that β-cells die mainly by apoptosis in response to TNF and that necroptosis does not occur even when cells are licensed to die. Of note, under conditions that efficiently induce cell death in pancreatic islets, we could not observe differences between wildtype and *Ripk1*$^{\beta\text{-}KO}$ islets, providing further evidence that TNF-induced cell death is independent of RIPK1 in these cells.

4. Discussion

TNF has long been associated with β-cell death, however, the mechanisms involved are not well-characterised. Moreover, the contribution of different cell death modalities to diabetes pathogenesis is not known. β-cell-specific deletion of Caspase-8 protected mice from

MLDSTZ-induced diabetes indicates that extrinsic apoptosis contributes to the disease. However, these mice develop spontaneous hyperglycemia with ageing, accompanied by increased cell death in the islets which could be explained by necroptosis induction in the absence of Caspase-8[33]. Although constitutive RIPK3 deficiency was shown to protect mice from MLDSTZ-induced diabetes[34], in a transplantation model, pancreatic islets lacking RIPK3 were as sensitive to T-cell killing as wild type islets, excluding a role of necroptosis in autoimmune diabetes[35]. Our study is in line with the latter and with Takiishi et al. who showed that RIPK1-mediated cell death does not play a role in type 1 diabetes by using *Ripk1*^{S25D} mice under the same type 1 diabetes challenge[18]. In addition, Karunakaran et al. reported that RIPK1 kinase inactive mice, *Ripk1*^{K45A}, are not protected from diet-induced metabolic syndrome[17]. We also demonstrated *ex vivo* that TNF-induced cell death induced by sensitisation with CHX, was fully blocked, rather than exacerbated, by caspase inhibition, providing further evidence that necroptosis does not occur in β-cells. Furthermore, Takiishi et al. showed that necroptotic stimuli do not translate into cell death although RIPK1 is phosphorylated, suggesting that β-cells have a mechanism downstream RIPK1 activation that protects from TNF-induced cell death.

Intriguingly, unlike many other cell types, we found that β-cells are not sensitive to cell death upon deletion of RIPK1 or HOIP under physiological conditions and diabetic challenges. It is particularly intriguing in the context of type 1 diabetes because Caspase-8 deficiency in β-cells protects from MLDSTZ-induced diabetes[33], indicating that death receptor-associated cell death machinery is engaged in this model. Curiously, it has been shown that death ligands such as TRAIL and FasL are dispensable for T-cell killing of β-cells[36,37]. Similarly, we and others showed that intact pancreatic islets are not sensitive to TNF along with cIAP1/2 depletion which is a widely used extrinsic apoptosis stimulus[18]. To understand what could be the mechanism that sustains β-cells survival upon check-point inhibition within the TNF pathway such as LUBAC deficiency, cIAP1/2 depletion and RIPK1 phosphorylation, we examined the expression profile of cell death proteins in β-cells. We found that β-cells express extremely low levels of MLKL and RIPK3. This goes in line with the observed negligible role of RIPK1 kinase activity in diabetes onset as discussed above. Moreover, we showed that β-cells express distinctively high levels of cFLIP compared to Caspase-8. The latter could represent a mechanism by which β-cells prevent TNF-induced cytotoxicity in conditions that were reported to licence TNF to kill in many other cell types and organs. Indeed, we found that CHX treatment which correlated with a depletion in cFLIP, sensitised cells to TNF-induced cell death. This goes in line with a report showing that overexpression of cFLIP in β-cell lines protects from TNF- and cytokine-induced cell death[38]. Although our data places cFLIP as the main checkpoint in TNF-cytotoxicity in β-cells, we cannot exclude the possibility that CHX also

targets other prosurvival factors that are important to preserve β-cell survival, e.g. MCL1[39,40]. Hence, the prominent role of cFLIP in β-cell death regulation, homeostasis and during pathological conditions warrants further investigation.

On one hand, high levels of cFLIP could explain why β-cells are protected from TNF-induced cell death. On the other hand, evidence suggests that Caspase-8 deletion in β-cells protects from diabetes onset[33]. Hence, how Caspase-8 gets activated in the presence of overwhelmingly high levels of cFLIP, especially upon MLDSTZ challenge, remains an open question. It is important to note that Caspase-8 expression was also increased upon MLDSTZ treatment, hence becoming available for activation. Emerging evidence suggests that Caspase-8 can be cleaved in an iNOS-dependent manner[41,42]. Considering the prominent role of iNOS in β-cell demise[43–45], and the fact that *Nos2* expression is induced by cytokine cocktail (Fig. S6a), it is possible that Caspase-8 cleavage and activation during diabetes occurs in an iNOS and NO-dependent manner potentially bypassing the inhibitory effect of cFLIP over Caspase-8. Overall, our results indicate that β-cells are resistant to TNF-induced apoptosis and necroptosis, upon loss of key survival nodes in TNF signalling, which can be a prosurvival adaptation in order to protect β-cell mass and maintain normoglycemia upon a plethora of inflammatory conditions.

Acknowledgements

We would like to thank all members of the Annibaldi, Liccardi and Walczak labs for sharing reagents and for helpful discussions. We particularly thank Erick Arroba and Anne Van Praet from A.K.C. group for their help with experiments with primary islets. We thank Hans Stauss for gifting Ins1-Cre mice and Lucy Walker and Chunjing Wang for protocols and discussions. We also thank the CECAD ivRF, CECAD Imaging facility and SFB1403 Histology Facility for their support. We thank Emma Deblangy for proofreading the manuscript. This work is supported by the Deutsche Forschungsgemeinschaft (DFG) (SFB1403 [414786233] to NP, HW and MP, SFB1399 [413326622] to NP, HW and MP, SFB1530 [455784452] to NP, HW and AA) and the NRW Network consortium CANTAR (NW21-062B) to NP, HW and AA. NP is further supported by the Center for Molecular Medicine Cologne, Career Advancement Program and by the Jurgen Manchot Stiftung (JMSF). Ö.V. is supported by JMSF. Work in the A.K.C. group was supported by Fonds National de la Recherche Scientifique (FNRS CDR J.0109.220). H.W. is supported by the Wellcome Trust Investigator Award (214342/Z/18/Z). Research in the M.J.M.B. group is supported by grants from FWO-Vlaanderen (3G046420, 3G044518W, EOS CD-INFLADIS (3G0I5722)) and Ghent University (iBOF ATLANTIS grant 01IB3920, 01G00123).

Author contribution

Ö.V. performed the majority of the experiments with the help of and Ö.K., A.B.V, X.H. P.X., Y.W, and A.K.C. contributed with experiments in pancreatic islets and provided helpful discussions. A.B.V performed analysis of sc-RNAseq and *Tabula Muris*. M.Z. and A.A. provided tissue samples from *cflar; VillinCre-ERT2* mice and helped with mouse work. Y.E and M.J.M.B. performed HFD experiments. M.P provided *Ripk1*-floxed and *Ripk1*^{D138N} mice and H.W. provided *Hoip*-floxed mice. N.P conceived the study. Ö.V and N.P wrote the manuscript with contribution from A.A. and A.K.C.

Supplementary figures

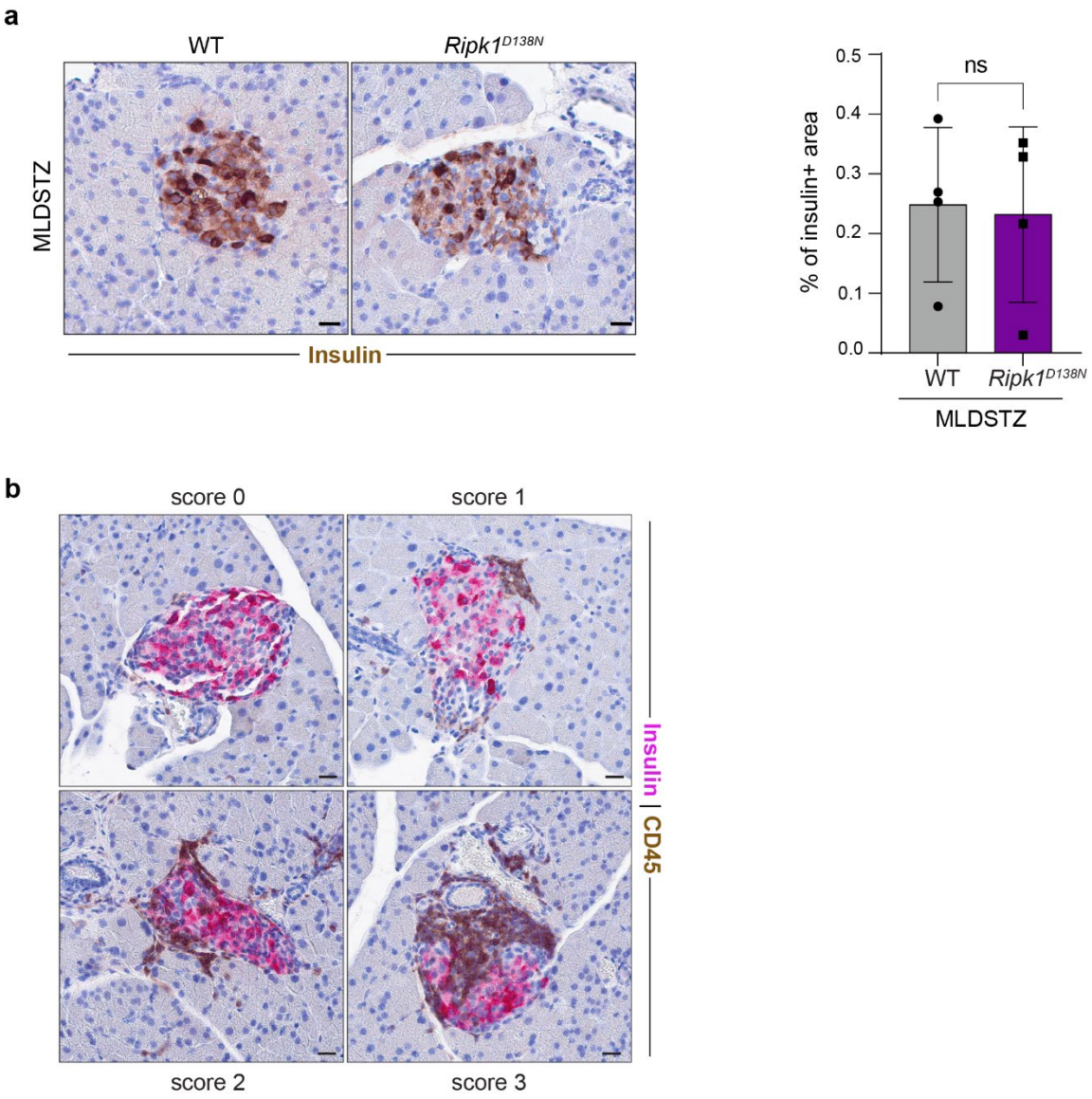

Figure S1. β-cell specific deletion of RIPK1 does not affect islet area and immune infiltration upon MLDSTZ. (a) Representative images of insulin IHC (left) and quantification of insulin positive area in MLDSTZ-treated *Ripk1*^{D138N} and WT. **(b)** Insulitis scoring strategy in MLDSTZ-treated *Ripk1*^{D138N} and WT. Scale bars represent 20 µm. Means ± SD. Unpaired t-test (a).

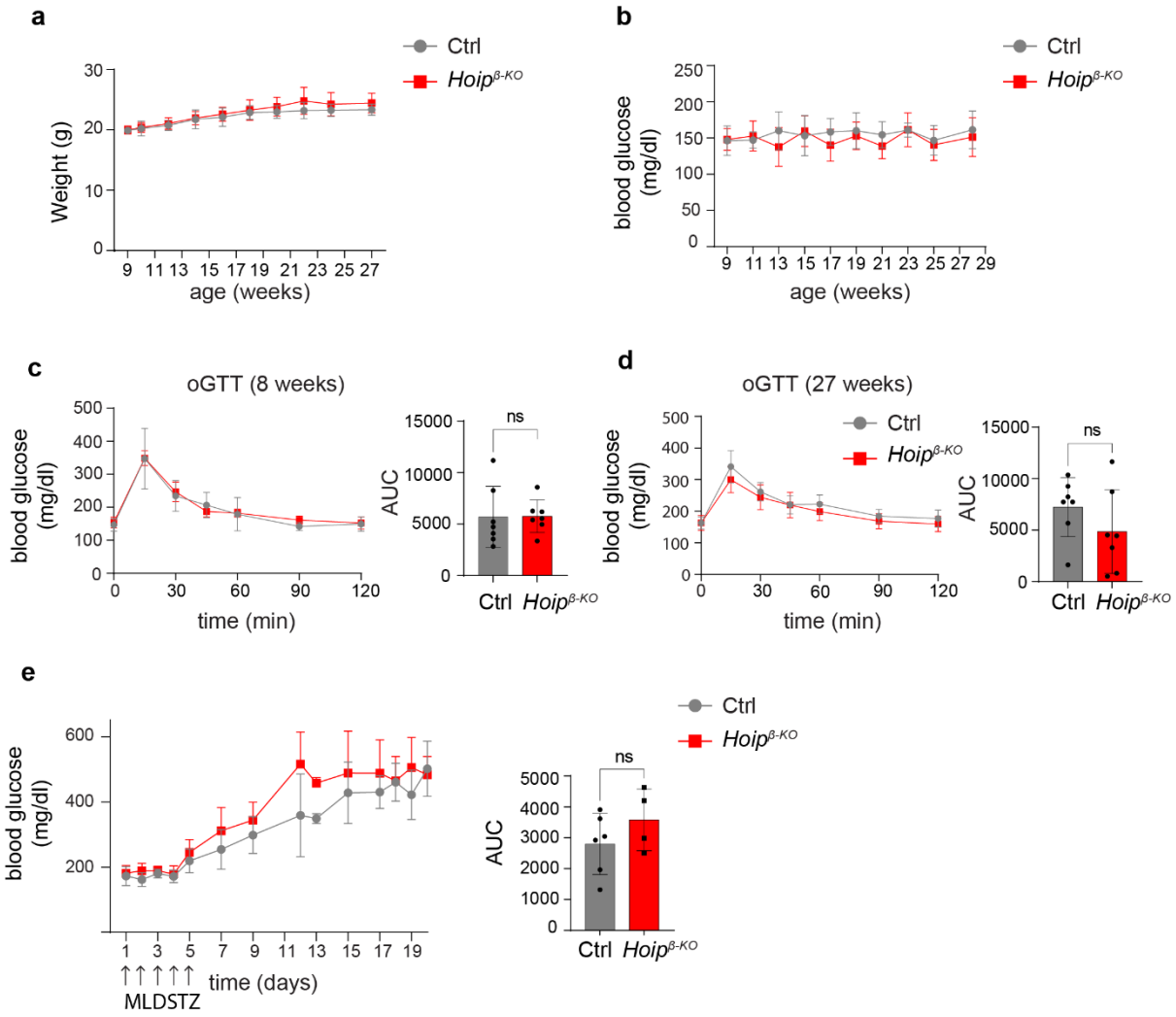

Figure S2. β-cell specific deletion of HOIP does not cause spontaneous metabolic disorder. (a) Blood glucose and **(b)** body weight was monitored weekly for 28 weeks in *Hoip*$^{β-KO}$ and littermate controls (n=7 per group). **(c)** oral GTT (oGTT) in 8 weeks-old mice **(d)** and in 28-weeks old *Hoip*$^{β-KO}$ and littermate controls. Area under curve (AUC) is shown on the right of each histogram (n=7 per group). *Hoip*$^{β-KO}$ and littermate controls were treated with buffer or MLDSTZ. **(e)** Fed-blood glucose levels were monitored over 20 days in (left) and AUC was calculated (right) (n=4-6 per group). Means ± SD. Unpaired t-test (c,d,e).

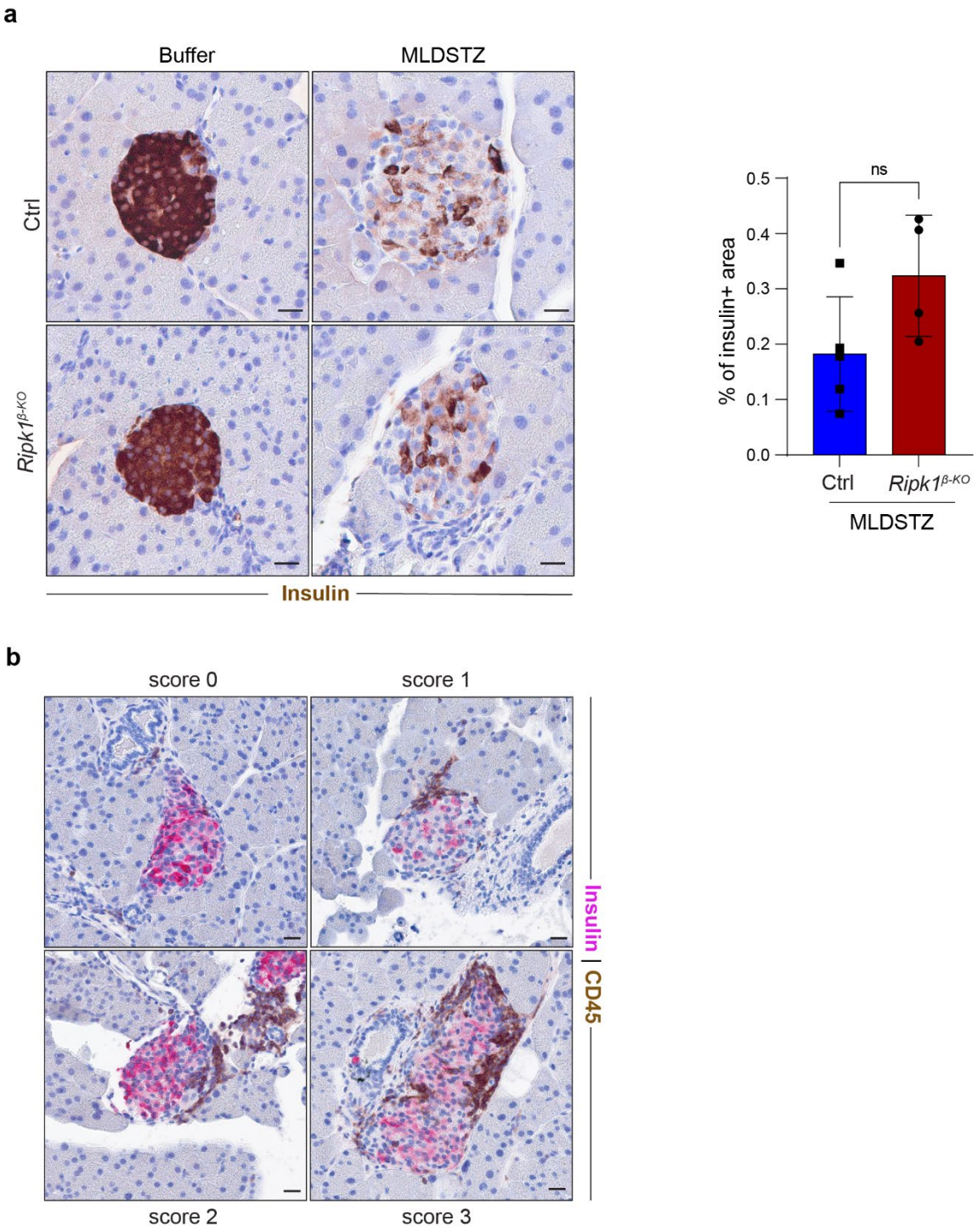

Figure S3. β-cell-specific deletion of RIPK1 does not affect islet area and immune infiltration upon MLDSTZ. (a) Representative images of insulin IHC (left) and quantification of insulin positive area in MLSTZ-treated *Ripk1*$^{β\text{-}KO}$ and littermate controls. **(b)** Insulitis scoring strategy in MLDSTZ-treated Ripk*1*$^{β\text{-}KO}$ and littermate controls. Scale bars represent 20 µm. Means ± SD. Unpaired t-test (a).

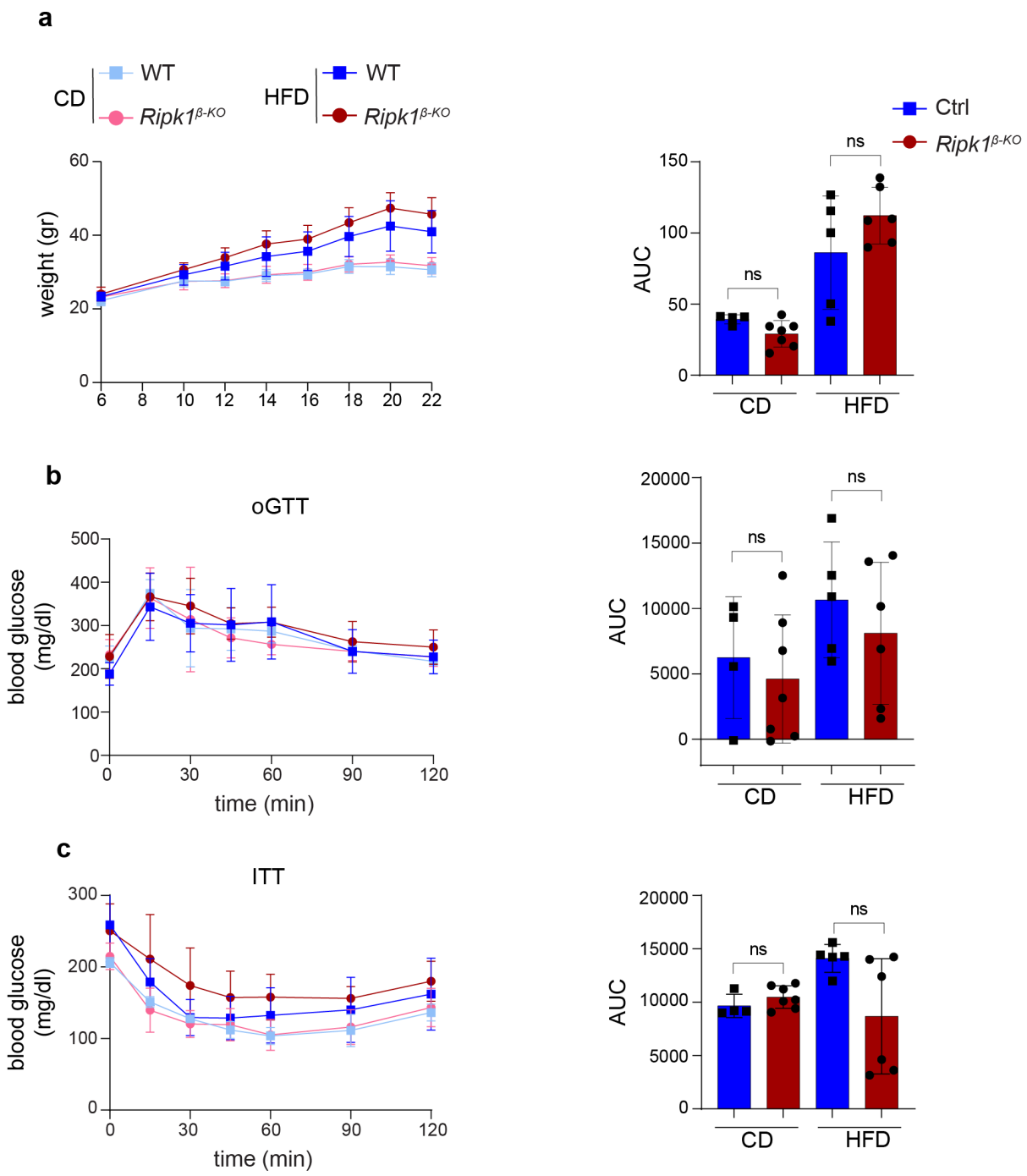

Figure S4: Hyperglycemia induced by HFD is not affected by RIPK1 deficiency in β-cells. (a) *Ripk1*$^{β\text{-}KO}$ and littermate controls were fed with CD or HFD for 16 weeks. **(a)** Weekly body weight measurements (left) and AUC was calculated (right). **(b)** Oral GTT (oGTT) was performed at 16 weeks after the start of diet (left) and AUC was calculated (right) (n=6 per group). Means ± SD. Unpaired t-test (a, b) **(c)** Intraperitoneal ITT was performed at 16 weeks after the start of diet (left) and AUC was calculated (right) (n=6 per group). Means ± SD. Unpaired t-test (a, b).

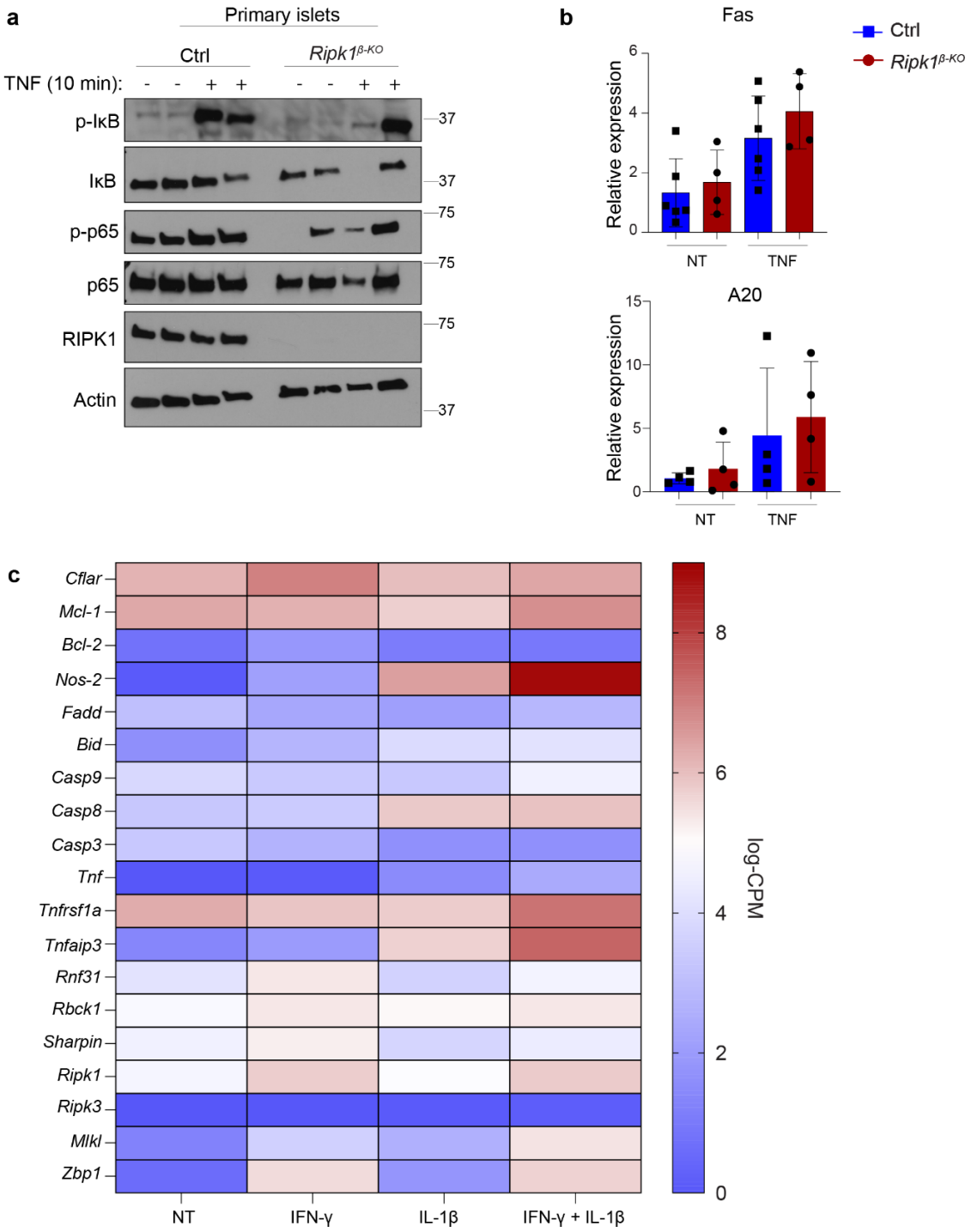

Figure S5. Primary islets have a mild NF-κB activation in response to TNF stimulation. (a) Primary islets isolated from *Ripk1*$^{β\text{-}KO}$ and littermate controls were stimulated with TNF for 10 mins. NF-κB activation was assessed by western blotting of the indicated proteins (p=phospho). **(b)** Gene expression analysis by qRT-PCR of primary islets isolated from *Ripk1*$^{β\text{-}KO}$ mice and littermate controls in response to 6h of TNF stimulation. Data is represented as relative to littermate control non-treated condition. **(c)** Gene expression profile of different cell death proteins in β-cells obtained from publicly available scRNAseq datasets. Means ± SD. 2-way ANOVA (b).

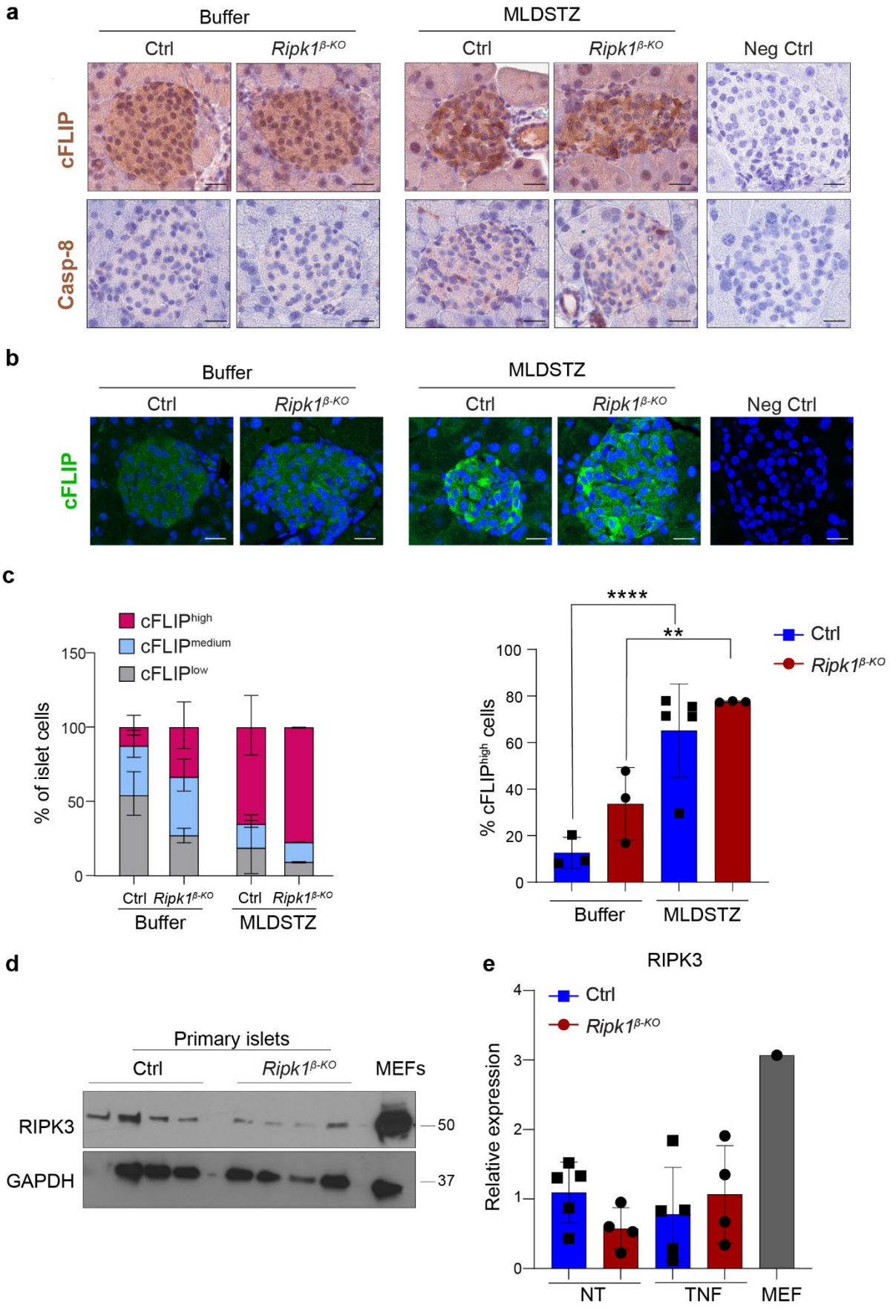
a
Buffer
MLDSTZ
Ctrl
Ripk1β-KO
Ctrl
Ripk1β-KO
Neg Ctrl
cFLIP
Casp-8
b
Buffer
MLDSTZ
Ctrl
Ripk1β-KO
Ctrl
Ripk1β-KO
Neg Ctrl
cFLIP
c
cFLIPhigh
cFLIPmedium
cFLIPlow
% of islet cells
150
100
50
0
Ctrl
Ripk1β-KO
Ctrl
Ripk1β-KO
Buffer
MLDSTZ
****
**
Ctrl
Ripk1β-KO
% cFLIPhigh cells
100
80
60
40
20
0
Buffer
MLDSTZ
d
Primary islets
Ctrl
Ripk1β-KO
MEFs
RIPK3
GAPDH
50
37
e
RIPK3
Ctrl
Ripk1β-KO
Relative expression
4
3
2
1
0
NT
TNF
MEF

Figure S6. MLDSTZ upregulates cFLIP and Caspase-8 expression in pancreatic islets. (a) Representative images of cFLIP and Caspase-8 IHC staining in the pancreas of buffer and MLDSTZ-treated *Ripk1*$^{\beta\text{-}KO}$ mice and littermate controls. **(b)** Representative images of cFLIP immunofluorescence in the pancreas of buffer and MLDSTZ-treated *Ripk1*$^{\beta\text{-}KO}$ mice and littermate controls. **(c)** Quantification of the percentage of islet cells expressing cFLIP at different fluorescent intensities as shown in (b) (left panel). Percentage of cells expressing cFLIP^{high} with statistical analysis (right panel). **(d)** RIPK3 expression was confirmed by western blot isolated from *Ripk1*$^{\beta\text{-}KO}$ mice and littermate controls. **(e)** RIPK3 expression analysis by qRT-PCT isolated from *Ripk1*$^{\beta\text{-}KO}$ mice and littermate controls under 6h TNF-treated or non-treated (NT) conditions. Data was represented as relative to littermate control non-treated condition. Scale bars represent 20 μm (a,b). Means ± SD. 2-way ANOVA Tukey's multiple comparisons test (c), 2-way ANOVA (e).

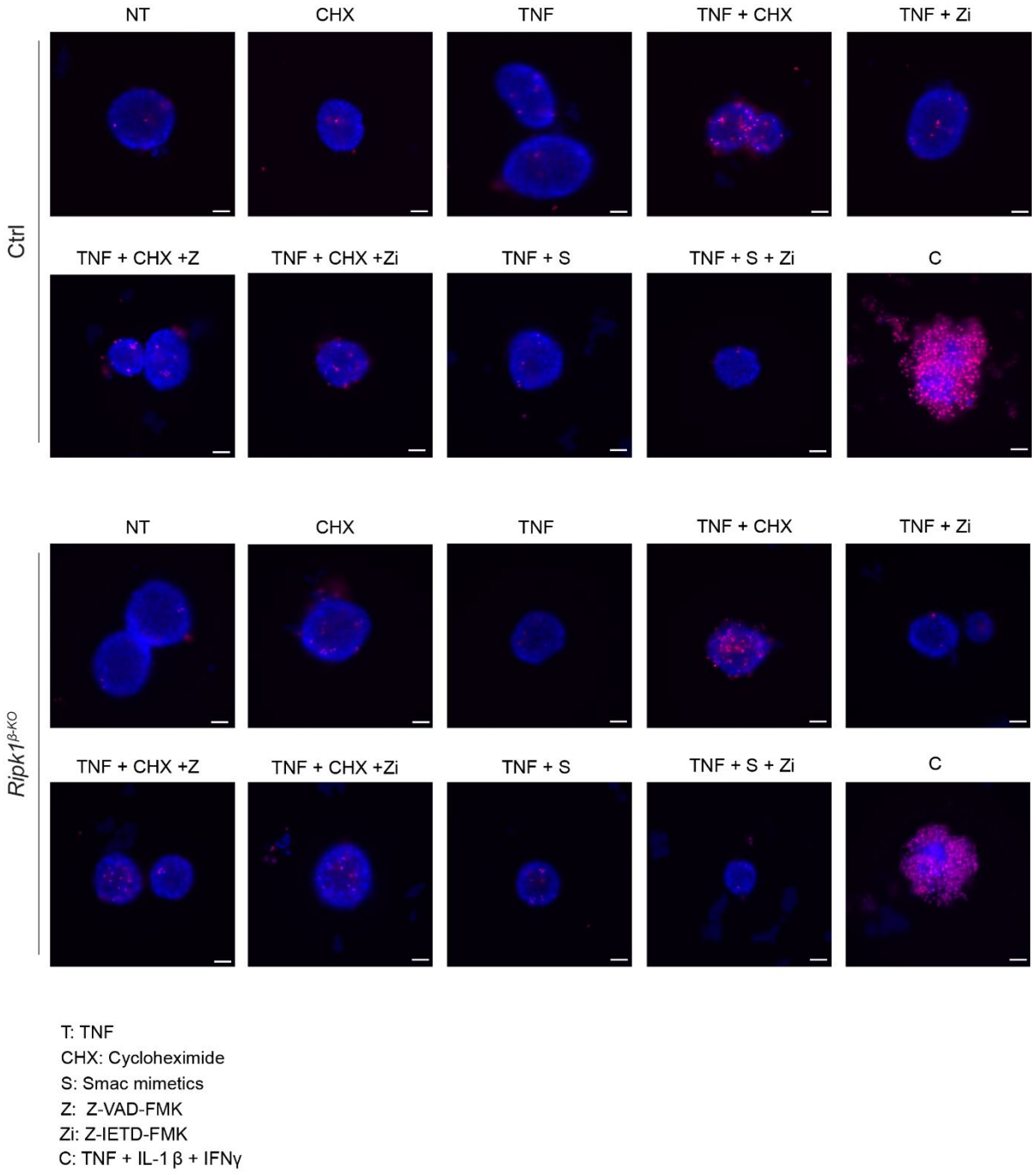

Figure S7. Cycloheximide treatment renders pancreatic islets sensitive to TNF-induced cell death, an implication of c-FLIP. (a) Extended representative images of pancreatic islets isolated from *Ripk1*$^{β\text{-}KO}$ mice and littermate controls and treated with indicated conditions for 24h. Scale bars represent 100 μm.

References

1. Katsarou, A. *et al.* Type 1 diabetes mellitus. *Nat Rev Dis Primers* **3**, 17016 (2017).
2. DeFronzo, R. A. *et al.* Type 2 diabetes mellitus. *Nat Rev Dis Primers* **1**, 15019 (2015).
3. Peltzer, N. & Walczak, H. Cell death and inflammation--a vital but dangerous liaison. *Trends Immunol.* **40**, 387–402 (2019).
4. Martinez Lagunas, K. *et al.* Cleavage of cFLIP restrains cell death during viral infection and tissue injury and favors tissue repair. *Sci Adv* **9**, eadg2829 (2023).
5. Oberst, A. *et al.* Catalytic activity of the caspase-8–FLIPL complex inhibits RIPK3-dependent necrosis. *Nature* **471**, 363–367 (2011).
6. Delanghe, T., Dondelinger, Y. & Bertrand, M. J. M. RIPK1 Kinase-Dependent Death: A Symphony of Phosphorylation Events. *Trends Cell Biol.* **30**, 189–200 (2020).
7. Dillon, C. P. *et al.* RIPK1 blocks early postnatal lethality mediated by caspase-8 and RIPK3. *Cell* **157**, 1189–1202 (2014).
8. Kelliher, M. A. *et al.* The death domain kinase RIP mediates the TNF-induced NF-kappaB signal. *Immunity* **8**, 297–303 (1998).
9. Rickard, J. A. *et al.* RIPK1 regulates RIPK3-MLKL-driven systemic inflammation and emergency hematopoiesis. *Cell* **157**, 1175–1188 (2014).
10. Huyghe, J., Priem, D. & Bertrand, M. J. M. Cell death checkpoints in the TNF pathway. *Trends Immunol.* **44**, 628–643 (2023).
11. Kim, H.-E. *et al.* Tumour necrosis factor-α-induced glucose-stimulated insulin secretion inhibition in INS-1 cells is ascribed to a reduction of the glucose-stimulated Ca2+ influx. *J. Endocrinol.* **198**, 549–560 (2008).
12. Tai, N., Wong, F. S. & Wen, L. The role of the innate immune system in destruction of pancreatic beta cells in NOD mice and humans with type I diabetes. *J. Autoimmun.* **71**, 26–34 (2016).
13. Quattrin, T. *et al.* Golimumab and Beta-Cell Function in Youth with New-Onset Type 1 Diabetes. *N. Engl. J. Med.* **383**, 2007–2017 (2020).
14. Liang, H. *et al.* Blockade of tumor necrosis factor (TNF) receptor type 1-mediated TNF-alpha signaling protected Wistar rats from diet-induced obesity and insulin resistance. *Endocrinology* **149**, 2943–2951 (2008).
15. Borst, S. E. & Bagby, G. J. Neutralization of tumor necrosis factor reverses age-induced impairment of insulin responsiveness in skeletal muscle of Sprague-Dawley rats. *Metabolism* **51**, 1061–1064 (2002).
16. Uysal, K. T., Wiesbrock, S. M., Marino, M. W. & Hotamisligil, G. S. Protection from obesity-induced insulin resistance in mice lacking TNF-alpha function. *Nature* **389**, 610–614 (1997).
17. Karunakaran, D. *et al.* RIPK1 gene variants associate with obesity in humans and can be therapeutically silenced to reduce obesity in mice. *Nat Metab* **2**, 1113–1125 (2020).
18. Takiishi, T. *et al.* Inhibition of RIPK1 kinase does not affect diabetes development: β-Cells survive RIPK1 activation. *Mol Metab* **69**, 101681 (2023).
19. Xu, H. *et al.* The pseudokinase MLKL regulates hepatic insulin sensitivity independently of inflammation. *Mol Metab* **23**, 14–23 (2019).
20. Peltzer, N. *et al.* HOIP deficiency causes embryonic lethality by aberrant TNFR1-mediated endothelial cell death. *Cell Rep.* **9**, 153–165 (2014).
21. Newton, K., Sun, X. & Dixit, V. M. Kinase RIP3 Is Dispensable for Normal NF-κBs, Signaling by the B-Cell and T-Cell Receptors, Tumor Necrosis Factor Receptor 1, and Toll-Like Receptors 2 and 4. *Mol. Cell. Biol.* **24**, 1464–1469 (2004).
22. Salmena, L. *et al.* Essential role for caspase 8 in T-cell homeostasis and T-cell-mediated immunity. *Genes Dev.* **17**, 883–895 (2003).
23. el Marjou, F. *et al.* Tissue-specific and inducible Cre-mediated recombination in the gut epithelium. *Genesis* **39**, 186–193 (2004).
24. Stancill, J. S., Kasmani, M. Y., Khatun, A., Cui, W. & Corbett, J. A. Single-cell RNA sequencing of mouse islets exposed to proinflammatory cytokines. *Life Sci Alliance* **4**, (2021).

25. Polykratis, A. *et al.* Cutting edge: RIPK1 Kinase inactive mice are viable and protected from TNF-induced necroptosis in vivo. *J. Immunol.* **193**, 1539–1543 (2014).
26. Taraborrelli, L. *et al.* LUBAC prevents lethal dermatitis by inhibiting cell death induced by TNF, TRAIL and CD95L. *Nat. Commun.* **9**, 3910 (2018).
27. Shimizu, Y. *et al.* The Linear ubiquitin chain assembly complex acts as a liver tumor suppressor and inhibits hepatocyte apoptosis and hepatitis. *Hepatology* **65**, 1963–1978 (2017).
28. Sakamoto, Y. *et al.* Differential involvement of LUBAC-mediated linear ubiquitination in intestinal epithelial cells and macrophages during intestinal inflammation. *J. Pathol.* **259**, 304–317 (2023).
29. Dannappel, M. *et al.* RIPK1 maintains epithelial homeostasis by inhibiting apoptosis and necroptosis. *Nature* **513**, 90–94 (2014).
30. Takahashi, N. *et al.* RIPK1 ensures intestinal homeostasis by protecting the epithelium against apoptosis. *Nature* **513**, 95–99 (2014).
31. Ortis, F. *et al.* Cytokine-induced proapoptotic gene expression in insulin-producing cells is related to rapid, sustained, and nonoscillatory nuclear factor-kappaB activation. *Mol. Endocrinol.* **20**, 1867–1879 (2006).
32. McKenzie, M. D. *et al.* Proapoptotic BH3-only protein Bid is essential for death receptor-induced apoptosis of pancreatic beta-cells. *Diabetes* **57**, 1284–1292 (2008).
33. Liadis, N. *et al.* Distinct in vivo roles of caspase-8 in beta-cells in physiological and diabetes models. *Diabetes* **56**, 2302–2311 (2007).
34. Contreras, C. J. *et al.* RIPK1 and RIPK3 regulate TNFα-induced β-cell death in concert with caspase activity. *Mol Metab* **65**, 101582 (2022).
35. Zhao, Y. *et al.* Autoreactive T cells induce necrosis and not BCL-2-regulated or death receptor-mediated apoptosis or RIPK3-dependent necroptosis of transplanted islets in a mouse model of type 1 diabetes. *Diabetologia* **58**, 140–148 (2015).
36. Knight, R. R. *et al.* Human β-cell killing by autoreactive preproinsulin-specific CD8 T cells is predominantly granule-mediated with the potency dependent upon T-cell receptor avidity. *Diabetes* **62**, 205–213 (2013).
37. Apostolou, I., Hao, Z., Rajewsky, K. & von Boehmer, H. Effective destruction of Fas-deficient insulin-producing beta cells in type 1 diabetes. *J. Exp. Med.* **198**, 1103–1106 (2003).
38. Cottet, S. *et al.* cFLIP protein prevents tumor necrosis factor-alpha-mediated induction of caspase-8-dependent apoptosis in insulin-secreting betaTc-Tet cells. *Diabetes* **51**, 1805–1814 (2002).
39. Stewart, D. P. *et al.* Ubiquitin-independent degradation of antiapoptotic MCL-1. *Mol. Cell. Biol.* **30**, 3099–3110 (2010).
40. Meyerovich, K. *et al.* MCL-1 Is a Key Antiapoptotic Protein in Human and Rodent Pancreatic β-Cells. *Diabetes* **66**, 2446–2458 (2017).
41. Simpson, D. S. *et al.* Interferon-γ primes macrophages for pathogen ligand-induced killing via a caspase-8 and mitochondrial cell death pathway. *Immunity* **55**, 423–441.e9 (2022).
42. Dubey, M. *et al.* Nitric oxide-mediated apoptosis of neutrophils through caspase-8 and caspase-3-dependent mechanism. *Cell Death Dis.* **7**, e2348 (2016).
43. Oyadomari, S. *et al.* Nitric oxide-induced apoptosis in pancreatic β cells is mediated by the endoplasmic reticulum stress pathway. *Proceedings of the National Academy of Sciences* **98**, 10845–10850 (2001).
44. Liu, D. *et al.* Cytokines induce apoptosis in beta-cells isolated from mice lacking the inducible isoform of nitric oxide synthase (iNOS-/-). *Diabetes* **49**, 1116–1122 (2000).
45. Meyerovich, K., Ortis, F., Allagnat, F. & Cardozo, A. K. Endoplasmic reticulum stress and the unfolded protein response in pancreatic islet inflammation. *J. Mol. Endocrinol.* **57**, R1–R17 (2016).

5. Extended results

Pyroptosis is another cell death type which can promote inflammation through IL-1β and DAMP release. The fact that β-cells do not express RIPK3, an essential kinase for necroptosis induction, made us question whether β-cell also silence the expression of pyroptotic proteins. We therefore check the expression levels of pyroptotic proteins in β-cells using the same publicly available sc-RNA seq. GSDME (*Dfna5*) expression is basally low in β-cells and does not increase in response to cytokines (Figure C1-5). On the contrary, despite being basally low, GSDMD and Caspase1/8 expression increase in response to cytokines, suggesting that GSDMD-mediated pyroptosis may occur under inflammatory conditions.

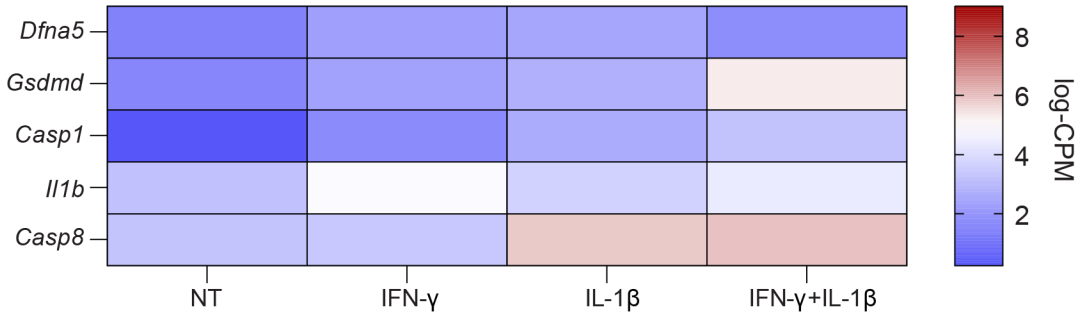

Figure CI-5. Expression of pyroptosis-related genes in β-cells. Pancreatic islets were treated with IL-1β, IFNγ, IL-1β + IFNγ for 6 hours. scRNA-seq dataset generated by Stancill et al.,[1] was re-analyzed for the expression of indicated pyroptosis-related genes.

6. Extended Discussion

TNF is a proinflammatory cytokine which can also induce cell death. While TNF has been linked to β-cell loss and dysfunction, the mechanism of TNF-induced cell death in β-cell is not well characterized. Moreover, the contribution of necroptosis to diabetes pathogenesis is not clear. In zebrafish, overnutrition led to RIPK3-dependent β-cell loss which was prevented by Nec-1s (RIPK1 inhibitor) and GSK'872 (RIPK3 inhibitor). Recently, it has been shown that RIPK3 deficiency protects from MLDSTZ-induced diabetes [2]. In contrast, in an islet transplantation model, RIPK3-deficient islets were as prone to T-cell killing as WT islets [3]. *Ripk1*$^{S25D/S25D}$ mice which are shown to be resistant to TNF-induced necroptosis were not protected from MLDSTZ-induced diabetes or HFD-feeding [4]. Our results also suggest that necroptosis does not play a significant role in autoimmune diabetes. We showed that *Ripk1*$^{D138N/D138N}$ mice are not protected from MLDSTZ-induced diabetes [5]. Moreover, primary islets subjected to TSZ (TNF + Smac mimetics + zVAD) *in vitro*, widely used necroptotic stimuli, do not induce cell death in islets despite RIPK1 being phosphorylated [4]. This finding

suggested that islets have a downstream mechanism protecting them from necroptosis. Indeed, our analysis of publicly available sc-RNA seq data shows that murine islet cells express very low levels of necroptotic proteins, RIPK3 and MLKL, which explains the lack of necroptotic arm in these cells [5]. However, we cannot exclude the possibility that RIPK3 can play a role in hematopoietic cells independent of its role in necroptosis. Indeed, there is growing evidence suggesting that RIPK3 have necroptosis-independent roles in inflammation [6,7]. This might explain the discrepancy between Conteras et al and our results.

In contrast to other cell types, we showed that the deficiency of RIPK1 or HOIP is not required for β-cell survival under basal conditions and under diabetic challenges [5]. We directly subjected control and RIPK1-deficient islets to apoptotic stimuli, TS (TNF + Smac mimetics) and found that islet cells are resistant to both TNF-induced apoptosis and necroptosis. sc-RNA seq suggested that this could potentially be explained by high levels of cFLIP vs low Caspase-8 expression. This appears to be specific to islet cells among other tissues which are sensitive to RIPK1 deficiency and TNF-induced cell death. Indeed, when we combined Cycloheximide (CHX) with TNF, we observed cell death which was blocked by both specific Caspase-8 or pan caspase inhibition. These results tempted us to speculate that cFLIP is the primary checkpoint of TNF signaling in β-cell. However, we cannot exclude the possibility that CHX targets also other short-lived proteins such as MCL-1 to trigger cell death. Indeed, MCL-1 was shown to protect β-cells from cytokine-induced cell death [8] . Interestingly, MCL-1 was found to be reduced in the β-cells of T1D patients [9]. Since cFLIP is one of the most important prosurvival proteins in extrinsic cell death pathways, it would be of significant interest to explore if the levels of cFLIP is altered in T1D patients. The downstream of other death receptors, FAS, and TRAIL, are also regulated by cFLIP-Caspase-8 heterodimers. Therefore, it raises the question whether β-cells or pancreatic islets are sensitive to cell death by FAS and TRAIL and if cFLIP depletion would sensitize them to cell death. The role of cFLIP in the regulation of β-cell death warrants further investigation.

Intriguingly, β-cell-specific Caspase-8 deficiency was shown to protect from MLDSTZ and HFD-induced diabetes suggesting that Caspase-8 is activated and plays a role in the pathogenesis of these diseases [10]. It is an open question how Caspase-8 gets activated in the presence of such high levels of cFLIP. One possible explanation is that under inflammatory conditions, elevated Caspase-8 expression may reach levels sufficient to bypass cFLIP-mediated protection. Indeed, sc-RNA data shows that IL-1β increases the expression level of Caspase-8 in β-cells. Therefore, a potential follow-up experiment could involve IL-1β pre-treatment before subjecting β-cells to TS (TNF + Smac mimetics). It would be interesting to investigate whether RIPK1 acts as a checkpoint of TNF signaling under these settings.

Reports also suggest that Caspase-8 can be activated in a NO-dependent manner [11,12]. Considering the prominent role of iNOS and NO reported in β-cell demise [13] and a sharp increase in its expression in response to cytokines, it is possible that NO can lead to cleavage of Caspase-8 bypassing the cFLIP protection. As previously explained, proinflammatory cytokine cocktail (IL-1β + IFNγ + TNF) is a potent inducer of cell death in pancreatic islets. The synergistic effect of IFNγ + TNF on cell death poses a big question also in the cell death field. A recent report suggested that the transcriptional upregulation of Caspase-8 levels in response to IFNγ + TNF levels mediate cell death in cancer cells [14]. By using a genetic screening, they identified ELAVL1 which sustains the levels of Caspase-8 via binding and stabilizing its mRNA. However, it is not known if Caspase-8 is activated in response to IL-1β + IFNγ + TNF treatment in β-cells. It would be very interesting to test if Caspase-8 is activated in cytokine-induced β-cell death and whether it is iNOS-dependent.

We and others showed that β-cells are resistant to TNF-induced cell death and they have a modest activation of NF-κB in response to TNF [4,5,15]. Therefore, it is an open question how TNF blockade improves glucose metabolism during diabetes. It has been shown that the deficiency of TNFR1 increases the number of T regulatory cells in NOD mice. Moreover, NOD mice lacking TNFR1 specifically in their islets are not protected from T-cell killing [16]. Taken together, these findings suggest that the protective effects of therapeutic TNF blockade may arise from the immune cells rather than the β-cells themselves.

In T1D, the classical view is that β-cells are attacked and killed by the immune system. In recent years, this view has been challenged since immunotherapies at best only delay T1D [17]. Therefore, it is proposed by some studies that β-cells are not only the victims of immune systems, but they also contribute to their own demise. One of the proposed mechanisms is the presentation of viral antigens by β-cells. It has been suggested that β-cell might be susceptible to viral infection during insulin secretion. Indeed, coxsackie and adenovirus infection was detected in some patients [18]. Therefore, it can be the case that the immune system is just doing its job by killing the infected β-cells. Another proposed mechanism is the presentation of neo-antigens by β-cells. Due to ER stress and increased levels of misfolded proteins, β-cells may present epitopes that are not native to the immune system. Therefore, the immune system might perceive them as non-self[17].

We hypothesize that β-cells contribute to their own demise simply by dying. It is widely accepted that cell death can be both cause and consequence of inflammation. We, therefore, hypothesize that inflammatory cell death types such as necroptosis and pyroptosis may feed the loop and contribute to β-cell demise. During the span of my PhD project, we and others showed that necroptosis does not happen in β-cells [4,5]. We also showed that this is due to the

very low to null expression of RIPK3 [5]. Interestingly, RIPK3 expression appears to be silenced in β-cells since treatment with IL-1β or IFNγ does not increase its expression. The role of pyroptosis in β-cell demise is not well characterized. Moreover, it is not known if β-cells have the machinery to undergo pyroptosis. Our sc-RNA analysis shows that β-cells express very low levels of pyroptotic proteins at the basal level. GSDME expression is low in β-cells, and it does not increase with cytokines. Therefore, it is unlikely that β-cells undergo GSDME-mediated pyroptosis. However, treatment with IL-1β and IFNγ increases the expression of GSDMD, Caspase1/8. Furthermore, it was shown that the GSDMD expression increases by two-fold in T1D patients [19]. Therefore, it is possible that, unlike necroptosis, pyroptosis might contribute to β-cell demise, warranting further investigation.

Outstanding questions

What is the role of cFLIP in β-cell homeostasis and during diabetes? Could the loss of cFLIP in β-cell trigger a metabolic disorder by causing spontaneous β-cell death?

If β-cells are resistant to TNF-induced cell death and potentially to other death receptors, why does β-cell-specific loss of Caspase-8 ameliorate MLDSTZ-induced diabetes? Through which mechanisms is Caspase-8 activated during diabetes?

β-cells are not sensitive to cIAP depletion or RIPK1 deficiency, suggesting that these do not act as checkpoints in β-cells. Can this be explained solely by the high expression of cFLIP versus the low expression of Caspase-8?

Does pyroptosis contribute to β-cell demise during diabetes? Could blockade of pyroptosis ameliorate diabetes onset and progression?

7. Author contribution

Önay Veli and **Prof. Nieves Peltzer** were responsible for securing the grant funding. The experimental design was developed by **Önay Veli** and **Prof. Nieves Peltzer**, while the majority of the experiments were conducted by **Önay Veli**. **Öykü Kaya** contributed to the immunofluorescence and immunohistochemistry staining procedures and their subsequent analysis. In vivo experiments were performed by **Önay Veli**, with assistance from **Ximena Hildebrandt** and **Öykü Kaya**. The analysis of sc-RNA sequencing datasets was carried out by **Ana Beatriz Varanda**. The islet viability assay and RT-qPCR were conducted in the Cardozo Lab at the Université libre de Bruxelles, Brussels, Belgium. These experiments were performed by **Peng Xiao**, **Erick Arroba**, **Anne Van Praet**, **Prof. Alessandra K. Cardozo**, and **Önay Veli**. **Matea Poggenberg** and **Dr. Alessandro Annibaldi** provided the Cflar; VillinCre-ERT2 samples. **Prof. Henning Walczak** provided the *Hoip*$^{fl/fl}$ mice, and **Prof. Manolis Pasparakis** supplied the *Ripk*$^{fl/fl}$ mice. Western blot analysis of the islets was performed by **Önay Veli**. The study was conceived by **Prof. Nieves Peltzer**. The manuscript was written by **Önay Veli** and **Prof. Nieves Peltzer**, with contributions from **Dr. Alessandro Annibaldi** and **Prof. Alessandra K. Cardozo.**

8. Extended Material & Methods

This section is provided as extended version of Material & Methods in Veli et al., included in the results section of this chapter [5]**.**

Table CI-1. List of general buffers and their composition used in this study.

	Buffers	Composition
Genotyping	Alkaline Lysis Buffer	25 mM NaOH, 0.2 mM EDTA
	Tris-HCl buffer	40 mM Tris-HCl, pH 5
	50X TAE buffer	2 M Tris, 50mM EDTA, 1 M Acetic acid
Histology	20X TBS	1M Tris base, 18% NaCl, pH 7.6
	1X TBS-T	1X TBS + 0.5 % Tween® 20
	Tris- EDTA buffer	10 mM Tris base, 1 mM EDTA, pH 9.5
Western Blot	10X TBS-T	1.5 M NaCl, 2M Tris, 0.1 % Tween® 20 pH 7.2
	10X Running Buffer	25 mM Tris base, 192 mM Glycine, 1 % SDS
	Blocking buffer	2.5 % Milk in TBST
	Primary antibody dilution buffer	2.5 % BSA in TBST

Table CI-2. List of chemicals and their corresponding suppliers used in general buffers.

Chemical	Supplier
NaOH	Carl Roth, 1CCX.2
Tris base	Fisher Scientific10376743
EDTA	Carl Roth, 8043.2
Acetic acid	Carl Roth, 6755.2
Tween® 20	Carl Roth, 9127.1
NaCl	Carl Roth, 3957.1
SDS	Carl Roth, 1057.1
Glycine	Carl Roth, 0079.4
Milk	Panreac AppliChem, A0830,500
BSA	Sigma-Aldrich, 3117057001

8.1. Mice

Ripk1$^{\beta\text{-}KO}$ and *Hoip*$^{\beta\text{-}KO}$ mice were generated by crossing *Ripk1*$^{fl/fl}$ (Dannappel et al., 2014) and *Hoip*$^{fl/fl20}$, respectively, with B6(Cg)-Ins1tm1.1(cre)Thor/J (Thorens et al., 2015) mice kindly gifted by Hans Stauss (UCL, London, UK). *Ripk1*^{D138N} mice were previously described and kindly provided by Manolis Pasparakis. (Polykratis et al., 2014). FFPE samples from *Ripk3/Caspase-8* double knockout (DKO) and *Cflar;VillinCre-ERT2* mice were provided by Henning Walczak and Alessandro Annibaldi, respectively[5, 21–23]. Mice were maintained in SPF animal facilities of CECAD research center, respecting 12-hour light and dark cycle. All experimental procedures were approved by local authorities (Landesamt für Natur, Umwelt und Verbraucherschutz Nordrhein-Westfalen) in Germany. For the genotyping of the mice, DNA was extracted by using alkaline lysis buffer (Table CI-1). The ear biopsies were incubated with 50 µl of alkaline lysis buffer at 95 °C for 30 mins. Then, the samples were neutralized with 50 µl Tris-HCl buffer (Table CI-1). For PCR reaction, 4 µl of polymerase, 4 µl MiliQ water, 0.5 µl 10 µM forward and reverse primer and 2 µl DNA was used (see Table CI-3 for the details for *Ripk1*$^{fl/fl}$*, Hoip*$^{fl/fl}$*, and Cre* primers and PCR programs). PCR products were separated by using 2 % agarose gel prepared with 1X TAE buffer (Table CI-1). GeneRuler 1 kb DNA Ladder (Thermo, SM0314) was used to determine the size of PCR products.

To withdraw blood at the endpoint, mice were injected with 100 mg/kg Ketamine and 20 mg/kg Xylazine (10 µl per 10 g, i.p.). Blood was collected by heart puncture after anesthesia. The blood serum was seperated by using Microvette® 500 Serum Gel CAT (Sarsted) and stored at -80 °C. The organs were fixed in neutral buffered 10 % Formalin solution (Sigma,

HT501128-4L) overnight at 4 °C. The following day, they were transferred into PBS and submitted to SFB1403 histology facility for paraffin embedding and sectioning.

Table CI-3. Genotyping protocol for *Ripk1$^{fl/fl}$*, *Hoip$^{fl/fl}$*, and *Cre*.

Target	Forward Primer (5 - 3)	Reverse Primer (5 - 3)	Band size	PCR Mastermix	PCR program (1-5)	Cycles (2-4)
Ripk1$^{fl/fl}$	CATGGCTGCAAACACCTAAA	GGGCAGTTACAACATGCAAA	Fl: 290 bp WT: 210 bp	AccuStart™ II GelTrack PCR SuperMix (VWR, 733-2239)	94 °C 2 min 94 °C 30 sec 58 °C 30 sec 72 °C 30 sec 72 °C 5 min	35
Hoip$^{fl/fl}$	CTCATTTGAATTCTATGATGC	GAAACAGGGACCAGGAGT	Fl: 650 bp WT: 500 bp	AccuStart™ II GelTrack PCR SuperMix (VWR, 733-2239)	95 °C 5 min 95 °C 30 sec 54 °C 30 sec 72 °C 60 sec 72 °C 7 min	33
Cre	TTGCCCCTGTTTCACTATCCAG	TGCTGTTTCACTGGTTATGCGG	Band present if positive for Cre	Red-Taq DNA-Polymerase 2X MasterMix VWR, 733-2546	95 °C 5 min 95 °C 30 sec 57 °C 30 sec 72 °C 60 sec 72 °C 7 min	33

8.2. Histology, Immunohistochemistry and Immunofluorescence

The slides were deparaffinized by using Histol (Carl Roth, 6640.4) 2 times for 5 minutes. Slides were rehydrated using decreasing grades of ethanol (100 %, 90 %, 70 %, 50 %). After a brief wash with distilled water, the slides were incubated in the appropriate antigen retrieval buffer for 10 mins (see Table CI-4). In this study, two types of antigen retrieval buffer were used, 1X citrate buffer pH 6 (commercially available, Sigma - Aldrich, C9999) and Tris - EDTA buffer pH 9.5 (Table CI-1). The type of antigen retrieval buffer that would be used for each antibody was decided during the optimization process and can be found in Table CI-4. After antigen retrieval in microwave with indicated antigen retriever and duration, the slides were left to cool down. The slides were washed with TBS and TBS-T for 5 minutes, respectively. The tissues were circled with a hydrophobic pen (BIOZOL, VEC-H-4000-Sample). Only for immunohistochemistry stainings, BLOXALL blocking solution (BIOZOL, VEC-H-4000) was used to block endogenous peroxidases. Then, tissues were permeabilized and blocked by 0.5% Triton-X (T8787, Sigma Aldrich) in Animal-Free Blocker (SP-5035-100, Vector Laboratories) and 0.3% Triton-X (T8787, Sigma Aldrich) in Animal-Free Blocker (SP-5035-100, Vector Laboratories). Tissues were incubated with antibodies of interest overnight at 4

°C (Table C1-4). The following day, slides were washed with TBS-T 3 times for 10 minutes. For immunofluorescence stainings, secondary antibodies were incubated for 1 hour at room temperature (Table CI-4) and then washed with TBS-T for 6 times 15 mins. Tissues were counterstained with DAPI (1 µg/ml) for 10 mins. Slides were mounted with ProLong Gold Antifade Mountant mounting media (P36934, Invitrogen). The images were acquired by using confocal microscope Stellaris 5, Leica Microsystems, provided by the CECAD imaging facility. The images were analyzed by QuPath0.4.0 and FIJI. For immunohistochemistry stainings, secondary antibodies were incubated for 30 mins at room temperature (Table CI-4) and then washed with TBS-T for 3 times 10 mins. Importantly, only for the double staining of insulin and CD45, the slides were first incubated with a rabbit secondary antibody (MP-7451 Vector Laboratories) and then a rat secondary antibody (MP-5404, Vector Laboratories) for 30 mins at RT. The color development was performed sequentially using a red alkaline phosphatase kit (BIOZOL, SK-5105) followed by the HIGHDEF® DAB Chromogen/Substrate Set (ENZ-ACC105-0200, Enzo). For the rest of the stainings, color was developed by using HIGHDEF® DAB Chromogen/Substrate Set (ENZ-ACC105-0200, Enzo) and counterstained with hematoxylin (BIOZOL, VEC-H-3401) for 3 mins. After dehydration with 100 % ethanol, slides were mounted with HIGHDEF IHC mount (Enzo Life Sciences, ADI-950-261-0030). The slides were scanned by slidescanner (Hamamatsu S360) provided by CECAD imaging facility. The insulin+ area was calculated by using QuPath0.4.0.

Table CI-4. Antibodies and antigen retrieval conditions for each staining.

	Target protein	Antibody	Antigen retrieval	Secondary antibody
Immunofluorescence	Insulin	1:100 5330-0104G, Bio-Rad	Citrate buffer, pH 6 5 mins in microwave	1:300 SA5-10094, Invitrogen
	Glucagon	1:100, C.S. 2760	Citrate buffer, pH 6 5 mins in microwave	1:300 A-11011, Invitrogen
	cl. Casp-3	1:50 C.S. 9661	Citrate buffer, pH 6 5 mins in microwave	1:300 A-11011, Invitrogen
	cFLIP	1:100 ab8421	Tris-EDTA buffer, pH 9.5 10 mins in microwave	1:300 A-1108, Invitrogen
Immunohistochemistry	Insulin	1:6400 C.S. C279	Citrate buffer, pH 6 5 mins in microwave	MP-7451 Vector Laboratories

	CD45	1:100 Thermofischer, 14-0451-82	Citrate buffer, pH 6 5 mins in microwave	MP-5404 Vector Laboratories
	Casp-8	1:200 ALX-804-447-C100	Tris-EDTA buffer, pH 9.5 10 mins in microwave	MP-7404 Vector Laboratories
	cFLIP	1:100 ab8421	Tris-EDTA buffer, pH 9.5 10 mins in microwave	MP-7451 Vector Laboratories

8.3. Pancreatic islet isolation

Mice were sacrificed by cervical dislocation and 3 mL collagenase solution (1 mg/ml) was injected through the bile duct for pancreas perfusion. After processing all the mice, pancreas was incubated in a shaking water bath at 37 °C for 17 mins. At the end of incubation, 20 ml of cold M199 medium (Gibco, 22350) with 10% FBS was added to stop the collagenase. The digested pancreas was spun at 250 RCF for 2 min at 4℃ with a break on setting. Then, the supernatants were carefully removed, and pellets were washed 3 times with M199 medium with 10% FBS. At the end of the wash, pellets were resuspended in 15 mL M199 medium with 10% FBS and passed through 100 µm wire mesh. After a centrifugation step, the pellets were resuspended in 10ml of Histopaque -1077 (Sigma,10771) and 10 mL M199 medium was added slowly, keeping the interphase sharp. A centrifugation step was carried at 1600 RCF for 20 min at 4°C with a break-off setting. After the centrifugation, the islets form a ring in the interface between the medium and the histopaque and the exocrine tissue is found in the pellet. The pellet was discarded and medium + histopaque was transferred to a new 50 ml tube. After adding M199 + 10 % FBS up to 45 mL, islets were spun down at 250 RCF for 2 min. After 2 washes, islets were picked up under a stereomicroscope and cultured in islet culturing medium. For the preparation of the islet culturing medium, Ham F10 medium (Gibco,11550043) supplemented with 10 mM glucose, 50 µM IBMX (Sigma 15879), 10% FBS, 50 U/ml penicillin, 50 µg/ml streptomycin (BioWhittaker 17-603/Lonza 17-603 E) and 2 mM glutaMAX (Gibco 35050-038).

8.4. Islet viability assay

For viability assay, the islets were transferred to Ham F10 medium (Gibco,11550043) supplemented with 10 mM glucose, 1% FBS, 50 U/ml penicillin, 50 µg/ml streptomycin (BioWhittaker 17-603/Lonza 17-603 E) and 2 mM glutaMAX (Gibco 35050-038). 10 islets per condition were seeded in 96-well plates (Thermo Scientific™, 243656). Islets were treated with the indicated concentrations in Table CI-5. 20 minutes before the evaluation of islet cell death,

PI and HO were added to the wells. The islet cell death was scored by using a fluorescence microscope by two independent researchers, and the results were represented as the average score from both assessments.

Table CI-5. Chemicals and cytokines used in the islet viability assay.

Chemical/Cytokine	Concentration	Supplier
SM	5 uM	Selleck Chemicals
zVAD-FMK	50 uM	Selleck Chemicals
CHX	5 ug/mL	Merck, C7698
zIETD-FMK	50 uM	Selleck Chemicals
TNF	1000 U/mL	R&D, MT-025
IFNγ	1000 U/mL	Peprotech,315-05
IL-1β	50 U/mL	R&D, 201-LB-005
Hoechst 33342	5 mg/ mL	Sigma-Aldrich
Propidium iodide	5 mg/ mL	Sigma-Aldrich

8.5. RT-qPCR

For qPCR analysis of primary islets, 50 islets were seeded per condition and treated with 1000 U/mL TNF for 6 hours. At the end of 6 hours, islets were collected and washed twice with cold PBS. For mRNA extraction, Dynabeads™ mRNA DIRECT™ Purification Kit (Thermofisher, 61012) was followed. Briefly, the islets were lysed in 200 µL of lysis/binding buffer. 12 µL of Dynabeads® Oligo(dT)25 was used for each condition. After the wash steps of the beads, 200 µL lysates were added into the tubes. This mixture was incubated at RT for 3-5 mins to allow the hybridization of polA tail and Oligo(dT)25 beads. Then, tubes were placed in DynaMag™-2 Magnet (Thermofisher). The supernatant was removed, and appropriate washes were carried out with Buffer A and Buffer B. mRNA elution was carried out with 20 µL of 10 mM Tris-HCl pH 7.5 (Elution Buffer). Reverse transcription was performed by using LunaScript RT SuperMix Kit (NEB E3010) according to the manufacturer's protocol. For RT-PCR, Luna Universal qPCR Master Mix (NEB M3003) was used. The primer list can be found in the Material & Methods section of Veli et al [5].

8.6. Western Blot (WB)

For WB analysis of primary islets, 100 islets were seeded per condition and treated with 1000 U/mL TNF for 10 mins or 24 hours as indicated in the figure legends. Following the treatment, islets were collected and washed twice with cold PBS. Islets were lysed in 40 µL of 30 mM Tris-Hcl, pH 7.5, 150 mM NaCl, 10 % glycerol, 1 % Triton X-100, 2 mM EDTA supplemented

with PhosSTOP and cOmplete™, Mini Protease Inhibitor Cocktail (Roche). The protein amount was quantified by using Pierce™ BCA® Protein Assay Kits (Thermo Scientific, 23227) and normalized to the lowest concentration. Following the denaturation step using 1X NuPAGE™ LDS Sample Buffer (4X) and DTT (20 mM), lysates were run using precast protein gels (4568084, Bio-rad) using running buffer for WB (Table CI-1). This was followed by transfer to the membrane (1704158, Bio-Rad) by using Trans-Blot® Turbo™ Transfer System (Bio-Rad). The membrane was blocked in blocking buffer (Table CI-1) for 1 hour at RT. Following the blocking step, the membrane was probed with the primary antibody (Table CI-6) diluted in primary antibody solution (Table CI-1) overnight at 4 °C. The following day, the membrane was washed with PBST- WB wash buffer (Table CI-1) 5 mins three times. Then, the membrane was incubated with the secondary antibody (Table CI-6) diluted in TBST WB wash buffer. Following three washes with PBST- WB wash buffer, the color was developed with ECL (PerkinElmer, NEL103001EA). The signal from the bands was developed by using X-ray films and western blot film developer.

Table CI-6: Antibodies and their corresponding dilutions used for WB analysis.

Protein	Primary Antibody	Secondary Antibody
RIPK1	1:1000 BD, 610459	1:10000 Mouse IgG2alpha SouthernBiotech
p-IκB	1:1000 C.S. 9246	1:10000 Mouse IgG1 SouthernBiotech
p-p65	1:1000 C.S. 3033	1:10000 Rabbit SouthernBiotech
NF-κB p65	1:1000 C.S. 8242	1:10000 Rabbit SouthernBiotech
Total IκB	1:1000 C.S. 9242	1:10000 Rabbit SouthernBiotech
RIPK3	1:1000 ab62344	1:10000 Rabbit SouthernBiotech
cFLIP	1:1000 ab8421	1:10000 Rabbit SouthernBiotech
cFLIP	1:1000 C.S. 56343	1:10000 Rabbit SouthernBiotech
Caspase-8	1:1000 MAB3429	1:10000 Rat SouthernBiotech
Insulin	1:300 BS-0862R	1:10000 Rabbit SouthernBiotech
Actin	1:10000 Sigma	1:10000 Mouse SouthernBiotech
GAPDH	1:10000 Sigma	1:10000 Rabbit SouthernBiotech

9. References

1. Stancill, J. S., Kasmani, M. Y., Khatun, A., Cui, W. & Corbett, J. A. Single-cell RNA sequencing of mouse islets exposed to proinflammatory cytokines. *Life Sci Alliance* **4**, (2021).
2. Contreras, C. J. *et al.* RIPK1 and RIPK3 regulate TNFα-induced β-cell death in concert with caspase activity. *Mol Metab* **65**, 101582 (2022).
3. Zhao, Y. *et al.* Autoreactive T cells induce necrosis and not BCL-2-regulated or death receptor-mediated apoptosis or RIPK3-dependent necroptosis of transplanted islets in a mouse model of type 1 diabetes. *Diabetologia* **58**, 140–148 (2015).
4. Takiishi, T. *et al.* Inhibition of RIPK1 kinase does not affect diabetes development: β-Cells survive RIPK1 activation. *Mol Metab* **69**, 101681 (2023).
5. Veli, Ö. *et al.* RIPK1 is dispensable for cell death regulation in β-cells during hyperglycemia. *Mol Metab* **87**, 101988 (2024).
6. Moriwaki, K. & Chan, F. K. M. Necrosis-dependent and independent signaling of the RIP kinases in inflammation. *Cytokine Growth Factor Rev.* **25**, 167–174 (2014).
7. Shlomovitz, I., Zargrian, S. & Gerlic, M. Mechanisms of RIPK3-induced inflammation. *Immunol. Cell Biol.* **95**, 166–172 (2017).
8. Meyerovich, K. *et al.* MCL-1 Is a Key Antiapoptotic Protein in Human and Rodent Pancreatic β-Cells. *Diabetes* **66**, 2446–2458 (2017).
9. Richardson, S. J., Leete, P., Bone, A. J., Foulis, A. K. & Morgan, N. G. Expression of the enteroviral capsid protein VP1 in the islet cells of patients with type 1 diabetes is associated with induction of protein kinase R and downregulation of Mcl-1. *Diabetologia* **56**, 185–193 (2013).
10. Liadis, N. *et al.* Distinct in vivo roles of caspase-8 in beta-cells in physiological and diabetes models. *Diabetes* **56**, 2302–2311 (2007).
11. Dubey, M. *et al.* Nitric oxide-mediated apoptosis of neutrophils through caspase-8 and caspase-3-dependent mechanism. *Cell Death Dis.* **7**, e2348 (2016).
12. Simpson, D. S. *et al.* Interferon-γ primes macrophages for pathogen ligand-induced killing via a caspase-8 and mitochondrial cell death pathway. *Immunity* **55**, 423–441.e9 (2022).
13. Corbett, J. A. *et al.* Nitric oxide production in islets from nonobese diabetic mice: aminoguanidine-sensitive and -resistant stages in the immunological diabetic process. *Proc. Natl. Acad. Sci. U. S. A.* **90**, 8992–8995 (1993).
14. Deng, B. *et al.* TNF and IFNγ-induced cell death requires IRF1 and ELAVL1 to promote CASP8 expression. *J. Cell Biol.* **223**, (2024).
15. Ortis, F. *et al.* Cytokine-induced proapoptotic gene expression in insulin-producing cells is related to rapid, sustained, and nonoscillatory nuclear factor-kappaB activation. *Mol. Endocrinol.* **20**, 1867–1879 (2006).
16. Chee, J. *et al.* TNF receptor 1 deficiency increases regulatory T cell function in nonobese diabetic mice. *J. Immunol.* **187**, 1702–1712 (2011).
17. Rodriguez-Calvo, T., Johnson, J. D., Overbergh, L. & Dunne, J. L. Neoepitopes in Type 1 Diabetes: Etiological Insights, Biomarkers and Therapeutic Targets. *Front. Immunol.* **12**, 667989 (2021).
18. Vehik, K. *et al.* Prospective virome analyses in young children at increased genetic risk for type 1 diabetes. *Nat. Med.* **25**, 1865–1872 (2019).
19. Colglazier, K. A., Mukherjee, N., Contreras, C. J. & Templin, A. T. RISING STARS: Evidence for established and emerging forms of β-cell death. *J. Endocrinol.* **262**, (2024).
20. Peltzer, N. *et al.* HOIP deficiency causes embryonic lethality by aberrant TNFR1-mediated endothelial cell death. *Cell Rep.* **9**, 153–165 (2014).
21. Newton, K., Sun, X. & Dixit, V. M. Kinase RIP3 Is Dispensable for Normal NF-κBs, Signaling by the B-Cell and T-Cell Receptors, Tumor Necrosis Factor Receptor 1, and Toll-Like Receptors 2 and 4. *Mol. Cell. Biol.* **24**, 1464–1469 (2004).
22. Salmena, L. *et al.* Essential role for caspase 8 in T-cell homeostasis and T-cell-mediated immunity. *Genes Dev.* **17**, 883–895 (2003).
23. el Marjou, F. *et al.* Tissue-specific and inducible Cre-mediated recombination in the gut epithelium. *Genesis* **39**, 186–193 (2004).

CHAPTER II

Characterizing the role of LUBAC in glycogen metabolism

In this chapter, I provide a detailed overview of the Linear Ubiquitin Assembly Complex (LUBAC). Mutations in different components of LUBAC have been linked to distinct pathological conditions, and I present an in-depth review of the clinical symptoms observed in patients with LUBAC deficiencies. Specifically, individuals with mutations in HOIP and HOIL-1 show toxic polyglucosan accumulation—less branched glycogen—in their muscles and heart, indicating a potential but yet unidentified role for LUBAC in glycogen metabolism. This chapter introduces a new project aimed at uncovering the molecular connection between LUBAC and glycogen metabolism, addressing this critical gap in our understanding. At the end of the chapter, I pose several key questions that arise from this project.

1. Introduction

1.1. Linear Ubiquitin Assembly Complex (LUBAC)

Ubiquitin is a small protein, consisting of 76 amino acids (~8.5 kDa). Ubiquitination is a post-translational modification, involved in nearly all cellular processes [1]. Ubiquitin can be attached to seven lysine residues of proteins — K7, K11, K27, K29, K33, K48, and K63. Additionally, it has been shown that methionine, serine and threonine can be ubiquitinated [2–4]. Proteins can be attached with a single ubiquitin (monoubiquitination) or polymeric ubiquitin chains (polyubiquitination) [5]. Importantly, polyubiquitin chains can be homotypic or heterotypic and branched. This gives rise to a vast "ubiquitin code," each serving as a different signal and regulating a plethora of cellular processes. Intriguingly, recent findings have shown that molecules such as LPS and glycogen, in addition to proteins, can also be ubiquitinated [6]. These findings broaden the range of cellular events regulated by ubiquitination.

Ubiquitination is a three-step enzymatic process which involves E1, E2 and E3 enzymes. Ubiquitin is first attached to an E1-activating enzyme, and this is an ATP-dependent reaction[7]. It is then transferred to an E2-ubiquitin conjugating enzyme. There are two types of E3 ligases. RING-type E3 ligases mediate the transfer of the ubiquitin directly to the substrate from the E2-conjugating enzyme. Whereas HECT-type E3 ligases act as intermediates in the ubiquitination process, where ubiquitin is first transferred to the HECT-type E3 ligase and then subsequently to the substrate [5].

Linear Ubiquitin Assembly Complex (LUBAC) is the only known E3 ligase that can conjugate linear ubiquitin (M1) chains [2]. LUBAC is composed of three subunits, HOIP, HOIL-1, and SHARPIN [8–10]. Crucially, both HOIP and HOIL-1 have E3 ligase activity (Figure CII-1). HOIP is the catalytic center of LUBAC since cells expressing catalytically inactive version of HOIP (C879S) completely abolish M1 chain formation [11]. Moreover, mice expressing this version of HOIP die embryonically around E11 similar to full deficiency of HOIP [12]. The embryonic lethality caused by HOIP was shown to be due to TNF-induced cell death. These findings showed that HOIP is the main catalytic component of LUBAC while raising questions about the function of HOIL-1 in the complex. The deficiency of HOIL-1 phenocopies the deficiency of HOIP [13]. The reason for this was nicely demonstrated by Peltzer et al. The authors showed that the UBL domain of HOIL-1 is essential for linear ubiquitination since it mediates the HOIP recruitment to the TNFR1 (Figure CII-1). Additionally, they showed that the NZF domain of HOIL-1 is critical for optimal LUBAC function by binding to M1 chains and ensuring LUBAC retention at TNFR1 (Figure CII-1). On the contrary, the cells bearing catalytic inactive HOIL-1 had augmented levels of linear ubiquitination [13]. Later, it was shown that HOIL-1 conjugates

monoubiquitin on itself and other LUBAC components [14]. This limits HOIP activity on other targets by making LUBAC components preferred substrates. Therefore, cells expressing a catalytically inactive version of HOIL-1 (C458S) have increased levels of M1 chains. Hence, while the loss of HOIL-1 catalytic activity causes sustained levels of M1 chains, the complete loss of HOIL-1 abrogates the M1 chain formation [13,14] (Figure CII-2). SHARPIN, the third component of the complex, does not have catalytic activity. Similarly, it also plays an important role in the stability of the complex. The loss of SHARPIN does not result in a complete loss of the LUBAC activity however, it significantly reduces it [13].

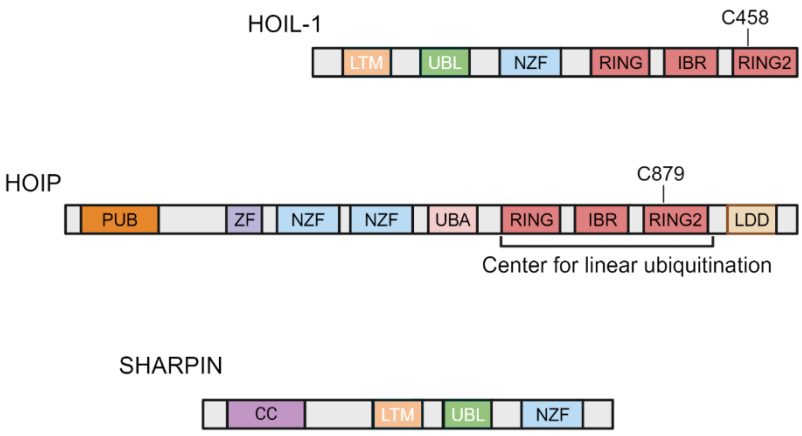

Figure CII-1. Domains of three LUBAC components, HOIP, HOIL-1, SHARPIN. LUBAC is composed of HOIP, HOIL-1 and SHARPIN. Both HOIP and HOIL-1 are RING- type E3 ligases however, HOIP is the center for linear ubiquitination. HOIL-1 and SHARPIN bind to HOIP via their UBL(Ubiquitin-like) domain. NZF (Npl4 Zinc Finger) domain of HOIL-1 is important for binding to M1 chains and retention of LUBAC at TNFR1 complex [1,13]. LTM: LUBAC-tethering motifs, PUB: PNGase/UBA or UBX-containing proteins, UBA: Ubiquitin-associated domains, LDD: Linear ubiquitin chain-determining domain, CC: Amino-terminal coiled-coil domain. Created with BioRender.

The role of LUBAC is extensively studied in innate immune and cytokine signaling [15]. LUBAC plays a key role by generating M1 chains downstream of various immune and cytokine receptors including TLRs, IL-1R and CD40 [1]. NEMO, an adaptor protein for the recruitment of IKKα/β, has 100-fold more affinity to M1 chains than K63 chains. Therefore, LUBAC function is essential for the effective activation of NF-κB. Moreover, LUBAC has a prosurvival function in TNF signaling by enabling NF-κB activation and preventing cell death [12,13]. The deficiency of HOIP and HOIL-1 in mice is embryonically lethal due to aberrant endothelial cell death [12,13]. SHARPIN deficiency causes chronic proliferative dermatitis phenotype (*cpdm*). These mice develop chronic dermatitis, liver inflammation, splenomegaly, etc [8–10]. Importantly, studies have shown that deficiencies in HOIP and HOIL-1 completely abolish linear chain formation in

response to TNF (Figure CII-2), while SHARPIN deficiency only reduces it [12,13]. This likely explains why SHARPIN deficiency leads to the *cpdm* phenotype, whereas HOIP and HOIL-1 deficiencies result in embryonic lethality. Notably, the *cpdm* phenotype can be rescued by the concomitant deletion of TNF or cross with *Ripk1*^{K45A} (RIPK1 kinase inactive) mice [9,16]. However, these interventions only delay the embryonic lethality caused by HOIP and HOIL-1 deficiencies. Full prevention of cell death, achieved by additional deletion of Caspase-8 and MLKL, is required for the survival of HOIP- and HOIL-1-deficient embryos [13].

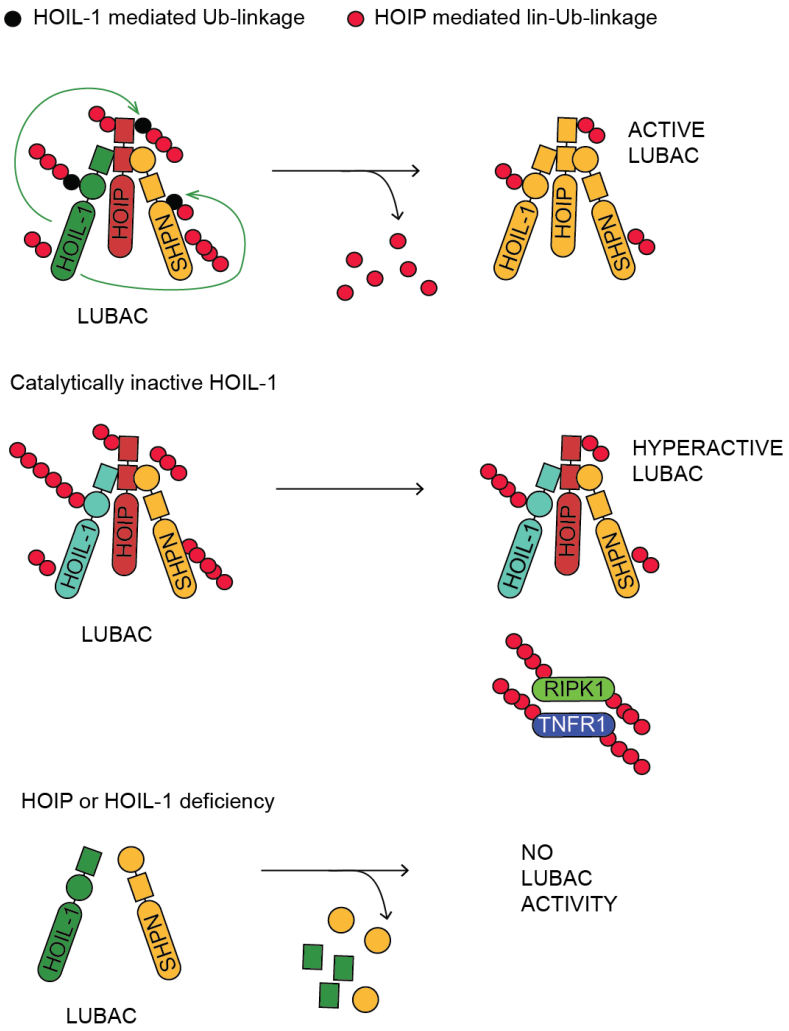

Figure CII-2. Schematic representation of LUBAC activity with different mutations. Under normal circumstances, HOIL-1 monoubiquitinates itself and other LUBAC components and HOIP further conjugates M1 chains. The monoubiquitination of the LUBAC components by HOIL-1 makes them preferred *cis* targets for HOIP-mediated linear ubiquitination. This limits the activity of HOIP on other *trans* targets. When HOIL-1 is catalytically inactive, HOIP continues to generate M1 chains on *trans* targets such as TNFR1 and RIPK1. Therefore, the catalytic activity of HOIL-1 is important for preventing the hyperactivity of LUBAC on trans targets. The deficiency of HOIL-1 or HOIP abrogates M1 chain formation.

The physiological importance of LUBAC and linear ubiquitination was further elucidated by patients who were reported to have mutations in different LUBAC components. Patients with HOIL-1 and HOIP mutations commonly develop autoinflammation, immunodeficiency, and amylopectinosis [17–19]. Amylopectinosis is a glycogen storage disease, characterized by a toxic accumulation of polyglucosan bodies in skeletal muscle, heart, and liver [20]. Recently, two SHARPIN-deficient patients were identified. These patients also presented with autoinflammation and immunodeficiency [21]. Although in a broad definition, LUBAC-deficient patients suffer from autoinflammation and immunodeficiency, each patient has different clinical manifestations. Therefore, mutations in different patients are discussed below in detail.

1.2. LUBAC deficiency in humans

1.2.1. Mutations in HOIP

Two patients with HOIP (RNF31) mutations have been reported [17,19]. In the first case of HOIP deficiency, the patient presented with autoinflammation in multiple organs, lymphangiectasia, weakness at the lower extremities, amylopectinosis, chronic diarrhea, and recurrent viral and bacterial infections due to immunodeficiency and defects in T-cell function [19]. Additional molecular analysis showed that the patient carries a missense mutation (L72P) in the PUB domain of HOIP which is shown to be important for OTULIN and CYLD binding [19,22,23]. This mutation is shown to impair the expression of HOIP leading to loss of expression [19]. Fibroblasts from the patient showed impaired NF-κB activation in response to TNF and IL-1β [19]. B cells isolated from the patient did not respond to CD40L and monocytes showed enhanced response to IL-1β stimulation [19]. Importantly, the biopsy from the sternocleidomastoid muscle showed PAS-positive patches of amylopectin-like depositions resistant to amylase treatment. However, there were no signs of myopathy or cardiomyopathy after further clinical examinations [19].

In the second case of HOIP deficiency, the patient presented with polyarticular juvenile idiopathic arthritis, recurrent fever, and bacterial, viral, and fungal infections [17]. Unlike the first patient, this patient showed no signs of lymphangiectasia [17]. The patient was identified with two single nucleotide variants in RNF31 (c.1197G>C; p.Q399H and c.1737+3A>G) which gave rise to aberrantly spliced variants [17]. The mutations abolished the binding of HOIP to SHARPIN and HOIL-1, thereby affecting the stability of LUBAC [17]. Following the first case of HOIP deficiency, peripheral blood mononuclear cells (PBMCs) from this patient showed impaired activation of NF-κB in response to TNF [17]. This patient was not examined for amylopectinosis due to the lack of clinical manifestations [17].

1.2.2. Mutations in HOIL-1

Numerous reports have been published on *RBCK1* (gene coding for HOIL-1) mutations. The first report describes three patients from two unrelated families [18]. Similar to HOIP-deficient patients, HOIL-1-deficient patients presented with autoinflammation, immunodeficiency, and amylopectinosis. The patients suffered from invasive pyogenic bacterial infections. Patient 1 (P1) and Patient 2 (P2) are siblings and were heterozygous for deletion from their mother spanning the first four exons of *HOIL1* (Table CII-1). P1 and P2 were also heterozygous for a paternally derived nonsense mutation (c.553C>T) which causes premature stop codon in exon 5 (mid-domain of the protein) [18]. By contrast, Patient (P3) bears a homozygous deletion in exon 2 (N-terminal) of *HOIL1* which causes frameshift and premature stop codon. The mutation causes the deletion of all functional domains of HOIL-1 [18]. The level of *HOIL1* mRNA was significantly reduced in the fibroblast isolated from the patients and HOIL-1 was undetectable at the protein level by immunoblot analysis [18]. Moreover, the deficiency of HOIL-1 affected the stability of other LUBAC components, HOIP and SHARPIN [18]. These results suggested that HOIL-1 is essential for LUBAC stability and function also in humans. Patient-derived fibroblast showed attenuated NF-κB activation in response to IL-1β and TNF. In contrast, PBMCs and monocytes showed hypersensitivity to IL-1β suggesting that HOIL-1 and LUBAC are essential for optimal NF-κB activation. Importantly, the patients showed myopathy and cardiomyopathy due to amylopectin-like deposits in their muscles [18]. Phadke et al. also reported patients with HOIL-1 mutations. Curiously, among these patients, only the patient bearing a mutation in the N-terminal of HOIL-1 showed signs of immunodeficiency in addition to myopathy and cardiomyopathy due to amylopectin-like deposits (polyglucosan bodies) [24]. Other patients carrying mutations in the C-terminal and mid-domain of HOIL-1 only showed signs of myopathy and cardiomyopathy due to amylopectin-like deposits [24]. These findings suggest that mutations in the C-terminal and mid-domains of HOIL-1 result in amylopectinosis, also known as polyglucosan body accumulation, while mutations in the N-terminal region additionally lead to immunodeficiency and autoinflammation. Indeed, other reports described patients only with myopathy and cardiomyopathy due to polyglucosan accumulation [25–28]. Among twenty-four patients identified, three patients with N-terminal mutations presented with immunodeficiency as their primary symptom (Table CII-1). Twenty of the patients with mid-domain and C-terminal presented with muscle weakness and nineteen of them presented with cardiomyopathy (Table CII-1). Exceptionally, Krenn et al reported two patients with mid-domain mutations. These patients mainly suffered from myopathy and cardiomyopathy but differently from the other patients with mid-domain or C-terminal mutations, they also had mild symptoms of immunodeficiency [28]. However, it is not well understood why different mutations give rise to different disease manifestations. In the latest literature, the disease caused by

HOIL-1 deficiency is named RBCK1-associated polyglucosan body myopathy-1 (PGBM1). PGBM1 is defined as an autosomal recessive rare genetic disorder which leads to myopathy and cardiomyopathy due to the accumulation of toxic polyglucosan bodies. Patients may also have signs of immunodeficiency and autoinflammation [29]. It is important to note that patients with HOIL-1 mutations often had a mild increase in ALT and AST levels, and hepatomegaly, suggesting that the liver is also affected by the deficiency of HOIL-1 [18,26,28,30,31].

Table CII-1. Clinical findings of patients with different HOIL-1 mutations.

	Patient	Sex	Initial symptom	Skeletal muscle	Cardiac muscle	ID	AI	Mutation
1	[18]	Female	Infections	Myopathy	Dilated Cardiomyopathy	+	+	N-terminal (deletion of E1-4) Mid-domain E5 (nonsense)
2	[18]	Female	Infections	Myopathy	Cardiomyopathy	+	+	N-terminal (deletion of E1-4) Mid-domain E5 (nonsense)
3	[18]	Male	Infections	-	Dilated Cardiomyopathy	+	+	N-terminal E2 (frameshift)
4	[32]	Female	Delayed motor development	Myopathy	Dilated Cardiomyopathy	+	+	Mid-domain E6 (frameshift)
5	[32]	Female	Muscle weakness, breathlessness	Wheelchair	Cardiomyopathy	+	-	Mid-domain E6 (frameshift)
6	[32]	Male	Abdominal Pain	Difficulty in walking	Cardiomyopathy	-	-	Mid-domain E7 (nonsense) C-terminal E12 (frameshift)
7	[32].	Male	Muscle weakness, learning difficulties	Skeletal and respiratory myopathy	Cardiomyopathy	-	+	Mid-domain E7 (frameshift) C-terminal E12 (frameshift)
8	[26]	Female	Leg weakness	Leg weakness	Dilated Cardiomyopathy	-	+	Mid-domain E6 (truncation) Mid-domain E9 (missense)
9	[26]	Female	Leg weakness	Leg weakness	N/A	-	+	Mid-domain E6 (non-sense) Mid-domain E9 (missense)

	Patient	Sex	Initial symptom	Skeletal muscle	Cardiac muscle	ID	AI	Mutation
10	[26]	Female	Leg weakness	Leg weakness	Cardiomyopathy	-	-	Mid-domain E7 (frameshift)
11	[26]	Male	Running difficulty	Running difficulty	Dilated Cardiomyopathy	-	-	Mid-domain E7 (frameshift)
12	[26]	Male	Running difficulty	-	Dilated Cardiomyopathy	-	+	Mid-domain E6 (frameshift)
13	[26]	Male	N/A	-	Dilated Cardiomyopathy	-	-	N-terminal E2 (missense)
14	[26]	Male	Running difficulty	Wheelchair	Dilated Cardiomyopathy	-	+	Mid-domain E6 (frameshift) N-terminal (deletion of E1-4)
15	[26]	Male	Leg weakness	-	Dilated Cardiomyopathy	-	-	Mid-domain E9 (missense)
16	[26]	Female	Leg weakness	Myopathy	Dilated Cardiomyopathy	-	-	Mid-domain E7 (frameshift)
17	[26]	Male	Running difficulty	Difficulty in walking	Dilated Cardiomyopathy	-	-	Mid-domain E5 (frameshift)
18	[25]	Male	N/A	Myopathy	Cardiomyopathy	-	-	Mid-domain E5 (frameshift) Mid-domain E6 (nonsense)
19	[25]	Female	N/A	Myopathy	Cardiomyopathy	-	-	Mid-domain E5 (frameshift) Mid-domain E6 (truncation)
20	[25]	N/A	N/A	Myopathy	Cardiomyopathy	-	-	Mid-domain E5 Splicing variant
21	[28]	Female	Dyspnea	Mild myopathy	Cardiomyopathy	+	+	Mid-domain E7 (frameshift)
22	[28]	Female	Dilated Cardiomyopathy	Myopathy	Dilated Cardiomyopathy	+	+	Mid-domain E7 (frameshift)
23	[33]	Male	Leg weakness	Myopathy	-	-	-	Mid-domain E7 (frameshift)
24	[30]	Female	Exercise intolerance, liver enlargement	-	-	-	-	Mid-domain E7 (frameshift)

ID, AI, N/A stands for immunodeficiency, autoinflammation and not available, respectively.

1.2.3. Mutations in SHARPIN

Oda and colleagues reported two patients with SHARPIN mutations [21]. Unexpectedly, these patients did not show dermatological phenotypes different from SHARPIN-deficient *cpdm* mice. Patients commonly showed autoinflammatory symptoms such as fever. Patient 1 (P1) developed fever, joint inflammation, colitis and chronic otitis. P2 had fever episodes and lymphadenopathy. Fibroblasts from P1 had impaired NF-κB activation in response to TNF. Moreover, fibroblasts from P1 were sensitive to TNF-induced cell death as compared to fibroblasts from controls.

1.3. Glycogen and glycogen storage diseases

1.3.1. Regulation of glycogen metabolism

Glycogen is a highly branched glucose polymer that serves as a glucose reservoir in the body in case of need. It is mainly stored in the liver and skeletal muscle [34]. The liver uses glycogen to supply glucose into the bloodstream when blood glucose is under normal range. The skeletal muscle uses glycogen as an energy source during contraction. Other organs such as the heart and brain store small amounts of glycogen, however, the function of glycogen in these tissues is not well understood.

Glycogen synthesis and breakdown in the liver are mainly regulated by insulin and glucagon hormones that are secreted by pancreatic islets [35]. Insulin is secreted when the blood glucose is above normal range and stimulates glycogen synthesis in the liver. Insulin controls glycogen synthesis in two different mechanisms. It increases the glucose uptake by the cells which allosterically activates glycogen synthase. Of note, glycogen synthase has two forms. While GYS1 is expressed by muscle, GYS2 is expressed by the liver. Insulin promotes the dephosphorylation of glycogen synthase which is normally phosphorylated and inactivated by GSK3 [36]. In contrast to insulin, glucagon is secreted when blood glucose is below the normal range and stimulates glycogen breakdown (glycogenolysis). In this pathway, PKA activates glycogen phosphorylase kinase which in turn phosphorylates and activates GP to start glycogenolysis. G6Pase is the enzyme responsible for converting glucose-6-phosphate into glucose, which can then exit the cell via glucose transporters to supply other tissues with glucose. Glucagon also suppresses glycogen synthesis by inhibiting the activation of glycogen synthase [37].

The regulation of glycogen metabolism in muscle is slightly different from that in the liver. The glycogen in skeletal muscle is used as an energy supply during muscle contraction. Unlike in the liver, glucagon does not stimulate glycogenolysis in skeletal muscle since it lacks

expression of glucagon receptors [38]. Instead, muscle glycogen phosphorylase kinase increases its activity in the presence of calcium released to the cytoplasm during contraction [37]. Moreover, different from the liver, glucose released by glycogenolysis in myocytes (muscle cells) cannot be used by other organs. Since skeletal muscle lacks the expression of this enzyme, the glucose-6-phosphate is only used by myocytes [39].

1.3.2. Glycogen synthesis and breakdown

Glycogen synthesis requires the concerted action of multiple enzymes. When glucose enters the cell via glucose transporters (GLUTs), it is converted to UDP-glucose via sequential action of numerous enzymes [34]. Then, Glycogenin autoglycosylates itself and forms a short oligosaccharide which is then further elongated by GYS via 1→ 4 glycosidic bonds. GBE adds branches to glycogen molecules via 1→ 6 glycosidic bonds. The formation of branch points by GBE ensures the solubility of glycogen molecules (Figure CII-3).

Glycogen breakdown, also known as glycogenolysis, can take place both in cytosol and lysosomes [40]. In the cytosol, GP phosphorylates glycogen and releases glucose-1-phosphate from the non-reducing ends (Figure CII-3). Glucose-1-phosphate is then converted to glucose-6-phosphate by hexokinase. The glycogen debranching enzyme transfers four glucose residues to neighbouring branches. The 1, 6 debranching enzyme cleaves the remaining 1→ 6 glycosidic bonds and frees a glucose molecule (Figure CII-3). In lysosomes, the glycogen breakdown is achieved via GAA (Figure CII-3). Importantly, there is no debranching enzyme in lysosomes, therefore GAA is responsible for the cleavage of both 1→ 4 and 1→ 6 glycosidic bonds [34].

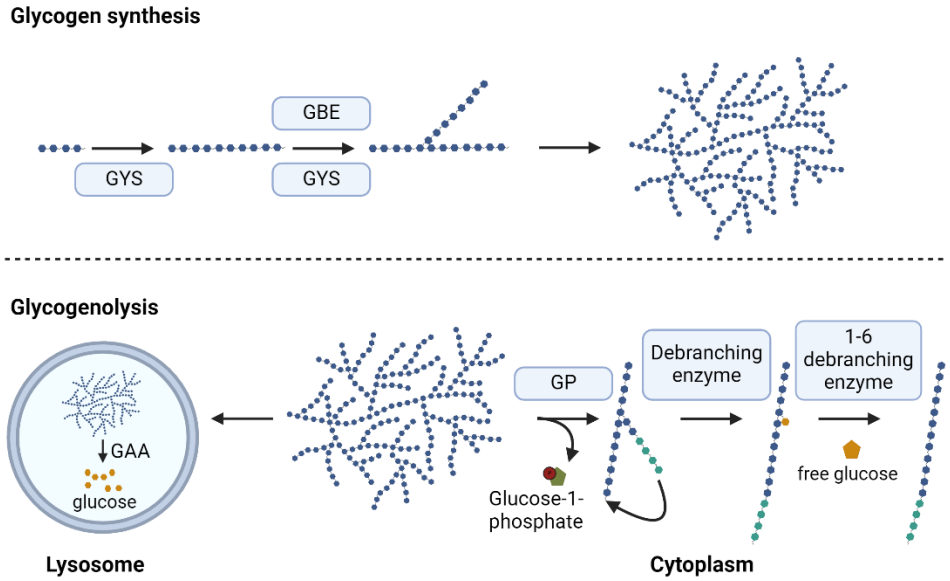

Figure CII-3. An overview of glycogen synthesis and glycogenolysis. Glycogen synthase (GYS)

elongates the chain via a 1→ 4 glycosidic bond. GBE adds branches to the glucose chain via 1→ 6 glycosidic bonds. The concerted action of GYS and GBE ensures the solubility of glycogen molecules. For glycogenolysis, GP phosphorylates glycogen and releases glucose-1-phosphate. The debranching enzyme transfers glucose residues to the neighboring branch. The 1-6 debranching enzyme cleaves the remaining glucose residue, releasing a glucose molecule. Besides cytoplasm, glycogen breakdown can also take place in lysosomes. Importantly, GAA is responsible for the hydrolysis of glycogen into glucose within lysosomes. Created with BioRender.

1.3.3. Glycogen storage diseases and polyglucosan bodies

Mutations in the enzymes that regulate glycogen synthesis or breakdown lead to glycogen storage diseases (GSD) [40]. Glycogen storage diseases (GSDs) primarily affect the liver, skeletal muscles, and heart, but other tissues, such as the kidneys and brain, can also be impacted. Importantly, there are at least nineteen different types of glycogen storage diseases classified according to the affected gene. For example, the deficiency of GYS2 (liver glycogen synthase) is named GSD type 0a. It causes decreased levels of glycogen in the liver, resulting in hypoglycemia [41]. The deficiency of GYS1 (muscle glycogen synthase) is called GSD type 0b. It leads to a reduction of glycogen levels in muscle and heart, resulting in muscle weakness and cardiac arrest [42]. The deficiency of GAA is called GSD type II, also known as Pompe disease. In this disease, glycogen accumulates in lysosomes, resulting in muscle weakness and respiratory failure [43].

The term “polyglucosan body” refers to the accumulation of less-branched glycogen molecules in the cells [44]. Polyglucosan bodies react with Periodic acid-Schiff (PAS) staining and are resistant to amylase treatment, unlike normally branched glycogen molecules. In certain types of GSDs, the accumulation of polyglucosan bodies can be observed in several organs. GSD type IV, also known as Andersen disease, is one of the most studied GSDs with polyglucosan accumulation and occurs due to mutations in the *GBE* gene [45]. It can manifest at different ages with a variety of symptoms including hepatic, cardiac, myopathic and neurological involvement. Unfortunately, this disease can cause premature death. Crucially, mutations in Malin (an E3 ligase) and Lafora (a glycan phosphatase) can lead to polyglucosan accumulation and a GSD, known as Lafora disease [46]. Lafora disease mostly affects neurons and the brain, causing cognitive decline, dementia and ataxia. It is currently not well understood how Malin and Lafora regulate glycogen metabolism. However, it is widely accepted that Lafora is a glycogen phosphatase. Malin is an E3 ligase, and it has been shown that it ubiquitinates several proteins that play a role in glycogen metabolism, such as Lafora, and GYS [47]. However, the exact role of Malin in glycogen metabolism remains to be elucidated. Other genes that cause polyglucosan body accumulation are listed in Table CII-2. Crucially,

the deficiency of HOIP, another subunit of LUBAC, was also reported to cause polyglucosan accumulation in one out of two identified patients. These findings suggest LUBAC plays a yet unidentified role in the regulation of glycogen metabolism.

Table CII-2. Mutations associated with polyglucosan accumulation.

Genes	Protein	Disorder	Clinical Manifestation
RBCK1	HOIL-1	Polyglucosan body myopathy-1 (PGBM1)	Myopathy and cardiomyopathy with/out immunodeficiency
EPM2A *NHLRC1*	Lafora Malin	Lafora disease	Neurodegenerative disorder with cognitive decline, ataxia, dementia
GYG1	Glycogenin	Glycogen storage disease XV (GSD XV)	Dilated cardiomyopathy Skeletal myopathy
PFKM	6-Phosphofructokinase	Glycogen storage disease VII (GSD VII)	Exercise intolerance Polyglucosan accumulation in some cases
PRKAG2	AMPK subunit gamma 2	Wolff-Parkinson-White syndrome	Polyglucosan deposition in cardiac muscle

Adapted from [48].

2. Aims of the study

There is growing evidence that, besides its role in immune signaling and cell death, LUBAC also regulates metabolism. Notably, the deficiencies of HOIP and HOIL-1, two components of LUBAC, have been linked to the accumulation of polyglucosan bodies in the skeletal and cardiac muscle. Currently, there is no treatment for myopathy and cardiomyopathy caused by polyglucosan bodies [29]. The patients require heart transplantation and have limited movement capacity due to muscle weakness. Unfortunately, this disease may cause premature death.

There is an urgent medical need to characterize the role of LUBAC in the regulation of glycogen metabolism. Therefore, we generated a mouse model, lacking the main catalytic subunit of LUBAC, HOIP, specifically in skeletal and cardiac muscle (*Hoip*$^{Muscle\text{-}KO}$). We showed that the muscle-specific deletion causes polyglucosan accumulation, particularly in the heart. In addition to the detailed phenotypic characterization of *Hoip*$^{Muscle\text{-}KO}$ mice, the primary aim of this project is to uncover the precise molecular mechanism by which LUBAC regulates glycogen metabolism, ultimately identifying therapeutically actionable targets.

3. Results

To study the role of LUBAC in muscle, we generated a mouse line that lacks HOIP, the catalytically active component of LUBAC, specifically in skeletal and cardiac muscle tissue by crossing *Hoip fl/fl* and *Ckmm-Cre* (*Hoip*$^{Muscle\text{-}KO}$) mice [12,49]. *Hoip*$^{Muscle\text{-}KO}$ mice are viable and do not show any overt phenotype until 21 months of age, the oldest mouse in the cages. We investigated the effect of muscle-specific LUBAC deficiency in mature or old mice. The initial cohort we analyzed consisted of female mice aged 7 to 8 months. The weight did not differ between control and *Hoip*$^{Muscle\text{-}KO}$ mice (Figure CII-4a). Moreover, we did not detect any gross differences such as immune infiltration in the H&E stainings of the heart of control and *Hoip*$^{Muscle\text{-}KO}$ mice (Figure CII-4b). However, since LUBAC is an important regulator of cell death and inflammation, a more detailed analysis for immune infiltration is needed [12,13,50]. Therefore, we will perform CD45 (pan-immune cell marker) and CD68 (pan-macrophage marker) stainings to evaluate the possibility of inflammation in the heart of *Hoip*$^{Muscle\text{-}KO}$ mice. Unlike glycogen, polyglucosan bodies are resistant to diastase digestion, which involves enzymes that catalyze the breakdown of starch into maltose [51]. Periodic acid-Schiff (PAS) which stains carbohydrates such as glycogen or glycoproteins, is a widely used diagnostic method for detecting polyglucosan bodies. If PAS-positive material is still detected after diastase digestion, this would suggest the presence of polyglucosan bodies [48]. We performed a diastase digestion before PAS (Periodic acid-Schiff) staining. Unlike controls, *Hoip*$^{Muscle\text{-}KO}$ mice showed polyglucosan deposition in their heart that is resistant to diastase digestion (Figure CII-4b). GYS1 is responsible for 1→ 4 glycosidic bond formation between glucose molecules during glycogen synthesis. It has been shown that GYS1 is sequestered and inactivated in the polyglucosan bodies [52]. Therefore, GYS1 can be used as a marker for polyglucosan bodies. We did a GYS1-glycogen co-staining in the heart of control and *Hoip*$^{Muscle\text{-}KO}$ mice (Figure CII-4c). We showed that indeed GYS1 and glycogen colocalize (Figure CII-4d). Hence, we can unmistakably conclude that HOIP deficiency in muscle leads to accumulation of toxic polyglucosan bodies in the heart and potentially other muscle tissues. Considering the role of HOIP in cell death regulation, we performed a TUNEL staining to look at the cell death levels in the heart of control and *Hoip*$^{Muscle\text{-}KO}$ mice (Figure CII-4d). Interestingly, we observed significantly more TUNEL+ nuclei in *Hoip*$^{Muscle\text{-}KO}$ mice compared to controls (Figure CII-4d).

Since LUBAC-deficient patients suffer from myopathy, we also analyzed the quadriceps, a major skeletal muscle group. We did not detect any gross differences in the H&E staining of the quadriceps between control and *Hoip*$^{Muscle\text{-}KO}$ mice (Figure CII-5a). Surprisingly, we detected only minimal diastase-resistant PAS-reactive material in the quadriceps of one out

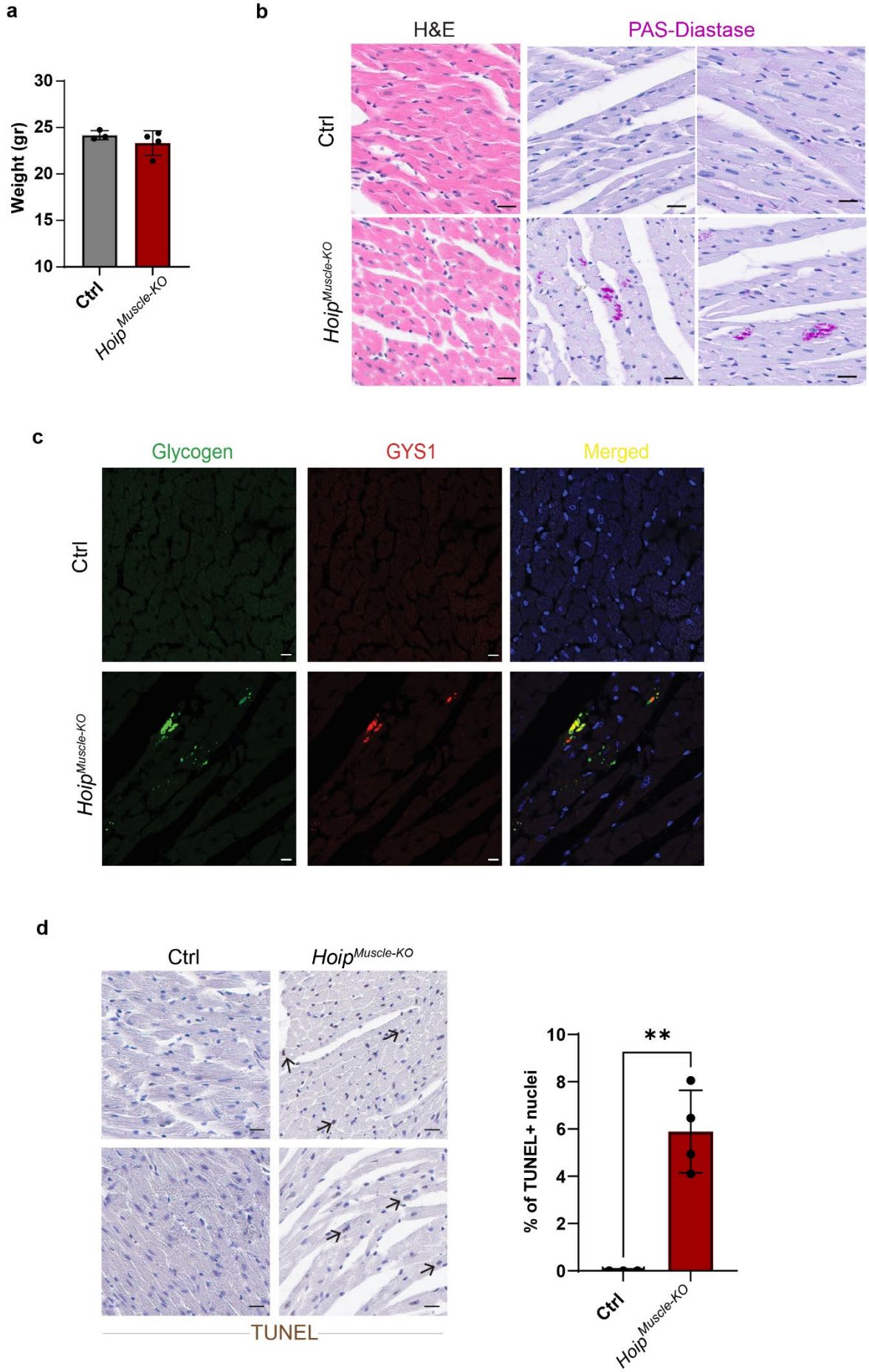
a
Weight (gr)
30
25
20
15
10
Ctrl
Hoip Muscle-KO
b
H&E
PAS-Diastase
Ctrl
Hoip Muscle-KO
c
Glycogen
GYS1
Merged
Ctrl
Hoip Muscle-KO
d
Ctrl
Hoip Muscle-KO
TUNEL
% of TUNEL+ nuclei
10
8
6
4
2
0
**
Ctrl
Hoip Muscle-KO

Figure CII-4. HOIP deficiency in muscle leads to the accumulation of polyglucosan bodies in the heart. a. The weight of 7-8 months female control and *Hoip*$^{Muscle\text{-}KO}$ mice (n=3-4 per group). **b.** H&E and PAS-D staining in the heart control and *Hoip*$^{Muscle\text{-}KO}$ mice. **c.** GYS1 and glycogen co-staining the heart control and *Hoip*$^{Muscle\text{-}KO}$ mice. **d.** TUNEL staining in the heart control and *Hoip*$^{Muscle\text{-}KO}$ mice. Scale bars represent 10 µM for GYS1 and glycogen co-staning. Scale bars represent 20 µM for PAS-Diastase and TUNEL staining. Means ± SD. Unpaired t-test (a,d).

of the four *Hoip*$^{Muscle\text{-}KO}$ mice. Moreover, unlike in the heart, we did not observe any cell death in the quadriceps (Figure CII-5b). Of note, we detected TUNEL-positive nuclei only in the positive control, which was treated with DNase I before TUNEL staining, ensuring that the staining was successfully performed. These results suggest that polyglucosan accumulation in the heart occurs earlier than in skeletal muscle and that the heart may be more affected than skeletal muscle, at least in our model. However, this finding needs to be investigated in more detail, across different life stages and in larger cohorts of mice.

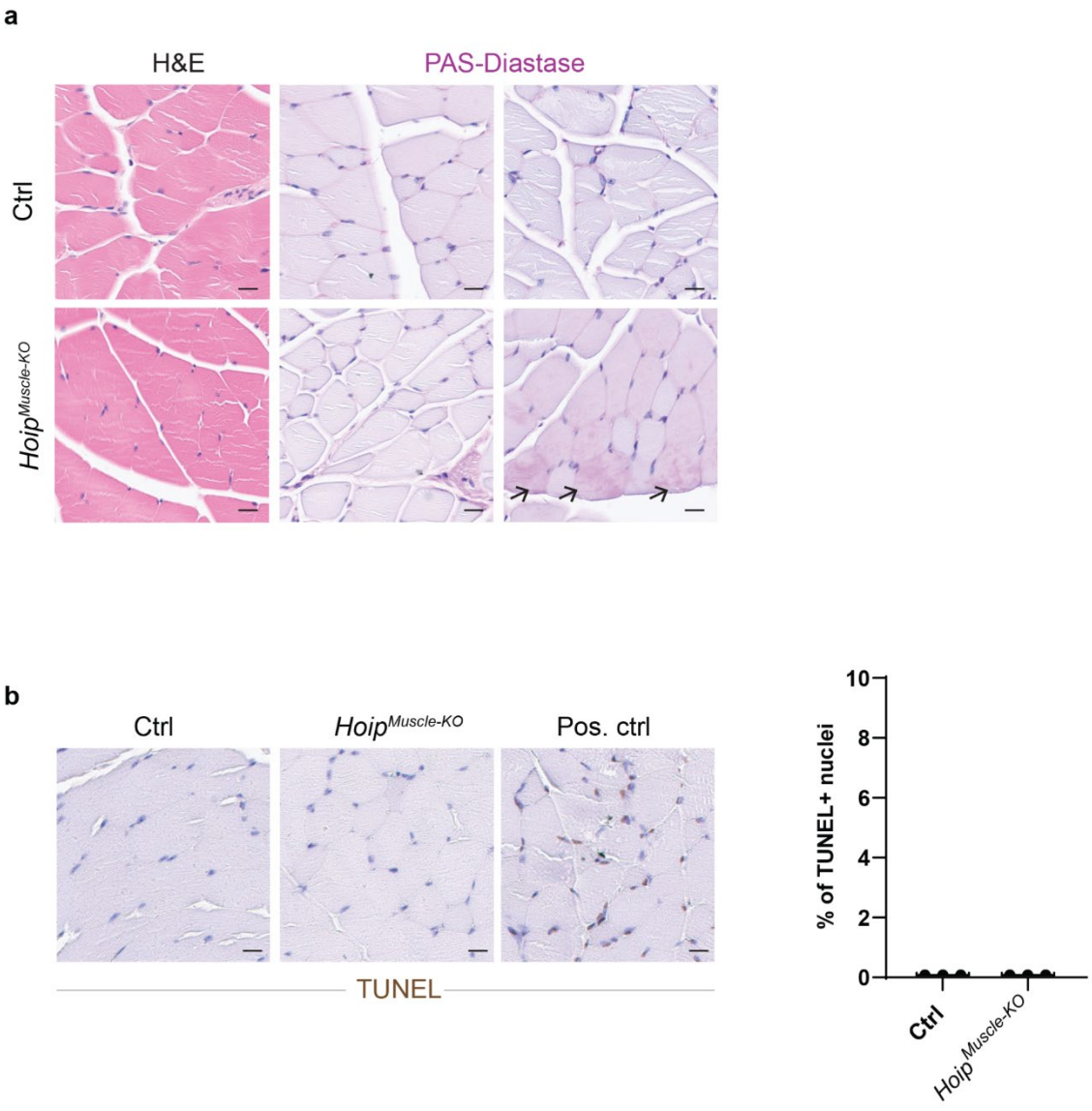

Figure CII-5. HOIP deficiency in muscle leads to mild accumulation of polyglucosan bodies in the quadriceps. a. H&E and PAS-D staining in the quadriceps of 7-8 months female control and *Hoip*$^{Muscle\text{-}KO}$ mice (n=3-4 per group). **b.** TUNEL staining in the quadriceps control and *Hoip*$^{Muscle\text{-}KO}$ mice. The positive control was treated with DNaseI before staining. Scale bars represent 20 µM for PAS-Diastase and TUNEL staining. Means ± SD.

The analysis of a second cohort consisted of 12-month-old males. Interestingly, *Hoip*$^{Muscle\text{-}KO}$ mice weighed significantly less than the controls which can indicate a reduction in muscle mass (Figure CII-6a). Moreover, 12-month-old males had larger polyglucosan aggregates (Figure CII-6b) compared to 7-8-month-old females (Figure CII-4b). This can be simply due to the age difference between male and female cohort or a different disease progression in males and females. The answers to these questions will be ultimately provided through detailed phenotypic studies using age-synchronized, larger cohorts of both male and female mice.

The overarching aim of this project is to understand the exact molecular mechanisms by which LUBAC regulates glycogen metabolism. To do so, we aimed to perform di-gly proteomics, a technique that enriches ubiquitinated proteins by utilizing an antibody specific to the di-glycine (Lys-ϵ-Gly-Gly) remnant [53]. This remnant is formed after the digestion of proteins with Lys-C and trypsin. The enriched proteins are then analyzed by liquid chromatography-mass spectrometry (LC-MS) [53]. This experiment aimed to determine whether LUBAC deficiency results in differential ubiquitination of proteins, which would give us potential targets of LUBAC. However, due to technical reasons, we could not enrich di-gly-modified proteins. The inability to enrich di-gly-modified proteins suggests an issue with the step of the di-gly antibody incubation, which should be addressed in future experiments. We, therefore, analyzed the normal proteome of the hearts from control and *Hoip*$^{Muscle\text{-}KO}$ mice (Figure CII-6c) as this data can help to identify differentially expressed proteins associated with HOIP deficiency. Indeed, the results showed that ATG16l, a scaffold protein that acts as a scaffold for LC3 lipidation during autophagy, is significantly downregulated (Figure CII-6c) [54]. Another interesting protein which was found to be significantly downregulated was TAX1BP1 (Figure CII-6c). TAX1BP1 is a selective autophagy receptor which recognizes ubiquitinated aggregates for autophagic degradation [55]. Interestingly, it has been proposed that TAX1BP1 binds to linear chains generated by LUBAC to initiate the detoxification of cell death-inducing, complex II of TNF signaling [56]. Indeed, GO enrichment analysis suggests that ubiquitin-dependent protein catabolic process and modification-dependent macromolecule catabolic process are downregulated in the heart of *Hoip*$^{Muscle\text{-}KO}$ (Figure CII-6d). It has been shown that the polyglucosan bodies colocalizes with ubiquitin and p62 (selective autophagy receptor) [57]. This reinforces the idea that indeed protein catabolic processes are impaired in the deficiency of HOIP. However, this raises the question whether somehow polyglucosan and protein

detoxification pathways merge. Therefore, it is tempting to speculate that LUBAC plays a yet uncharacterized role in the detoxification of protein and polyglucosan aggregates.

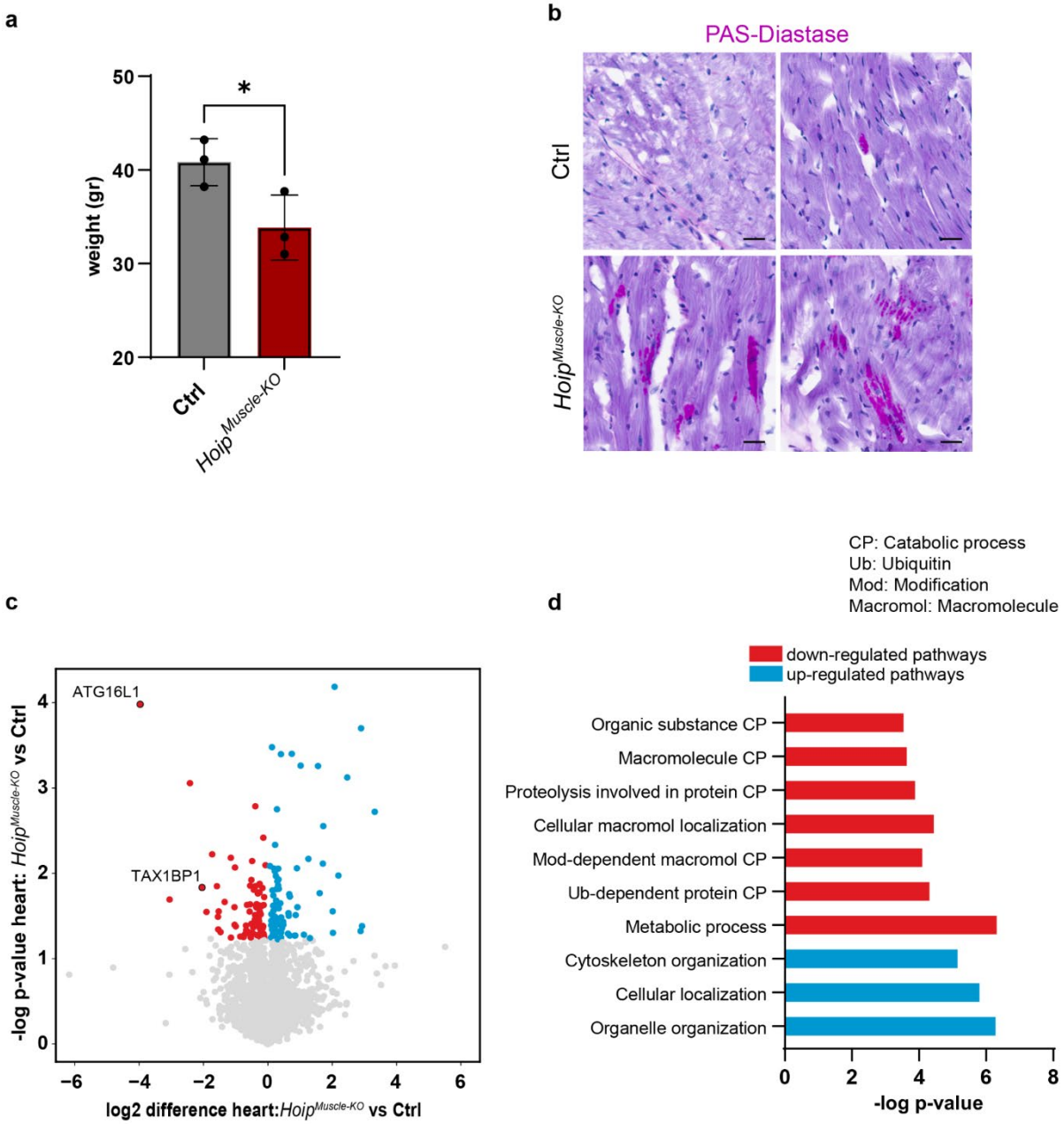

Figure CII-6. LUBAC Deficiency in muscle results in decreased macromolecule catabolic processes in the heart. a. Weight measurements of 12-month-old male control and *Hoip*$^{Muscle\text{-}KO}$ mice (n=3 per group). **b.** PAS-D staining of heart tissues from control and *Hoip*$^{Muscle\text{-}KO}$ mice. **c.** Proteomics analysis of heart samples from control and *Hoip*$^{Muscle\text{-}KO}$ mice. Proteins that were downregulated are highlighted in red, while upregulated proteins are highlighted in blue. A significance threshold of $p < 0.05$ (equivalent to -log p-value > 1.3) was applied. **d.** Gene Ontology (GO) enrichment analysis depicting downregulated and upregulated pathways in the heart, with downregulated pathways indicated in red and upregulated pathways in blue. Scale bars represent 20 µm for PAS-D staining. Data are presented as means ± standard deviation (SD)**.** Means ± SD. Unpaired t-test (a).

4. Discussion

The patients with LUBAC deficiency presented with cardiomyopathy and myopathy due to the deposition of toxic polyglucosan bodies in their hearts and muscles, a phenotype which appears to be unrelated to immune defects. This suggested that LUBAC has a yet unidentified role in glycogen metabolism. To be able to study the role of LUBAC in glycogen metabolism, we generated a mouse model in which HOIP, the primary catalytic subunit of LUBAC, is specifically deleted in skeletal and cardiac muscle. *Hoip*$^{Muscle\text{-}KO}$ mice are viable without any overt phenotype. Our histological examinations showed that the deletion of HOIP leads to polyglucosan accumulation in 7-8-month-old females. This finding further confirms the regulatory role of LUBAC in glycogen metabolism. Since LUBAC acts as a checkpoint in TNF signaling to prevent cell death (see general introduction), we performed a TUNEL staining in the heart of control and *Hoip*$^{Muscle\text{-}KO}$ mice. Intriguingly, *Hoip*$^{Muscle\text{-}KO}$ mice have significantly more cell death compared to controls. The reason for the increased amount of cell death can be polyglucosan accumulation within the cells that disrupts cellular function. However, it can also be due to TNF-induced cell death which is exacerbated due to LUBAC deficiency. The underlying cause of increased cell death can be tested by additional deletion of Caspase-8 and MLKL to block TNF-induced apoptosis and necroptosis. If the increased cell death phenotype still persists, this would strongly suggest that polyglucosan accumulation is the primary driver of cell death in the heart. Understanding the mechanisms by which polyglucosan accumulation induces cell death, as well as the specific cell death modalities involved, will be crucial for elucidating the cardiac complications associated with LUBAC deficiency.

We also started analysis of a second cohort, composed of 12-month-old males. Different from the 7-8-month-old females, 12-months *Hoip*$^{Muscle\text{-}KO}$ males weighed significantly less than the control littermates. Although this can be attributed to the age difference between the two cohorts, we cannot exclude the possibility of different disease progression in males and females. Indeed, another report using a mouse model with a truncated version of HOIL-1 showed that the polyglucosan deposition in male mice was significantly more than in female mice [52]. However, it is important to note that such a difference was not reported with the patients. Therefore, it is imperative to set up ageing cohorts of both male and female mice and follow the disease progression at different stages of life, for example, 3, 6, 12 and 18 months of age. Importantly, to understand if our model, *Hoip*$^{Muscle\text{-}KO}$ mice, fully recapitulate human LUBAC deficiency, it would be interesting to understand if these mice show signs of cardiomyopathy. Cohorts can be followed by echocardiography to evaluate the heart function at regular intervals [58]. Myopathy can also be evaluated by using non-invasive methods such

as grip strength test [59]. However, it is important to note that mild symptoms might not be detected in this test and additional histopathological examinations might be needed.

The exact molecular mechanism by which LUBAC regulates glycogen metabolism is not well understood. It has been shown that mice with a truncated version of HOIL-1 (lacking E3 ligase domain) accumulate polyglucosan bodies in the central nervous system, muscle, and heart [52]. Importantly, downregulation of GYS1 either by anti-sense oligomers (ASO) or by crossing with a monoallelic knockout of GYS1 (*Gys1*$^{+/-}$) mice rescues the polyglucosan accumulation caused by truncated HOIL-1. Another report showed that mice bearing a mutant catalytically inactive form of HOIL-1 (C458S) also accumulate polyglucosan bodies in their heart and brain [51]. As explained in the introduction of this chapter, HOIL-1 limits LUBAC activity by monoubiquitinating itself and other LUBAC components, making them preferred *cis* substrates for HOIP. This process prevents LUBAC from becoming hyperactive on other *trans* targets. Therefore, mice bearing catalytically inactive HOIL-1 (C458S) have augmented levels of M1 chains [14]. The fact that polyglucosan accumulation was also observed in HOIL-1 (C458S) mice raised the question if this phenotype is dependent on linear ubiquitination by HOIP or monoubiquitination by HOIL-1. Crucially, Kelsall et al showed that HOIL-1 can monoubiquitinate polysaccharides at the hydroxyl group of C6 [51]. They propose a model in which the monoubiquitination of glycogen is a “quality control mechanism” to remove unbranched glycogen/polyglucosan from the cells. Although this is a plausible explanation for why HOIL-1 (C458S) mice have polyglucosan accumulation, it does not exclude a possible role for linear ubiquitination in this process. It is known that HOIP either elongates the monoubiquitin which is conjugated by HOIL-1 or K63 chains that are conjugated by other E3 ligases such as cIAPs [1]. Therefore, M1 chains that are generated by HOIP may be also essential for this “quality control mechanism” for glycogen. The fact that HOIL-1 and HOIP stabilize each other within LUBAC complicates the efforts to understand how exactly LUBAC regulates this process. The deficiency of HOIL-1 would deplete HOIP and vice versa [12,13]. To address this challenge, one can take advantage of the catalytic inactive form of HOIP (C879S) [11]. The mice bearing catalytic inactive HOIP in their skeletal and cardiac muscle would still retain a functional HOIL-1. If these mice do not have polyglucosan accumulation, this would suggest that the catalytic activity of HOIL-1 is responsible for preventing polyglucosan accumulation.

Autophagy is a process which supplies energy to the cells in case of need, for example during starvation. Additionally, autophagy is important for removing protein aggregates, defective organelles, etc. During starvation-induced autophagy initiation, AMPK, the master regulator of energy homeostasis, phosphorylates and activates ULK1 to initiate autophagy [60]. Alternatively,

autophagy can be initiated by cargo receptors such as Optineurin, TAX1BP1, p62 that bind to ubiquitin-tagged cargo molecules [61]. In both cases, this leads to the recruitment of the ULK complex, which is composed of FIP200, ATG13, ATG101, and ULK kinases. ULK complex then recruits ATG9 vesicles which serve as the seed of autophagosome formation. ULK complex also recruits class III phosphatidylinositol 3-kinase complex I (PI3KC3–C1) that elongates the autophagic membrane [61]. The lipidation of LC3/ATG8 is the hallmark of autophagy. ATG12-ATG5-ATG16L1 complex is important for the lipidation of LC3. After the closure of autophagosomes, they fuse with lysosomes for the degradation of cargo. Importantly, this is a simple overview of the core autophagy process. There are alternative, unconventional pathways for autophagy.

It has been suggested that linear ubiquitination, conjugated by LUBAC on the previously existing ubiquitin coat of *S.* Typhimurium, recruits autophagic cargo receptor Optineurin to initiate autophagy and limit the bacterial proliferation in the cytosol [62]. Therefore, it seems like a possible scenario that LUBAC regulates the ubiquitin-dependent selective autophagy process for the degradation of unbranched glycogen/polyglucosan. In line with this, it was reported that polyglucosan bodies in HOIL-1 mutated patients colocalize with ubiquitin. This suggests that in the deficiency of LUBAC, there is a defective autophagy initiation or progression, at least in this hypothetical pathway.

To look at the differentially expressed proteins in the heart of *Hoip*$^{Muscle\text{-}KO}$ and control mice, we carried out a proteomics analysis. We found out that an ATG16L1, a scaffold protein that acts as a scaffold for LC3 lipidation, is significantly downregulated. This suggests that ATG16L1 might be ubiquitinated and stabilized by LUBAC. Indeed, ATG13, another protein which is required for phagophore formation, is stabilized by LUBAC [63]. Therefore, it is important to test whether LUBAC ubiquitinates ATG16L1. Next, we will perform an M1 pulldown to enrich the proteins linear ubiquitinated by LUBAC. Besides western blot analysis, we will perform a proteomics analysis to identify potential targets of LUBAC, specifically in the heart. Curiously, TAX1BP1, a selective autophagy receptor, was also significantly downregulated. Indeed, the gene ontology enrichment analysis suggested that protein catabolic process and ubiquitin-dependent catabolic pathways are downregulated in the heart of *Hoip*$^{Muscle\text{-}KO}$ compared to controls. These results raise the question of whether this pathway is also critical for polyglucosan accumulation, or if alternative pathways instead regulate it. It is also possible that LUBAC directly regulates the proteins that are directly involved in glycogen synthesis or breakdown. Indeed, a recent study analyzing the HOIP interactome across various tissues identified GYS1, GYS2, and GSK3 as interaction partners of HOIP [64]. However, we did not observe any difference in the expression of these proteins in our

proteomics analysis. HOIP may regulate the functionality of these proteins rather than their stability or expression, or it might simply interact with them without exerting any regulatory role.

In summary, while our results indicate that impaired autophagy is likely the primary cause of polyglucosan accumulation in the hearts of *Hoip*$^{Muscle\text{-}KO}$ mice, LUBAC may also influence glycogen metabolism through other pathways, which certainly requires further investigation.

Outstanding questions

How does LUBAC regulate glycogen metabolism, and is this process dependent on linear ubiquitination or HOIL-1-mediated monoubiquitination?

Is there a glycogen quality control mechanism which is regulated by LUBAC?

In addition to clearing protein aggregates, can autophagy also recycle unbranched glycogen or polyglucosans?

5. Material & Methods

5.1. Mice

Hoip$^{Muscle\text{-}KO}$ mice were generated by crossing *Hoip fl/fl* and *Ckmm Cre* mice [12,49]. Hearts were collected in 10% neutral buffered formalin solution for 30 minutes which were then transferred to 20% sucrose solution in PBS overnight at 4 °C. Quadriceps were fixed overnight in 10% neutral buffered formalin solution. The heart of the male cohort was cut into two pieces. One piece was directly frozen in liquid nitrogen. The other part was covered with OCT medium for cryosectioning. Tissues were sent to the SFB1403 Histology Facility for paraffin embedding and sectioning.

5.2. Periodic acid Schiff (PAS) staining

Cryosections were equilibrated at room temperature and paraffin sections were deparaffinized. Then, the slides were incubated with amylase enzyme (AR17192-2, Agilent Technologies) for 1 hour at 37 °C for enzyme digestion. Slides were then incubated 0.5% Periodic Acid (100482, Sigma Aldrich) for 7 minutes and washed with distilled water two times for 5 minutes. After washes, slides were incubated in Schiff's reagent (109033, Sigma Aldrich) for 10 minutes. The slides were washed under running water for 10 minutes. Counterstaining was performed with Hematoxylin (H-3401, Vector Laboratories) for 3 minutes. Slides were dehydrated, cleared, and mounted using a toluene-based mounting medium (Catalog#H-5700, Vector Laboratories). Slides were scanned using S360, Hamamatsu Slidescanner.

5.3. GYS1 and Glycogen double staining

Paraffin sections were deparaffinized and rehydrated by using graded alcohol series. A commercially available citrate buffer (C9999, Sigma Aldrich) was used for antigen retrieval. After 10 minutes of incubation with 1X citrate buffer, antigen retrieval was done by maintaining sub-boiling conditions in the microwave for 5 mins. After cooling down, they were washed with 1X PBS for 5 minutes and then with TBS-T for 5 minutes. Slides were permeabilized for 10 minutes by using 0.5% Triton-X (T8787, Sigma Aldrich) in Animal-Free Blocker (SP-5035-100, Vector Laboratories) and blocked for 1 hour in 0.3% Triton-X in Animal-Free Blocker. Primary antibodies, glycogen antibody (1:200, kindly provided from Reznick lab), and GYS1 antibody (1:100, 3886, Cell Signalling) were incubated overnight at 4 ℃. After three washes with PBS-T slides were incubated for 1 hour in the secondary antibodies at room temperature (1:300, A11011, Invitrogen and 1:400, A28175, Invitrogen). Slides were covered from the light and washed 6 times for 15 minutes. DAPI (1 µg/ml) staining was performed for 10 minutes. Slides were mounted with ProLong Gold Antifade Mountant mounting media (P36934, Invitrogen) and scanned using a confocal microscope Stellaris 5, Leica Microsystems.

5.4. TUNEL staining

DeadEnd Colorimetric TUNEL System (G7360, Promega) was used for TUNEL staining. The manufacturer's protocol was followed. Proteinase K (20 µg/mL) was used for 15 minutes for antigen retrieval. Bloxall Endogenous Blocking Solution was used to block endogenous peroxidases (#SP-6000-100, Vector Laboratories) for 5 minutes. Counterstaining was performed with Hematoxylin (H-3401, Vector Laboratories) for 3 minutes and slides were mounted using HIGHDEF IHC mount (ADI-950-261-0030, Enzo Life Sciences). TUNEL positive nuclei analysis was performed using QuPath Software.

5.5. Proteomics analysis

Proteomics analysis of the heart was performed in collaboration with Markus Krüger lab, at CECAD, following the protocol from their lab as in Schmidt et al [65]. Hearts from 12-month-old male mice were collected and directly frozen in liquid nitrogen. The tissues were lyzed in Urea-thiourea buffer (4 M urea and 2 M Thiourea in 0.1 M Tris-HCl, supplemented with PhosSTOP and cOmplete™, Mini Protease Inhibitor Cocktail (Roche)) to ensure the maximum solubility of proteins. The protein extraction was carried out TissueLyser III (Qiagen). The protein concentration was quantified by using a Bradford assay kit (BioRad, 5000002) according to the manufacturer´s instructions and 930 µg protein was used as input. 5 mM TCEP and 15 mM 2-chloroacetamid pH 7.5 were used to reduce and alkylate the proteins (Sigma-Aldrich, Merck, Darmstadt, Germany) for 20 min at 70 °C, shaking at 750 rpm. Protein digestion was performed as described in SP3 protocol [66]. Proteins were digested with trypsin (substrate: enzyme ratio 100:1) overnight at room temperature. Samples were acidified with TFA (pH < 2) and desalted using Sep-Pak C18 1 cc Vac Cartidge, 50 mg (Waters, Milford, US). Eluates were lyophilized by using a speed vacuum concentrator. 10 µg were resuspended in 5% formic acid, 2% acetonitrile. Peptide separation was performed on a nanoElute (upgraded) equipped with a 25 cm PepSep column (75 µm inner diameter, 1.9 µm particle size) with the column temperature maintained at 50 °C using an integrated column oven (all Bruker Daltonics). Peptides were separated using a binary buffer system of buffer A (0.1% FA) and buffer B (80% ACN, 0.1% FA). A 60 min segmented gradient of 4–32% Solvent B over 43 min, 32–55% Solvent B over 7 min and 55–95% over 10 min at a flow rate of 300 nL/min was applied to elute peptides and the peptides were measured with a timsTOF pro 2 using a CaptiveSpray source (both Bruker). Samples were measured in dia-PASEF mode with daily ion mobility calibration using three ions of Agilent ESI-Low Tuning Mix following vendor specifications. The DIA-PASEF window was ranging in dimension 1/k0 0.7-1.45, with 2 ion mobility windows with 12 segments in dimension m/z from 350 to 1250.

PTMScan Ubiquitin Remnant Motif (K-ε-GG) (Cell Signaling, 5562) was used to perform diGLY enrichment. Desalted peptides were reconstituted in 1 ml 1X IAP buffer (provided by the kit). The antibody beads were washed with 1x PBS and spun down at 2000 g for 30 seconds after each wash. The beads were resuspended in 40 µl of PBS and added to peptides which were then incubated for 2 hours at 4°C on a rotator. The samples were centrifuged at 2000 g for 30 seconds. The beads were washed with 1X IAP buffer two times and with HPLC water three times. Following the washes, the elution step was carried out 2 times with 55 µl 0.15% TFA. After the clean-up step with Stop-and-Go StageTips, purified peptides were analysed on an Orbitrap Eclipse Tribid Mass Spectrometer (Thermo) coupled with an easy nLC 1200 (Thermo). An in-house packed C18 analytical column (30 cm, 150 µm inside diameter, and 1.9-µm ReproSil-Pur C18 beads; Dr. Maisch, Germany) was used with an integrated column oven (50°C; PRSO-V1, Biberach, Germany). DiGly-remnant peptides were analysed using a 60 min gradient (0-47 min: 3-55 %B, 47-54 min: 55-65 %B, 54-60 min: 65-90 %B). Peptides were analysed in a data-dependent aquisiton (DDA) mode. Full MS scan was set to 120,000 at mass/charge ratio 350 to 1400 m/z, with AGC target at 300%. MS2 resolution was set to 30,000.

Acquired spectra from DiGly samples were processed using MaxQuant (version 2.4.2.0) and proteome were analyzed with DIA-NN 1.8.1 using library free search against UniProt mouse database (April 2024) complemented with protein sequences from collagens. Mass ranges were set according to the settings of the mass spectrometer, mass deviation was set to 15. Data was further processed using R (V 4.2.2), with the libraries: tidyverse, diann, data.table, magrittr, FactoMineR, factoextra and ggplot2, gprofiler, missForest, ggplot2. An in-house modified R-script based on the version by V. Demichev was used to calculate MaxLFQ values (Github page, cit MaxLFQ). Data input was filtered for unique peptides, q-Value <0.01, Lib.Q.Value <0.01, PG.Q.Value < 0.01, Global.Q.Value < 0.01, Quantity.Quality > 0.7, Fragment.count >= 4. Statistical analysis was performed on the MaxLFQ normalised data with R (V 4.2.2), and Perseus (V.1.6.5.0) and visualized with Instant clue (V 0.10.10.20210315). Data completeness of 70% was calculated on each group. Missing values were imputed by the random forest algorithm for groups with 70% data completeness, with more than 30% missing values. The random forest algorithm was downshifted of 0.3, width 1.5. Further analysis was performed in perseus (V 1.6.5.0) and InstantClue (V 0.10.10.20211105). ANOVA analysis and Student's T-test analysis was performed with an FDR with less than 0.05 and 500 randomizations. Quality control of iRT peptides were performed in Skyline-Daily (V 22.21.391).

6. Author contribution

Dr. Peter Kreuzaler generated *Hoip*$^{Muscle\text{-}KO}$ mice in Walzcak Lab. The experiments were designed by **Önay Veli** and **Öykü Kaya** (a master's student in the lab) under the supervision of **Prof. Nieves Peltzer**. Histological analysis of the heart and quadriceps was conducted in collaboration with **Öykü Kaya**. For the proteomics analysis, samples were prepared by **Önay Veli** for MS analysis in partnership with **Luisa Schmidt** from Marcus Krüger lab. **Luisa Schmidt** performed the sample acquisition, data analysis and visualization.

7. Software and Programs

Data was represented as Means ± SD and statistical analyses were carried out using GraphPad Prism 10.1.2. (GraphPad Software Inc., San Diego, CA, USA) unless otherwise stated such as in the proteomics analysis. Unpaired two-tailed t-test was carried out to compare the means of two groups. 2-way ANOVA was used to compare the means of groups with more than one variable. A $p<0.05$ is considered statistically significant.

The figures in this thesis were created by using Adobe Illustrator and Biorender. Grammarly was used for grammar corrections.

8. References

1. Cohen, P., Kelsall, I. R., Nanda, S. K. & Zhang, J. HOIL-1, an atypical E3 ligase that controls MyD88 signalling by forming ester bonds between ubiquitin and components of the Myddosome. *Adv. Biol. Regul.* **75**, 100666 (2020).
2. Kirisako, T. *et al.* A ubiquitin ligase complex assembles linear polyubiquitin chains. *EMBO J.* **25**, 4877–4887 (2006).
3. Pao, K.-C. *et al.* Activity-based E3 ligase profiling uncovers an E3 ligase with esterification activity. *Nature* **556**, 381–385 (2018).
4. Kelsall, I. R., Zhang, J., Knebel, A., Arthur, J. S. C. & Cohen, P. The E3 ligase HOIL-1 catalyses ester bond formation between ubiquitin and components of the Myddosome in mammalian cells. *Proc. Natl. Acad. Sci. U. S. A.* **116**, 13293–13298 (2019).
5. Damgaard, R. B. The ubiquitin system: from cell signalling to disease biology and new therapeutic opportunities. *Cell Death Differ.* **28**, 423–426 (2021).
6. Lechtenberg, B. C. & Komander, D. Just how big is the ubiquitin system? *Nat. Struct. Mol. Biol.* **31**, 210–213 (2024).
7. Metzger, M. B., Pruneda, J. N., Klevit, R. E. & Weissman, A. M. RING-type E3 ligases: master manipulators of E2 ubiquitin-conjugating enzymes and ubiquitination. *Biochim. Biophys. Acta* **1843**, 47–60 (2014).
8. Ikeda, F. *et al.* SHARPIN forms a linear ubiquitin ligase complex regulating NF-κB activity and apoptosis. *Nature* **471**, 637–641 (2011).
9. Gerlach, B. *et al.* Linear ubiquitination prevents inflammation and regulates immune signalling. *Nature* **471**, 591–596 (2011).
10. Tokunaga, F. *et al.* SHARPIN is a component of the NF-κB-activating linear ubiquitin chain assembly complex. *Nature* **471**, 633–636 (2011).
11. Emmerich, C. H. *et al.* Activation of the canonical IKK complex by K63/M1-linked hybrid ubiquitin chains. *Proc. Natl. Acad. Sci. U. S. A.* **110**, 15247–15252 (2013).
12. Peltzer, N. *et al.* HOIP deficiency causes embryonic lethality by aberrant TNFR1-mediated endothelial cell death. *Cell Rep.* **9**, 153–165 (2014).
13. Peltzer, N. *et al.* LUBAC is essential for embryogenesis by preventing cell death and enabling haematopoiesis. *Nature* **557**, 112–117 (2018).
14. Fuseya, Y. *et al.* The HOIL-1L ligase modulates immune signalling and cell death via monoubiquitination of LUBAC. *Nat. Cell Biol.* **22**, 663–673 (2020).
15. Jahan, A. S., Elbæk, C. R. & Damgaard, R. B. Met1-linked ubiquitin signalling in health and disease: inflammation, immunity, cancer, and beyond. *Cell Death Differ.* **28**, 473–492 (2021).
16. Berger, S. B. *et al.* Cutting Edge: RIP1 kinase activity is dispensable for normal development but is a key regulator of inflammation in SHARPIN-deficient mice. *J. Immunol.* **192**, 5476–5480 (2014).
17. Oda, H. *et al.* Second Case of HOIP Deficiency Expands Clinical Features and Defines Inflammatory Transcriptome Regulated by LUBAC. *Front. Immunol.* **10**, 479 (2019).
18. Boisson, B. *et al.* Immunodeficiency, autoinflammation and amylopectinosis in humans with inherited HOIL-1 and LUBAC deficiency. *Nat. Immunol.* **13**, 1178–1186 (2012).
19. Boisson, B. *et al.* Human HOIP and LUBAC deficiency underlies autoinflammation, immunodeficiency, amylopectinosis, and lymphangiectasia. *J. Exp. Med.* **212**, 939–951 (2015).
20. Koch, R. L. *et al.* Diagnosis and management of glycogen storage disease type IV, including adult polyglucosan body disease: A clinical practice resource. *Mol. Genet. Metab.* **138**, 107525 (2023).
21. Oda, H. *et al.* Biallelic human SHARPIN loss of function induces autoinflammation and immunodeficiency. *Nat. Immunol.* **25**, 764–777 (2024).
22. Elliott, P. R. *et al.* Molecular basis and regulation of OTULIN-LUBAC interaction. *Mol. Cell* **54**, 335–348 (2014).
23. Takiuchi, T. *et al.* Suppression of LUBAC-mediated linear ubiquitination by a specific interaction between LUBAC and the deubiquitinases CYLD and OTULIN. *Genes Cells* **19**, 254–272 (2014).
24. © 2020 SSIEM J Inherit Metab Dis. *J. Inherit. Metab. Dis.* **43**, 1002–1013 (2020).

25. Wang, K. *et al.* Whole-genome DNA/RNA sequencing identifies truncating mutations in RBCK1 in a novel Mendelian disease with neuromuscular and cardiac involvement. *Genome Med.* **5**, 67 (2013).
26. Nilsson, J. *et al.* Polyglucosan body myopathy caused by defective ubiquitin ligase RBCK1. *Ann. Neurol.* **74**, 914–919 (2013).
27. Phadke, R., Scalco, R. S., Oldfors, A. & Murphy, E. RBCK1 mid-domain mutations with a phenotype spanning the entire spectrum of the condition: A rare polyglucosan storage disorder causing multisystem autoinflammation, immunodeficiency, cardiac and skeletal myopathy. *Neuromuscul. Disord.* **27**, S43 (2017).
28. Krenn, M. *et al.* Mutations outside the N-terminal part of RBCK1 may cause polyglucosan body myopathy with immunological dysfunction: expanding the genotype–phenotype spectrum. *J. Neurol.* **265**, 394–401 (2018).
29. Sun, Q., Xie, Z., Song, L. & Fu, D. A case of polyglucosan body myopathy caused by an RBCK1 gene variant and literature review. *Mol. Genet. Genomic Med.* **12**, e2432 (2024).
30. AlAnzi, T., Al Harbi, F., AlGhamdi, A. & Mohamed, S. A novel variant of RBCK1 gene causes mild polyglucosan myopathy. *Neurosciences* **27**, 45–49 (2022).
31. © 2020 SSIEM J Inherit Metab Dis. *J. Inherit. Metab. Dis.* **43**, 1002–1013 (2020).
32. RBCK1-related disease: a rare multisystem disorder with polyglucosan storage, autoinflammation, recurrent infections, skeletal and cardiac myopathy - four additional patients and a review of the current literature. *J. Inherit. Metab. Dis.* **43**, 1002–1013.
33. Chen, L. *et al.* Polyglucosan body myopathy 1 may cause cognitive impairment: a case report from China. *BMC Musculoskelet. Disord.* **22**, 35 (2021).
34. Adeva-Andany, M. M., González-Lucán, M., Donapetry-García, C., Fernández-Fernández, C. & Ameneiros-Rodríguez, E. Glycogen metabolism in humans. *BBA Clin* **5**, 85–100 (2016).
35. Jensen, T. E. & Richter, E. A. Regulation of glucose and glycogen metabolism during and after exercise: Regulation of glucose and glycogen metabolism in exercise. *J. Physiol.* **590**, 1069–1076 (2012).
36. Bouskila, M., Hirshman, M. F., Jensen, J., Goodyear, L. J. & Sakamoto, K. Insulin promotes glycogen synthesis in the absence of GSK3 phosphorylation in skeletal muscle. *Am. J. Physiol. Endocrinol. Metab.* **294**, E28–35 (2008).
37. Paredes-Flores, M. A., Rahimi, N. & Mohiuddin, S. S. Biochemistry, glycogenolysis. *StatPearls [Internet]* (2024).
38. Kaneko, J. J. Carbohydrate metabolism and its diseases. in *Clinical Biochemistry of Domestic Animals* 45–80 (Elsevier, 2008).
39. Daghlas, S. A. & Mohiuddin, S. S. Biochemistry, glycogen. (2019).
40. Neoh, G. K. S. *et al.* Glycogen metabolism and structure: A review. *Carbohydr. Polym.* **346**, 122631 (2024).
41. Szymańska, E. *et al.* Pediatric patient with hyperketotic hypoglycemia diagnosed with glycogen synthase deficiency due to the novel homozygous mutation in GYS2. *Mol. Genet. Metab. Rep.* **4**, 83–86 (2015).
42. Sukigara, S. *et al.* Muscle glycogen storage disease 0 presenting recurrent syncope with weakness and myalgia. *Neuromuscul. Disord.* **22**, 162–165 (2012).
43. Kohler, L., Puertollano, R. & Raben, N. Pompe disease: From basic science to therapy. *Neurotherapeutics* **15**, 928–942 (2018).
44. Mochel, F. *et al.* Adult polyglucosan body disease: Natural History and Key Magnetic Resonance Imaging Findings. *Ann. Neurol.* **72**, 433–441 (2012).
45. Souza, P. V. S. *et al.* GBE1-related disorders: Adult polyglucosan body disease and its neuromuscular phenotypes. *J. Inherit. Metab. Dis.* **44**, 534–543 (2021).
46. Moreno-Estellés, M. *et al.* Deciphering the polyglucosan accumulation present in lafora disease using an astrocytic cellular model. *Int. J. Mol. Sci.* **24**, 6020 (2023).
47. Skurat, A. V. *et al.* Impaired malin expression and interaction with partner proteins in Lafora disease. *J. Biol. Chem.* **300**, 107271 (2024).
48. Akman, H. O., Lossos, A. & Kakhlon, O. GBE1 adult polyglucosan body disease. (2020).

49. Brüning, J. C. *et al.* A muscle-specific insulin receptor knockout exhibits features of the metabolic syndrome of NIDDM without altering glucose tolerance. *Mol. Cell* **2**, 559–569 (1998).
50. Taraborrelli, L. *et al.* LUBAC prevents lethal dermatitis by inhibiting cell death induced by TNF, TRAIL and CD95L. *Nat. Commun.* **9**, 3910 (2018).
51. Kelsall, I. R. *et al.* HOIL-1 ubiquitin ligase activity targets unbranched glucosaccharides and is required to prevent polyglucosan accumulation. *EMBO J.* **41**, e109700 (2022).
52. Nitschke, S. *et al.* Glycogen synthase downregulation rescues the amylopectinosis of murine RBCK1 deficiency. *Brain* **145**, 2361–2377 (2022).
53. Fulzele, A. & Bennett, E. J. Ubiquitin diGLY proteomics as an approach to identify and quantify the ubiquitin-modified proteome. *Methods Mol. Biol.* **1844**, 363–384 (2018).
54. Fujita, N. *et al.* The Atg16L complex specifies the site of LC3 lipidation for membrane biogenesis in autophagy. *Mol. Biol. Cell* **19**, 2092–2100 (2008).
55. Turco, E. *et al.* Reconstitution defines the roles of p62, NBR1 and TAX1BP1 in ubiquitin condensate formation and autophagy initiation. *Nat. Commun.* **12**, 5212 (2021).
56. Huyghe, J. *et al.* ATG9A prevents TNF cytotoxicity by an unconventional lysosomal targeting pathway. *Science* **378**, 1201–1207 (2022).
57. Fanin, M. *et al.* Familial polyglucosan body myopathy with unusual phenotype. *Neuropathol. Appl. Neurobiol.* **41**, 385–390 (2015).
58. Gao, S., Ho, D., Vatner, D. E. & Vatner, S. F. Echocardiography in mice. *Curr. Protoc. Mouse Biol.* **1**, 71–83 (2011).
59. Vogel, P., Read, R. W., Hansen, G. M. & Powell, D. R. Histopathology is required to identify and characterize myopathies in high-throughput phenotype screening of genetically engineered mice. *Vet. Pathol.* **58**, 1158–1171 (2021).
60. Kim, J., Kundu, M., Viollet, B. & Guan, K.-L. AMPK and mTOR regulate autophagy through direct phosphorylation of Ulk1. *Nat. Cell Biol.* **13**, 132–141 (2011).
61. Wang, S., Zhang, J., Zhang, H., Yang, Y. & Wen, Y. Exploration of mitochondrial autophagy related genes in the diagnosis model construction and molecular marker mining of Alzheimer's disease based on multi-omics integration. *Cell. Mol. Biol.* **70**, 114–121 (2024).
62. Noad, J. *et al.* LUBAC-synthesized linear ubiquitin chains restrict cytosol-invading bacteria by activating autophagy and NF-κB. *Nat. Microbiol.* **2**, 17063 (2017).
63. Chu, Y. *et al.* LUBAC and OTULIN regulate autophagy initiation and maturation by mediating the linear ubiquitination and the stabilization of ATG13. *Autophagy* **17**, 1684–1699 (2021).
64. Fu, Y. *et al.* Systematic HOIP interactome profiling reveals critical roles of linear ubiquitination in tissue homeostasis. *Nat. Commun.* **15**, 2974 (2024).
65. Schmidt, L. *et al.* Spatial proteomics of skeletal muscle using thin cryosections reveals metabolic adaptation at the muscle-tendon transition zone. *Cell Rep.* **43**, 114374 (2024).
66. Hughes, C. S. *et al.* Single-pot, solid-phase-enhanced sample preparation for proteomics experiments. *Nat. Protoc.* **14**, 68–85 (2019).

CONCLUDING REMARKS

The default response to TNF sensing is proinflammatory gene activation and cell survival [1]. However, TNF can also induce cell death and, as such, is tightly regulated by molecular breaks, known as checkpoints of TNF-induced cell death. Inhibition of these checkpoints may lead to cell death as explained in detail in General Introduction. The inhibition of these checkpoints can occur due to, e.g. microbial hijacking [2]. Some pathogens, such as *Yersinia*, can block kinases to evade proinflammatory responses. Through the acetyltransferase YopJ/P, Yersinia blocks the kinase activity of IKKs or TAK1, inhibiting kinase-dependent checkpoints [3–5]. The inhibition of these checkpoints leads to RIPK1-dependent cell death. Therefore, checkpoints of TNF signaling have evolved as a backup mechanism to limit pathogen invasion [2]. However, as with everything in life, this too comes at a cost. TNF-induced cell death must be tightly regulated and suppressed in healthy cells. The mutations that inhibit these cell death checkpoints can lead to severe inflammatory conditions, as evidenced by LUBAC-deficient patients (Chapter II). Another example is mutations that prevent the cleavage of RIPK1 by Caspase-8, resulting in an inflammatory syndrome known as cleavage-resistant RIPK1-induced autoinflammatory (CRIA) syndrome [6].

TNF plays a vital role in host defense. Indeed, TNF-deficient patients suffer from recurrent infections [7]. On the other hand, increased levels of TNF are associated with autoimmunity and autoinflammation [8]. TNF is associated with β-cell loss during diabetes and TNF blockade improves glucose metabolism in T1D patients [9,10]. However, the contribution of TNF-induced cell death to T1D pathogenesis remained unknown. Moreover, the mechanisms of TNF-induced cell death in β-cells were not well-characterized. By using RIPK1 kinase inactive mice, we and others show that the kinase activity of RIPK1 does not contribute to T1D pathogenesis [11,12]. RIPK1 deletion leads to cell death-dependent lethal inflammation in other cell types [13,14]. However, we show that β-cell-specific loss of RIPK1 does not cause any phenotype under physiological conditions or diabetic challenges [11]. Moreover, β-cell-specific deficiency of HOIP, the main catalytic activity of LUBAC, is also dispensable for β-cell survival [11]. This raises the question of how something essential for some cell types can be dispensable for β-cells. Moreover, it was unclear how β-cells can survive the inhibition of ubiquitination-dependent or Caspase-8-dependent checkpoints. Using sc-RNA-seq, we showed that β-cells do not express RIPK3, an essential kinase for necroptosis induction [11]. Interestingly, β-cells express high amounts of cFLIP compared to Caspase-8 to limit TNF-induced apoptosis [11]. This could render upstream cell death checkpoints dispensable for cell survival since cFLIP can inhibit the activation of Caspase-8. This finding positions cFLIP as the main checkpoint regulating the TNF signaling output in β-cells. Interestingly, cFLIP has been identified as a target gene of NF-κB in other cell types. In contrast, β-cells exhibit inherently high levels of cFLIP expression at baseline, with only a modest increase upon IL-1β stimulation, highlighting its

critical role in these cells. Therefore, it would be intriguing to investigate whether the β-cell-specific loss of cFLIP leads to a spontaneous phenotype induced by β-cell death.

β-cells have extremely limited proliferative activity, ranging from %0 - 0.4 [15]. Therefore, this might have evolved as a mechanism to protect the limited pool of β-cells upon a plethora of inflammatory conditions and maintain euglycemia. However, this might come at a cost as well. Research has shown that β-cells are susceptible to infections from certain viruses, such as the Coxsackie virus, due to their expression of the Coxsackie and adenovirus receptor (CAR) [16]. The Coxsackie virus infection was associated with islet autoimmunity in young children [17]. Besides the Coxsackie virus, cytomegalovirus and rotavirus were also implicated in the pathogenesis of T1D [18,19]. The fact that β-cells are resistant to TNF-induced cell death may impair their ability to effectively clear viral infections. This persistent viral infection in β-cells could potentially trigger autoimmunity in genetically susceptible individuals. Therefore, a better characterization of cell death mechanisms in β-cells could provide important insights into T1D pathogenesis.

Patients with LUBAC, specifically HOIL-1 and HOIP, deficiencies develop myopathy and cardiomyopathy due to toxic polyglucosan accumulation in muscle and heart (see Chapter II). This phenotype observed in LUBAC-deficient patients suggests that LUBAC may play an as-yet-unknown role in regulating glycogen metabolism. We generated a mouse line which lacks HOIP specifically in cardiac and skeletal muscle (*Hoip*$^{Muscle\text{-}KO}$). Importantly, these mice are viable and do not show any overt phenotype until 21 months of age (the oldest mice in our facility). We analyzed 7-12-month-old mice and showed that these mice have polyglucosan accumulation in their heart. The fact that the same phenotype was recapitulated in mice reinforces the hypothesis that LUBAC has a conserved role in the regulation of glycogen metabolism. The deletion of HOIP unleashes TNF-induced apoptosis in keratinocytes, leading to lethal dermatitis [20]. However, we did not observe a strong cell death phenotype upon deletion of HOIP in cardiac and skeletal muscle since the mice do not show any overt phenotype until 21 months of age. It is widely accepted that excessive TNF-induced cell death triggers inflammation [2]. However, we did not detect upregulation of inflammatory pathways in our proteomic analysis. Therefore, it is plausible to suggest that the cell death we observed in the heart of *Hoip*$^{Muscle\text{-}KO}$ is not due to TNF-induced cell death but to toxic polyglucosan accumulation. Indeed, in the quadriceps, we detected minimal polyglucosan accumulation and no cell death.

Our proteomics analysis did not show the upregulation of inflammatory cytokines or proteins. Instead, we found that ATG16L1 and TAX1BP1, autophagy-related proteins, are downregulated in the heart of *Hoip*$^{Muscle\text{-}KO}$. Gene ontology-enrichment analysis suggests that

protein and macromolecule catabolic pathways are downregulated in the heart of *Hoip*$^{Muscle\text{-}KO}$. Therefore, it is tempting to speculate that, in addition to protein aggregates, selective autophagy also clears polyglucosan aggregates as they form in the cells, and this process is regulated by LUBAC in an as-yet-unknown manner. However, we cannot exclude the possibility that autophagy and polyglucosan deposition are two independent processes and LUBAC regulates glycogen metabolism via a different mechanism. Therefore, it is important to identify metabolism-related targets of LUBAC not only in muscle and heart but also in the liver, as it is one of the major organs that stores glycogen.

In summary, my research suggests alternative regulatory mechanisms for TNF-mediated cell death pathways that operate independently of classical checkpoints. While cFLIP appears to play a central role, other molecular mechanisms that limit cell death may also be involved. Additionally, my work indicates that LUBAC may influence selective autophagy, facilitating the detoxification of insoluble polyglucosan. These findings could have important implications for autoimmunity and point to potential new targets of LUBAC relevant to patients with inherited mutations.

References

1. Huyghe, J., Priem, D. & Bertrand, M. J. M. Cell death checkpoints in the TNF pathway. *Trends Immunol.* 44, 628–643 (2023).
2. van Loo, G. & Bertrand, M. J. M. Death by TNF: a road to inflammation. *Nat. Rev. Immunol.* 23, 289–303 (2023).
3. Mukherjee, S. *et al.* Yersinia YopJ acetylates and inhibits kinase activation by blocking phosphorylation. *Science* 312, 1211–1214 (2006).
4. Haase, R., Richter, K., Pfaffinger, G., Courtois, G. & Ruckdeschel, K. Yersinia outer protein P suppresses TGF-beta-activated kinase-1 activity to impair innate immune signaling in Yersinia enterocolitica-infected cells. *J. Immunol.* 175, 8209–8217 (2005).
5. Paquette, N. *Serine/threonine Acetylation of TGFbeta-Activated Kinase (TAK1) by Yersinia Pestis YopJ Inhibits Innate Immune Signaling*.
6. Lalaoui, N. *et al.* Mutations that prevent caspase cleavage of RIPK1 cause autoinflammatory disease. *Nature* 577, 103–108 (2020).
7. Arias, A. A. *et al.* Tuberculosis in otherwise healthy adults with inherited TNF deficiency. *Nature* (2024) doi:10.1038/s41586-024-07866-3.
8. Jang, D.-I. *et al.* The role of tumor necrosis factor alpha (TNF-α) in autoimmune disease and current TNF-α inhibitors in therapeutics. *Int. J. Mol. Sci.* 22, 2719 (2021).
9. Mastrandrea, L. *et al.* Etanercept treatment in children with new-onset type 1 diabetes: pilot randomized, placebo-controlled, double-blind study. *Diabetes Care* 32, 1244–1249 (2009).
10. Quattrin, T. *et al.* Golimumab and Beta-Cell Function in Youth with New-Onset Type 1 Diabetes. *N. Engl. J. Med.* 383, 2007–2017 (2020).
11. Veli, Ö. *et al.* RIPK1 is dispensable for cell death regulation in β-cells during hyperglycemia. *Mol Metab* 87, 101988 (2024).
12. Takiishi, T. *et al.* Inhibition of RIPK1 kinase does not affect diabetes development: β-Cells survive RIPK1 activation. *Mol Metab* 69, 101681 (2023).
13. Takahashi, N. *et al.* RIPK1 ensures intestinal homeostasis by protecting the epithelium against apoptosis. *Nature* 513, 95–99 (2014).
14. Dannappel, M. *et al.* RIPK1 maintains epithelial homeostasis by inhibiting apoptosis and necroptosis. *Nature* 513, 90–94 (2014).
15. Linnemann, A. K., Baan, M. & Davis, D. B. Pancreatic β-cell proliferation in obesity. *Adv. Nutr.* 5, 278–288 (2014).
16. Ifie, E. *et al.* Unexpected subcellular distribution of a specific isoform of the Coxsackie and adenovirus receptor, CAR-SIV, in human pancreatic beta cells. *Diabetologia* 61, 2344–2355 (2018).
17. Vehik, K. *et al.* Prospective virome analyses in young children at increased genetic risk for type 1 diabetes. *Nat. Med.* 25, 1865–1872 (2019).
18. Hiemstra, H. S. *et al.* Cytomegalovirus in autoimmunity: T cell crossreactivity to viral antigen and autoantigen glutamic acid decarboxylase. *Proc. Natl. Acad. Sci. U. S. A.* 98, 3988–3991 (2001).
19. Honeyman, M. C. *et al.* Association between rotavirus infection and pancreatic islet autoimmunity in children at risk of developing type 1 diabetes. *Diabetes* 49, 1319–1324 (2000).
20. Taraborrelli, L. *et al.* LUBAC prevents lethal dermatitis by inhibiting cell death induced by TNF, TRAIL and CD95L. *Nat. Commun.* 9, 3910 (2018).

ACKNOWLEDGMENTS

"Life is not easy for any of us. But what of that? We must have perseverance and, above all, confidence in ourselves. We must believe that we are gifted for something, and that this thing, at whatever cost, must be attained." — Marie Curie

The PhD journey has been a long and challenging yet enjoyable experience filled with many ups and downs. First and foremost, I would like to thank everyone who has accompanied me on this journey, especially those who supported me during the down moments while celebrating the ups.

I thank my supervisor and mentor, Prof. Nieves Peltzer, for guiding me throughout this journey and providing me with the space and opportunities for growth. I thoroughly enjoyed our scientific discussions, which were always filled with enthusiasm and curiosity. I am especially grateful for the scientific freedom you offered, along with your limitless support and encouragement. I have learned so much from you!

I thank Jurgen Manchot Stiftung for funding my PhD salary and lab consumables for three years.

I would like to express my deepest gratitude to all our collaborators. I thank Prof. Alessandra K. Cardozo for her input and her team for their support with islet experiments. I thank Dr. Alessandro Annibaldi for his valuable input and providing us with FFPE samples from Cflar; VillinCre-ERT2 mice. I thank Prof. Mathieu Bertrand and Dr. Yann Estornes for the HFD experiments. I thank Prof. Henning Walczak for all his support including *Hoip*$^{fl/fl}$ mice and to Prof. Manolis Pasparakis for providing us with the *Ripk1*$^{fl/fl}$ mice. Finally, I thank Luisa Schmidt from Marcus Krüger lab for the proteomics analysis.

My gratitude to my TAC mentors, Prof. Silvia von Karstedt and Prof. Ana Garcia-Saez and for their inputs and discussions during the TAC meetings. Moreover, I thank the members of my examination committee, Dr. Alessandro Annibaldi, Prof. Ana Garcia-Saez, Prof. Andrea Morandi, Prof. Günter Schwarz and Prof. Nieves Peltzer.

The discussions during the joint lab meetings between Peltzer, Annibaldi and Liccardi labs were very insightful. I thank all members of Annibaldi, Liccardi and Walczak labs for the sharing reagents and protocols, and discussions.

Special thanks to Ana Beatriz Varanda from Walczak Lab for our long scientific discussions on cell death and optimization of staining protocols. Your contribution was significant for the paper. Moreover, thank you for all the support!

Special thanks to all the former and current members of Peltzer lab. My PhD journey wouldn't have been same without you. I particularly enjoyed sharing Mate with the Argentinian members of the lab. Now, I am a proper Mate drinker, with all the special equipment needed. I hope by now you also feel so strong about Halloumi and embrace it. I thank Lucas Valdez Capuccino for his suggestions and input especially in IT-related matters. I thank Ximena Hildebrandt for her help in vivo work and Mate drinking sessions which were a perfect occasion for long breaks. Dr. Mohammed Ibrahim has been certainly the funniest and most cheerful member of the Peltzer lab. Thanks for cheering us up.

I thank Öykü Kaya for making the long and late experiments enjoyable. Although you started as a master's student in the lab, we have also learnt many things from you. Thanks for all your endless support, friendship, coffee breaks, scientific discussions, hikes. I am certainly grateful that we have met.

My beloved aunt, teyze, you have certainly been one of the most influential people in my life. Thank you for teaching me the values of perseverance, honesty and courage. Your support has been a source of strength, not just during my PhD but throughout my entire life. I feel very lucky to have you by my side.

My dear wife, my life partner and my closest friend, Emma Deblangy, I feel like whatever I say will not be enough to explain my gratitude. PhD has been sometimes tough and overwhelming. Thank you for being there when I was feeling low and lifting me up. Thank you for cheering me up at the end of a very stressful and tiring day. Thank you for listening to all my presentations and proofreading every single document that was written by me during my PhD. Undoubtfully, this work wouldn't have been possible without your endless support.

Erklärung zur Dissertation
gemäß der Promotionsordnung vom 12. März 2020

Diese Erklärung muss in der Dissertation enthalten sein.
(*This version must be included in the doctoral thesis*)

„Hiermit versichere ich an Eides statt, dass ich die vorliegende Dissertation selbstständig und ohne die Benutzung anderer als der angegebenen Hilfsmittel und Literatur angefertigt habe. Alle Stellen, die wörtlich oder sinngemäß aus veröffentlichten und nicht veröffentlichten Werken dem Wortlaut oder dem Sinn nach entnommen wurden, sind als solche kenntlich gemacht. Ich versichere an Eides statt, dass diese Dissertation noch keiner anderen Fakultät oder Universität zur Prüfung vorgelegen hat; dass sie - abgesehen von unten angegebenen Teilpublikationen und eingebundenen Artikeln und Manuskripten - noch nicht veröffentlicht worden ist sowie, dass ich eine Veröffentlichung der Dissertation vor Abschluss der Promotion nicht ohne Genehmigung des Promotionsausschusses vornehmen werde. Die Bestimmungen dieser Ordnung sind mir bekannt. Darüber hinaus erkläre ich hiermit, dass ich die Ordnung zur Sicherung guter wissenschaftlicher Praxis und zum Umgang mit wissenschaftlichem Fehlverhalten der Universität zu Köln gelesen und sie bei der Durchführung der Dissertation zugrundeliegenden Arbeiten und der schriftlich verfassten Dissertation beachtet habe und verpflichte mich hiermit, die dort genannten Vorgaben bei allen wissenschaftlichen Tätigkeiten zu beachten und umzusetzen. Ich versichere, dass die eingereichte elektronische Fassung der eingereichten Druckfassung vollständig entspricht."

Teilpublikationen:

Veli, Ö., Kaya, Ö., Varanda, A. B., Hildebrandt, X., Xiao, P., Estornes, Y., Poggenberg, M., Wang, Y., Pasparakis, M., Bertrand, M. J. M., Walczak, H., Annibaldi, A., Cardozo, A. K., & Peltzer, N. (2024). RIPK1 is dispensable for cell death regulation in β-cells during hyperglycemia. Molecular metabolism, 87, 101988. https://doi.org/10.1016/j.molmet.2024.101988

Datum, Name und Unterschrift

06/10/2024 Önay Veli

Original article

MOLECULAR METABOLISM

RIPK1 is dispensable for cell death regulation in β-cells during hyperglycemia

Önay Veli[1,2,3], Öykü Kaya [1,2,3], Ana Beatriz Varanda[3,8], Ximena Hildebrandt [1,2,3], Peng Xiao [4], Yann Estomes[5,6], Matea Poggenberg[2], Yuan Wang [1,2,3], Manolis Pasparakis [3,7], Mathieu J.M. Bertrand [5,6], Henning Walczak[3,8], Alessandro Annibaldi[2], Alessandra K. Cardozo[4], Nieves Peltzer[1,2,3,*]

ABSTRACT

Objective: Receptor-interacting protein kinase 1 (RIPK1) orchestrates the decision between cell survival and cell death in response to tumor necrosis factor (TNF) and other cytokines. Whereas the scaffolding function of RIPK1 is crucial to prevent TNF-induced apoptosis and necroptosis, its kinase activity is required for necroptosis and partially for apoptosis. Although TNF is a proinflammatory cytokine associated with β-cell loss in diabetes, the mechanism by which TNF induces β-cell demise remains unclear.

Methods: Here, we dissected the contribution of RIPK1 scaffold versus kinase functions to β-cell death regulation using mice lacking RIPK1 specifically in β-cells (*Ripk1*$^{\beta\text{-}KO}$ mice) or expressing a kinase-dead version of RIPK1 (*Ripk1*^{D138N} mice), respectively. These mice were challenged with streptozotocin, a model of autoimmune diabetes. Moreover, *Ripk1*$^{\beta\text{-}KO}$ mice were further challenged with a high-fat diet to induce hyperglycemia. For mechanistic studies, pancreatic islets were subjected to various killing and sensitising agents.

Results: Inhibition of RIPK1 kinase activity (*Ripk1*^{D138N} mice) did not affect the onset and progression of hyperglycemia in a type 1 diabetes model. Moreover, the absence of RIPK1 expression in β-cells did not affect normoglycemia under basal conditions or hyperglycemia under diabetic challenges. *Ex vivo*, primary pancreatic islets are not sensitised to TNF-induced apoptosis and necroptosis in the absence of RIPK1. Intriguingly, we found that pancreatic islets display high levels of the antiapoptotic cellular FLICE-inhibitory protein (cFLIP) and low levels of apoptosis (Caspase-8) and necroptosis (RIPK3) components. Cycloheximide treatment, which led to a reduction in cFLIP levels, rendered primary islets sensitive to TNF-induced cell death which was fully blocked by caspase inhibition.

Conclusions: Unlike in many other cell types (e.g., epithelial, and immune), RIPK1 is not required for cell death regulation in β-cells under physiological conditions or diabetic challenges. Moreover, *in vivo* and *in vitro* evidence suggest that pancreatic β-cells do not undergo necroptosis but mainly caspase-dependent death in response to TNF. Last, our results show that β-cells have a distinct mode of regulation of TNF-cytotoxicity that is independent of RIPK1 and that may be highly dependent on cFLIP.

Keywords RIPK1; Necroptosis; TNF; Apoptosis; β-cell; Diabetes; cFLIP